THERMAL REMEDIATION OF STAINLESS STEEL ELECTRIC ARC FURNACE (EAF) DUST

A thesis submitted to the Faculty of Graduate Studies and Research in partial fulfilment of the requirements of the degree of Masters of Engineering

By: Neil S. D'Souza

9338343

Department of Mining & Metallurgical Engineering

November 1999

ACKNOWLEDGMENTS

I would like to take this opportunity to thank my co-supervisors Dr. Jerzy Szpunar and Dr. Janusz Kozinski for their tremendous guidance. I would especially like to thank Dr. Kozinski's constant support and assistance. He has provided me throughout the years with a true learning experience, not simply by enriching my academic career but by providing me a life experience which will serve me throughout my professional and personal endeavours.

I would also like to thank the following people for their support and technical assistance throughout my research: Sergio Di Lalla, Guohui Zheng, Slawomir Poplawski, Yang Cao, Yasmine Sarruf and Stacey Rodgers.

ABSTRACT

Along with the essential importance of the metallurgical sector, one must recognise that it is also one of the largest sources of environmental pollution. In particular, the problem of electric arc furnace (EAF) dusts is of a growing concern due to the increase in popularity of EAF steelmaking. This dust is classified as a hazardous product due to the elevated content of toxic metals (e.g., Cr).

Studies on the properties of EAF dusts are sparse. Experiments were performed in order to determine the chemical and physical characteristics of the dust. It was determined that EAF dust is constituted of randomly distributed agglomerations of homogeneously nucleated particles and entrained particles. The main elements present within the particular dust were iron and chromium, the latter due to the fact that the dust used was formed within a stainless steel mini-mill. The main phases present within the dust were Fe_2O_3/Fe_3O_4 and Cr_2O_3.

Thermal remediation experiments were then carried out in a computer controlled thermogravimetric system. The parameters studied during the tests included temperature, residence time and heating rate. In addition, the behaviour of the EAF dust during remediation was studied; in terms of weight and volume loss, gas evolution, particle morphology and resulting leachability of the treated product. Furthermore, it was observed that at temperatures greater than 1200°C metal leachability decreased significantly due to a decrease in toxic metal concentration within the treated product and the formation of a resistant, dense, plate-like morphology. At 1600°C, no toxic metals leached out of the remediated EAF dust and volume reduction was significant, resulting in a product that would be safe and more economical to landfill.

RÉSUMÉ

Avec l'importance essentielle du secteur métallurgique, on doit identifier qu'il est également un des plus grandes sources de pollution environnementale. En particulier, la poussière provenant des fours d'arc électrique (EAF) est devenue un problème croissant dû à la popularité de ce type d'aciérie. Cette poussière est classifiée comme déchet dangereux dû à la teneur élevée de métaux toxiques (par exemple, le chrome).

Les études sur les caractéristiques de ce type de poussière sont clairsemée. Des essais ont été exécutées afin de déterminer les caractéristiques chimiques et physiques de la poussière. Les études ont déterminé que la poussière EAF est constituée d'agglomérations aléatoirement distribuées de particules homogènement nucléées et de particules entraînées dans l'échappement du four. Les principaux éléments dans cette poussière particulière étaient le fer et le chrome; ce dernier étant donné que la poussière utilisée a été formée dans une usine d'acier inoxydable.

Des essais thermiques de remédiation ont ensuite été effectuées dans un système thermogravimétrique. Les paramètres étudiés durant les essais incluaient la température, le temps de séjour et la cadence de chauffage. En outre, le comportement de la poussière EAF pendant la remédiation a été étudié en terme de perte de poids et de volume, d'évolution de gaz, de morphologie de particule et de la lixiviation du produit traité. On a observé qu'a des températures supérieures à 1200°C, la lixiviation a diminué sensiblement en raison d'une diminution de concentration de métaux toxiques dans le produit traité et de la formation d'une morphologie dense et résistante. À 1600°C, aucun métal toxique a lixivié de la poussière EAF traité. Aussi, la réduction de volume dû au traitement termique était significative. Ceci avait pour résultat un produit qui serait sûr et plus économique à remblayer.

TABLE OF CONTENTS

A. LIST OF FIGURES

Chapter 1: LITERATURE REVIEW

Chapter 3: EXPERIMENTAL FACILITY AND ANALYTICAL INSTRUMENTS

Chapter 4: EAF DUST CHARACTERISTICS AND FORMATION

Chapter 5: EXPERIMENTAL METHODOLOGY

Chapter 6: BEHAVIOUR OF EAF DUST DURING THERMAL TREATMENT

Chapter 7: MORPHOLOGICAL CHANGES DURING THERMAL TREATMENT

B. LIST OF TABLES

Chapter 1: LITERATURE REVIEW

Chapter 3: EXPERIMENTAL FACILITY AND ANALYTICAL INSTRUMENTS

Chapter 4: EAF DUST CHARACTERISTICS AND FORMATION

Chapter 5: EXPERIMENTAL METHODOLOGY

Chapter 6: BEHAVIOUR OF EAF DUST DURING THERMAL TREATMENT

Chapter 7: MORPHOLOGICAL CHANGES DURING THERMAL TREATMENT

1 LITERATURE REVIEW

1.1 Electric Arc Furnace (EAF) Steelmaking

The electric arc furnace (EAF) was developed by a Frenchman, Pichon, for which a patent was granted on March 16, 1853 for his claim of economically melting minerals and metals. Thereafter, many furnace designs were conceptualized as seen in Figure 1.1, however, it was in France between 1888 and 1892 that Heroult built a direct arc furnace which provided the blueprint for EAF construction of today. A schematic of Heroult's design can be seen in Figure 1.2. The enhancement of this design was that the heat generated by the arc was held within the scrap during the melting process. This resulted in lower refractory erosion. The EAF was initially developed in the manufacture of ferroalloys and calcium carbide. However, its advantages were soon recognized in the growth of alloy steel melting[1]. The first arc furnace to be installed and operated successfully in North America was at the Halcomb Steel Company in Syracuse, New York in 1906.

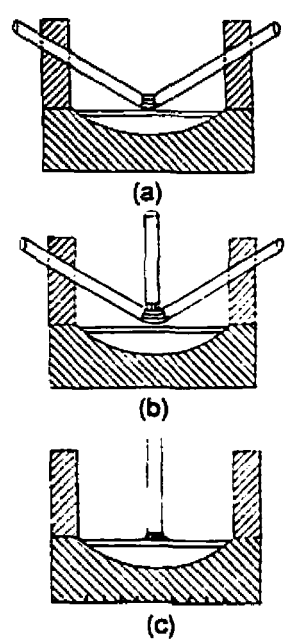

Figure 1.1: Schematic drawings of (a) indirect arc designed by Stassano, (b) special indirect arc designed by Rennerfelt, (c) Conducting-bottom, direct arc principle by Girod

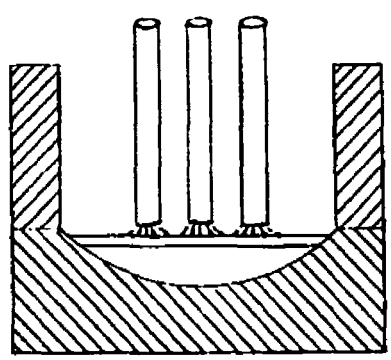

Figure 1.2: Three-phase electric arc furnace built by Heroult

Arc furnaces can be divided into three main categories based upon nature and form of the electrodes to which the current is supplied. Three types are as follow:

Indirect arc Furnaces
Direct arc Furnaces
Bottom Electrode Furnaces

The use of the indirect arc furnace is limited to the melting of cast irons and non-ferrous metals. It is rarely used in steelmaking operations due to the fact that it results in severe wall refractory wear.

The majority of steelmaking operations require the use of direct arc furnaces. Bottom electrode furnaces were constructed as an alternative to Heroult's strong patent. However, problems arose with bottom refractory wear as the furnaces got larger and their power ratings increased. Direct arc furnaces are manufactured in most steelmaking countries. Most manufacturers employ the basic principle: there are three electrodes, almost always of graphite and a cup shaped hearth, which forms the crucible for the molten metal. A current is passed through these electrodes and an arc is sparked between each electrode and the charge. The heating process takes place mainly through radiation and convection from the arcs, which can attain temperatures in excess of 20,000°C[2]. Due to these high temperatures, the dissipation of energy and the resulting heating rate are quite rapid. The high temperatures attainable within the furnace coupled with a highly reducing atmosphere and a very fluid slag which can be formed, results in the formation of chemical compounds which promote desulphurising and deoxidising conditions. As a result, a much larger range of raw materials can be used.

1.1.1 General Furnace Construction

Most direct arc furnaces used for industrial purposes are of the three phase type with three carbon or graphite electrodes, hanging vertically over the hearth. These large industrial furnaces consist of an external steel shell, which is cylindrical in shape, a dished bottom and a removable roof ring on which the domed refractory roof is supported. The roof contains three openings about the centreline symmetrically placed to form an equilateral triangle, through which the electrodes enter the furnace. Furnaces can either discharge the metal by means of a bottom tap or a side tap. In the latter case, the furnace should comprise a rocking mechanism. Above the furnace roof lie the electrode

arms, which not only mechanically support the electrodes above the furnace but also carry the conductors leading the current to the clamps.

As the furnace hearths increased, so did the methods used to charge the furnace. In earlier practice, the furnace was hand-charged through doors on the furnace sidewall. However, as the charges increased, a top charging method was developed. This required the need for the roof and superstructure to be removed quickly by mechanical means. Top charging can be seen in Figure 1.3. The charging bucket used is usually designed for a particular application. Two basic types of charging buckets are used: the clamshell type and the orange peel type. These two-bucket designs are illustrated in Figure 1.4.

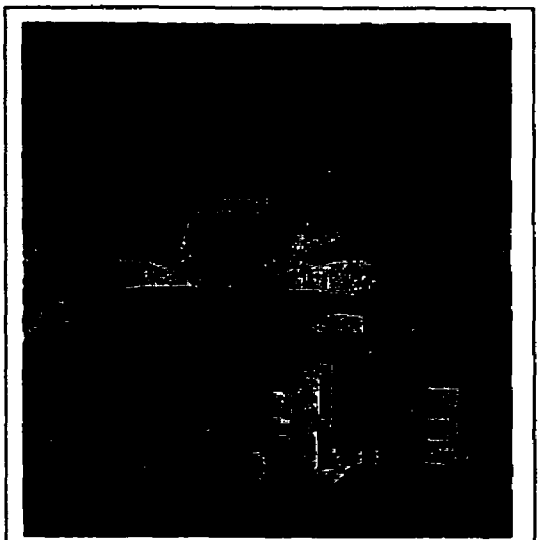

Figure 1.3: Top-charging of a 120 ton EAF

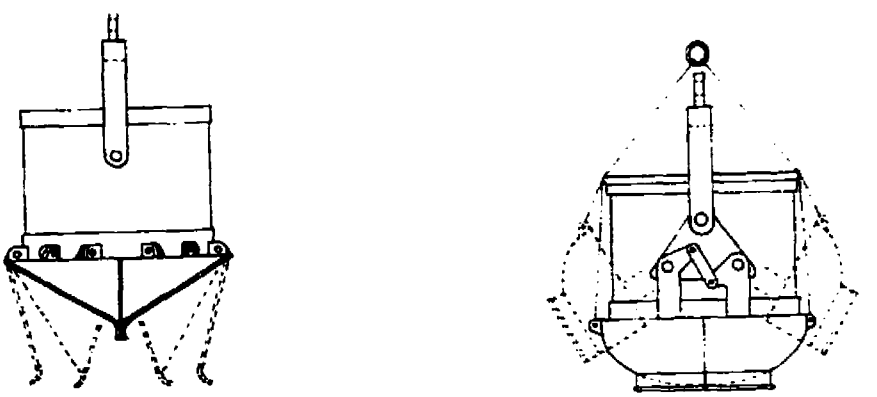

(a) (b)

Figure 1.4: (a) Orange peel type of charging bucket; (b) Clamshell type of charging bucket

1.1.2 Process Status

Electric arc steelmaking is a process option that is considerably increasing in popularity amongst steelmakers. Technology developments have resulted in increased

opportunities for EAF steelmakers since now, minimills are not limited to the production of simple steel products but rather, can compete with integrated steel mills in the more lucrative high end product range. Steel plants with EAFs once only consisted of furnaces, continuous casting equipment and elementary rolling machines. Previously, their production consisted mainly of construction steel, however, through technological development, they were involved in the production of wire rod and light and heavy profiles. Presently, EAF steelmakers are capable of manufacturing all types of long products; such as tubing, while increasing their share in the flat products market with the help of continuous casting[3].

In Canada, electric arc furnaces have a nominal capacity of over 8 million tons of steel a year. These arc furnaces consume around 10 billion kWh annually[4].

In 1991 U.S. and Canadian steelmakers operated some 240 electric furnaces[5]. Almost half of these furnaces tapped heats that can be classified as small (55 tons or less) while 27% of these EAF's had a capacity of 100 tons or more. More than 100 of the 240 EAFs were operated by minimills. Almost half these furnaces had a tapping capacity of 55 tons or less which would categorise them as small. 30 percent are of medium size (56 to 109 tons) and 21 percent as large (> 110 tons), as seen in Figure 1.5.

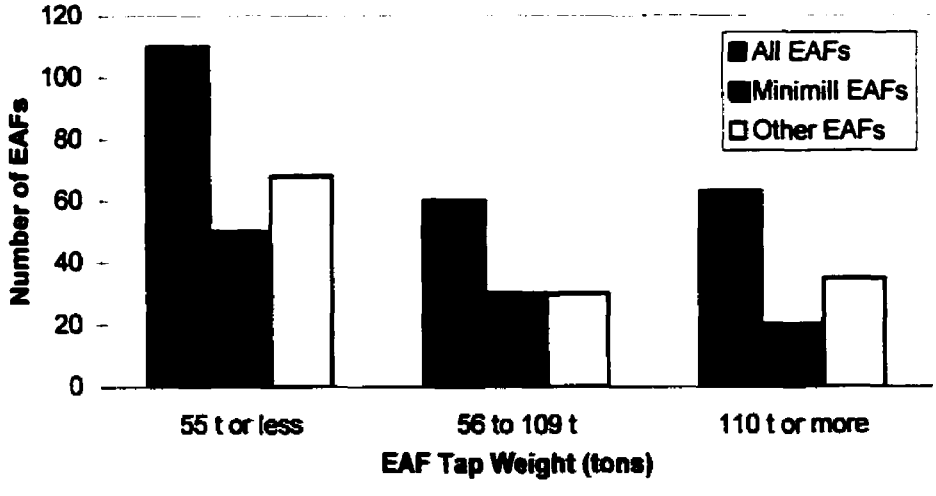

Figure 1.5: Distribution of U.S. and Canadian EAFs by heat size.

Merely 5 percent of the EAF output in 1991 was alloy, stainless and tool steels. Equally, 18 percent of EAFs made stainless and tool steels along with carbon grades.

Twenty-two percent made basically carbon and alloy steels while the remaining majority (42 percent) of EAFs were involved in the production of carbon and low alloy grades (Figure 1.6).

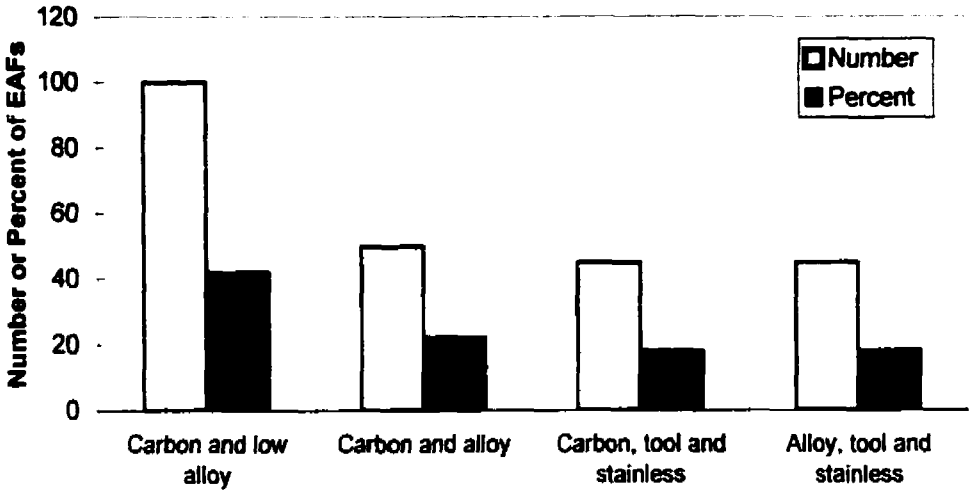

Figure 1.6: Distribution of U.S. and Canadian EAFs by steel product produced

1.1.3 Scrap in World Steel Production

The world-wide production of steel in 1993 reached 725 Mt. To produce this quantity, 503 Mt of hot metal, 24 Mt of sponge iron and about 400 Mt of scrap were used[6]. The share of EAFs in steel production has climbed to a high of around 30%, signifying that every third ton of steel produced world-wide was made from recycled scrap.

The share of electric arc furnaces in steelmaking greatly affects the demand for scrap in the medium and long terms, Figure 1.7 shows world steel production, the share of production by EAFs and the level of scrap consumption between 1976 and 1993. The share of EAFs in worldwide steel production climbed from a share of 19.2 percent in 1976 (130 Mt), to 30 percent in 1993 (225 Mt). The material required to feed this growing production is supplied through the following sources: hot metal, scrap and scrap substitutes. Although the demand for hot metal will remain stagnant until 2003, the demand for scrap will increase by 17.4 percent during this same period. Scrap used in the production of steel can be categorised into three groups:

Circulating scrap: scrap produced during the final transformation step of molten steel to the final products in steel plants and mills. The amount of circulating scrap is expected to decrease by the year 2003.

Process scrap: scrap produced in industrial plants where steel is the initial material in the fabrication of components. Due to the increase in efficiency of fabricating methods, one would expect a decrease in this type of scrap, however, this decrease is balanced by the increase in steel consumption. As a result there is expected to be a marginal increase in the level of process scrap until 2003

Capital scrap: scrap from components manufactured of steel that have served their useful life cycle. Due to the increase in direct and indirect consumption of steel, there is expected to be a significant increase in the level of capital scrap. Indeed, the level of capital scrap will increase by 31 percent by the year 2003.

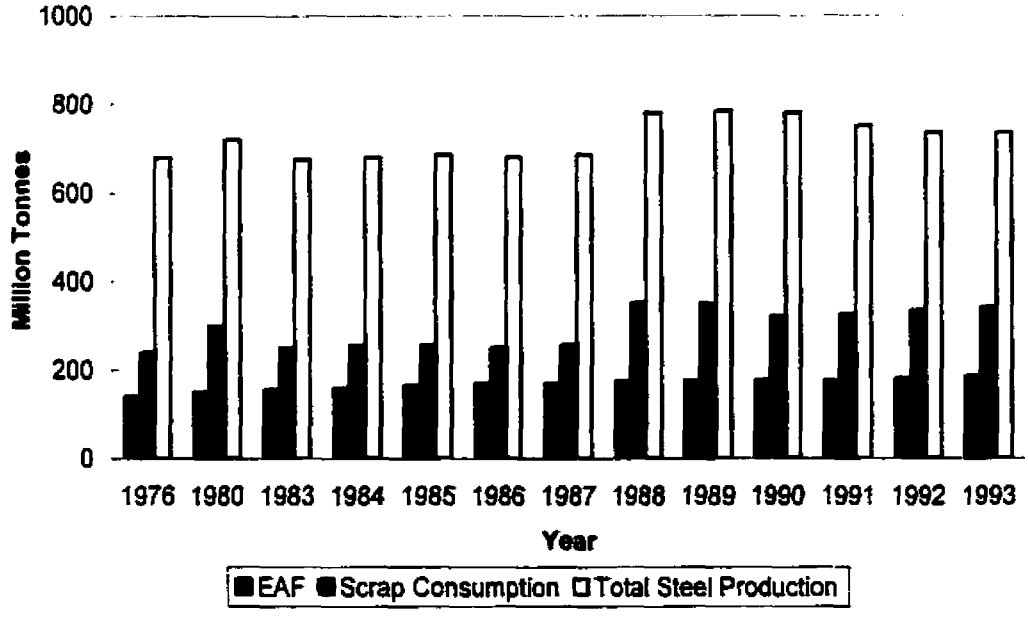

Figure 1.7: World steel production, EAF share and scrap consumption

1.2 Emission Control In Electric Arc Furnaces

Emission generation from the operation of electric arc furnaces is associated with all phases of normal furnace operations. Two categories exist for emissions: primary emissions and secondary emissions. Primary emissions are categorized as those occurring

during the melting and refining cycles of furnace operations. Secondary emissions are defined as those occurring during operations other than melting or refining, specifically, during furnace charging, metal tapping or slagging. Secondary emissions, which constitute less than 10 weight percent of all furnace emissions, occur over relatively short periods of time, and are associated with roof movements or furnace movements which make emission collection rather tedious.

1.2.1 Nature of Particulate Emissions

The principal contaminants formed during EAF steelmaking operations are carbon monoxide and particulate matter. In addition, depending on slag chemistry and furnace additives, traces of hydrocarbons, sulphur oxides, and fluorides will be present. Additional products of furnace combustion can also be found, such as oxides of nitrogen and ozone, which can be formed from the furnace arcs.

During the melting and refining stages, particulate matter is evolved from the furnace principally in the form of metallic oxides resulting from the oxidation of some metals and volatilization of others, resulting from the intense heat and turbulence generated. The thermal head in the furnace results in a positive pressure at the top of the furnace where the fumes escape through the electrode ports and roof rings in a furnace with no emission control system. The injection of oxygen during the refining process results in the greatest concentration of particulate matter. During the charging process, particulate matter and volatile matter are liberated from the scrap by the furnace heat and agitation as the charge drops into the bath. The heat and agitation that occurs during tapping results in noticeable particulate formation, especially if alloy additions are added as the metal is tapped into the ladle[7]. The temperature of the EAF steelmaking process is generally around 1600°C, which is above the vaporisation temperature of zinc, lead, and cadmium present in the charge[8]. In addition, small amounts of iron, nickel and manganese are volatilised. The level of chromium volatilisation depends on the charge to be melted; as stainless steel scrap contains high chromium levels. As the metal vapours exit, physically and chemically complex, microscopic agglomerates form on foreign nuclei such as fugitive dust.

The primary dust generators are electric furnace minimills who melt scrap in an EAF to produce a variety of steel products. While melting the scrap, approximately 2% of the scrap steel charged to the EAF arises as dust containing mostly zinc, lead, cadmium, and halides contained in the charge. Dust formation from EAFs ranges from 4.5-22.5 kg/ton of steel produced. In Canada and U.S., this adds up to 600,000 tons/yr. of furnace dust produced[9]. The range of dust produced can vary from plant to plant depending on such factors as charging methods, scrap quality, oxygen blowing rates, furnace operating practices, and the type of steel produced. Particulate matter concentrations in the off-gas generally exceed 23000 mg/m^3. Studies conducted on secondary emissions have concluded that charging and tapping emissions are generally equal in magnitude. In addition, operating parameters such as scrap quality and ladle additives greatly affect the amount of dust generation.

The range of chemical composition of EAF dust can be seen in Table 1.1. The variations can be attributed to the type of steel produced, as galvanised steel will produce a high zinc oxide content whereas stainless steel will yield high chromium oxide and nickel levels in the dust.

Table 1.1: Range of composition of EAF dust

Component	Range of Reported Values (wt%)
Fe_2O_3	19-65
FeO	4-11
Fe	5-36
SiO_2	1-9
Al_2O_3	1-13
CaO	2-22
MgO	2-15
MnO	1-12
Cr_2O_3	0-12
NiO	0-3
PbO	0-4
ZnO	0-44
P	0-1
S	0-1
C	0-4
Alkalies	1-11

The particle size distribution of the dust is quite difficult to determine due to uncertainties in sampling techniques. However, in general, EAF dust is classified as "sub-micron". Table 1.2 shows some reported ranges of particle size.

Table 1.2: Particle size distribution of EAF dust

Weight Percent Less Than, (μm)	Ranges of Reported Percentages
40	82-100
20	67-98
10	61-95
5	43-90

1.2.2 Status of Environmental Regulations

1.2.2.1 U.S. Environmental Protection Agency Standards

The water solubility of some of the elements in EAF dust exceeds prescribed US federal environmental limits. In 1984, the Environmental Protection Agency (EPA) classified this dust as a hazardous waste (K061) under the regulations of the Resource Conservation and Recovery Act (RCRA). EAF dust fails the EPA's Toxicity Characteristic Leaching Procedure (TCLP) for lead, cadmium and chromium[10]. The EPA regulatory level of metal toxicity is shown in Table 1.3[11]. A material is considered hazardous if the aqueous leachate of the material contains elements greater than the concentrations indicated in Table 1.3.

Table 1.3: EPA regulatory leachate levels for metals

Metal Contaminant	Regulatory Level (mg/l)
Arsenic	5.0
Barium	100.0
Cadmium	1.0
Chromium	5.0
Lead	5.0
Mercury	0.2
Selenium	1.0
Silver	5.0

The US EPA regulations regarding EAF dusts are continually evolving, however the current regulation is that EAF dust is designated by the EPA as hazardous waste No.K061. EAF dust is a listed waste because it contains hazardous constituents including hexavalent chromium, lead and cadmium. In 1995, the EPA ruled that stabilisation and subsequent disposal in conventional landfills is permissible for all EAF dust[12].

The current K061 regulations are the following:

If the dust is to be used for fertiliser manufacture, the dust is exempt from hazardous waste regulation.

Any dust treatment technology can be used if it meets the TCLP leachate standards. The treatment standards include fourteen elements:

Antimony	Mercury
Arsenic	Nickel
Barium	Selenium
Beryllium	Silver
Cadmium	Thallium
Chromium	Vanadium
Lead	Zinc

1.2.2.2 Quebec Ministry of the Environment Standards

EAF dust is considered to be hazardous waste by the Ministère de l'Environment et de la Faune (MEF). EAF dust is present in *"Regulation on Hazardous Waste (Q-2, r3.01)"*[13] and falls under the category of metallurgical hazardous waste: Art. 69. "Dust resulting from the purification of emissions from metal fusion in fusion furnaces"

EAF dust falls under the category of hazardous waste since its leachate produced using the leaching procedure *"Procédure d'évaluation des caractéristiques des déchets solides et des boues pompables"*[14]. contains levels of certain metals superior to the regulatory limits. These limits, found in Annex III of the *"Regulation on Hazardous Waste"*, are shown in Table 1.4. These levels are similar to EPA guidelines.

Table 1.4: MEF guidelines for maximum concentration of metals in leachate from solid residue

Metal Contaminants	Norms for the Leachate of Solid Residue (mg/L)
Total arsenic	5.0
Total cadmium	2.0
Total chromium	5.0
Total copper	10
Total mercury	0.2
Total nickel	10.0
Total lead	5.0
Total selenium	1.0
Total zinc	10

1.2.3 Methods of Fume Capture

Most of the effort to capture fumes has been concentrated on the capture of primary emissions, which occur during the melting and refining stages. Three basic methods of primary fume capture are employed: (a) direct shell evacuation, (b) roof-mounted hoods, and (c) canopy hoods.

1.2.3.1 Direct Shell Evacuation

The direct shell evacuation method of fume control employs a duct system, which removes emissions through a hole in the furnace roof. The water-cooled duct transports the gases to a point where further cooling can occur. Air is introduced in the duct gaps as to burn off the carbon monoxide produced. This process is primarily used on larger furnaces (greater than 4.6m in diameter) but can also be used on smaller furnaces. The advantages of direct shell evacuation are the following: (a) better control of furnace evacuation rates, (b) less system volume, (c) effective CO control, (d) best control of particulate emissions during melting and refining. The disadvantages of this process are: (a) possible effects on furnace metallurgy, (b) adverse affects on electrode consumption, furnace efficiency, refractory life and melting efficiency, (c) possible physical interference at the furnaces, and (d) no secondary emission control

1.2.3.2 Roof-Mounted Hoods

Roof mounted hoods have been in most common practice since the early 1960's[15] [16]. The most recognized roof-mounted system is that of side draft or lateral exhaust hood, as seen in Figure 1.8. This exhaust system is composed of a hood placed over the furnace roof laterally attached to ducts. Gas cooling is not of great importance since the hood will pull in sufficient dilution air from the surroundings. The advantages of roof mounted hoods are the following: (a) no effects on furnace conditions, (b) the absence of special cooling equipment and furnace pressure controls, and (c) simple system design. The disadvantages of this system include: (a) higher off-gas volumes, (b) physical interference with furnace operations, (c) less effective CO control, and (d) no control of furnace emissions.

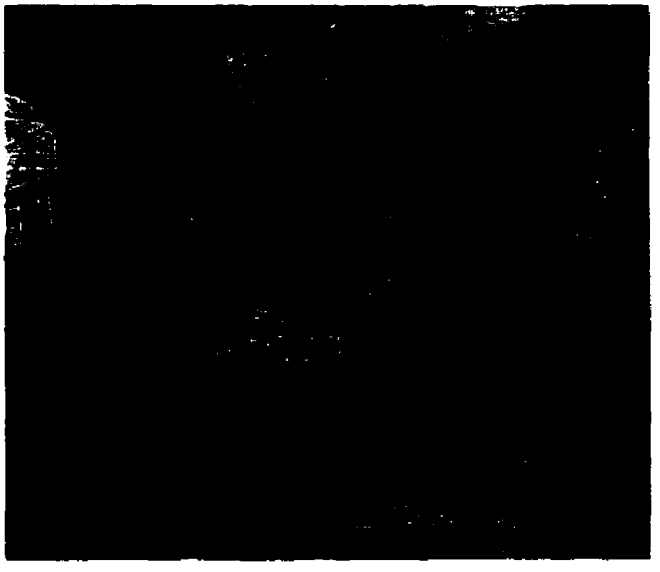

Figure 1.8: Side draft hood arrangement of roof mounted design

1.2.3.3 Canopy Hood Design

Canopy hoods are essentially large hoods located well above the furnace in the foundry building roof. The fumes generated from the furnace are permitted to escape in an uncontrolled manner until reaching the building roof[17]. The emission gas is cooled naturally by the great deal of infiltration air that is pulled up to the canopy with it. Canopy hoods have the following advantages: (a) absolutely no interference from furnace operations, (b) a simple design, (c) no gas cooling system required, and (d) partial control

of secondary emissions. The disadvantages of this system are: (a) absence of effective particulate control, (b) less effective CO control, (c) extremely high off-gas volume, and (d) polluted working and shop conditions.

1.2.4 Gas Cleaning Equipment

1.2.4.1 Electrostatic Precipitators

When dust-laden air is passed between two surfaces with a high electric potential difference, the particles are charged under the influence of an electric field. These particles migrate and precipitate on the surface having an opposite electrical charge. Removal of the collected material is obtained by vibrating or rapping the electrode plates, either continuously or at predetermined intervals.

The advantage of electrostatic precipitators is that they operate at high temperatures (260-316°C), which requires less cooling and can capture sub-micron dust. However, several disadvantages accompany this technique, such as a high initial cost, the need for proper temperature and moisture control to prevent corrosion, and the danger of explosion from carbon monoxide carry-over. Frequent cleaning of the electrode plates is also necessary to prevent a decrease in system efficiency.

The lack of proper moisture control, resulting in corrosion has discouraged the use of electrostatic precipitators in the steel industry[18].

1.2.4.2 Wet Scrubbers

A wet scrubbing system would utilize a quenching of the off-gas near the furnace and subsequent transport to a Venturi or orifice scrubber followed by cyclonic mist eliminators.

The feasibility of using wet scrubbers must be determined based on the cost of energy. High-energy scrubbers are in use in several direct evacuation systems, primarily on large furnaces[19]. The advantage of using a wet scrubbing system is that it can perform under temperature fluctuations that can be caused in furnace operations without any significant loss in performance. The many disadvantages of wet scrubbers include, (a) the high power requirements, (b) the need to build and maintain a water treatment system to deal with the effluents of the scrubbing system, and (c) the need to install a scrubber system for each furnace. In addition, since scrubber systems make an extensive use of

water, corrosion comes into play. The presence of chlorides and sulphurs will lead to corrosion problems. Thus, effluent water that is re-used must be treated in order to decrease or even eliminate the chloride and sulphur concentration in the water, control pH and treat dissolved solids.

1.2.4.3 Fabric Filters

The use of fabric filters as a gas-cleaning device in steelmaking operations is quite widespread. They present a simple solution at a relatively low cost. In the bag filter cleaners, furnace off-gases are filtered through fabric bags, which are located in the baghouse (Figure 1.9). Dacron polyester bags can be used up to temperatures of 200°C; fibreglass is used for gases up to 300°C. The bags are usually stored in air tight galvanised sheet steel boxes. As many as 84 bags can be used for a 30 ton furnaces stored in four separate compartments. To remove the dust, the bags are periodically vibrated, however, this increases bag wear. For this reason, most modern facilities employ periodic reverse flow through the bags to remove the dust accumulation. The system can be arranged so as to clean one compartment as the other ones are filtering.

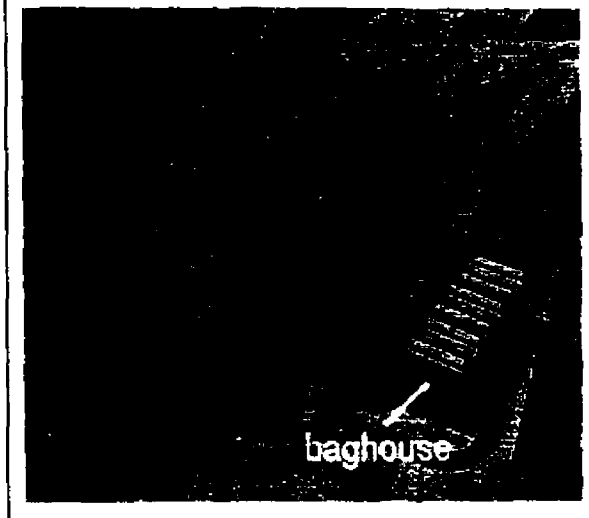

Figure 1.9: Electric furnace fabric filter installation

Fabric filters offer the advantages of ease of expansion, reliability and availability. This gas-cleaning device can treat a large volume of low temperature gases. However a main disadvantage lies in the fact that the gases must be cooled to a level compatible with the filter material of choice. Another disadvantage is the space required setting up a baghouse facility.

1.3 Exposure to Particulate Matter Produced During EAF Steelmaking

The exposure to airborne particles can be a hazard to human health as they can cause a variety of respiratory diseases affecting the lungs. Airborne particles can be

divided into two main categories: (a) dispersion, which involves the breakdown from solid or liquid matter resulting from such activities as milling or atomization, and (b) condensation, resulting from the build-up of matter after a heating and cooling cycle. In addition, airborne emissions can be further categorized into sub-categories as follows[20]:

- *Dusts*, which fall under the category of dispersion, are produced from solids as they are mechanically processed; such is the case in mines, mills and foundries; such is the case with EAF dusts.
- *Mists*, which are generated by liquid dispersion, or by evaporation and/or condensation of vapours
- *Smokes*, which are partially formed by very fine solid and liquid particles, are generated by the burning of carbonaceous material. Most smokes contain harmful carcinogens
- *Fumes*, which are produced from the vaporisation and condensation of hot solid species usually occur in metallurgical industries.

Particle behaviour in air and in the human body depends on their physical and chemical compositions. Size, density and shape are important parameters to consider since they determine particle settling rates, and thus determine the time that these particles remain airborne. If particles cause any harmful effects, it will be resultant upon their chemical and mineralogical composition, solubility, and biological activity.

1.3.1 Particle Size

Particle size is usually defined by its diameter. If the particle is a sphere, then its diameter will be a specific indication of its size, however, if the particle is non-spherical, then the following conventions are employed:

- The volume of the particle is given in terms of a sphere;
- The mass of the particle is given in terms of a sphere;
- The settling velocity of the particle is given in terms of that of a spherical particle;
- The diameter of the particle is determined in terms of a dimension of the projected area as seen through microscopy

Particles in the range of 0.005-0.05 μm are formed through the condensation of vapors either through high temperatures or chemical processes. Particles in the range of 0.5-2 μm are formed through coagulation of smaller particles or through small particles from vapor condensation. Fume particles, such as EAF dusts contain diameters ranging from 200 μm down to 0.01 μm. A wide spectra of different airborne particles can be seen in Figure 1.10[21].

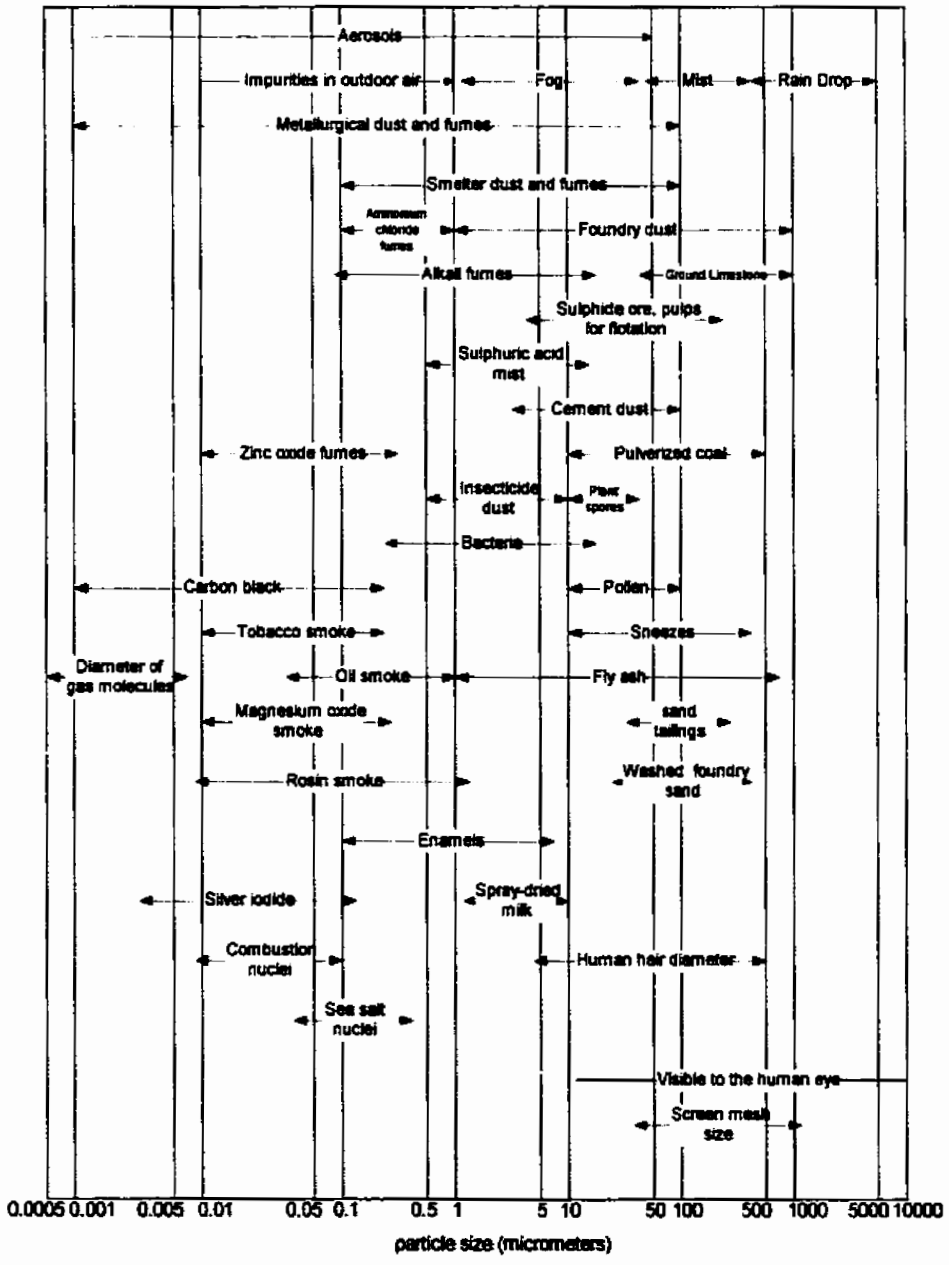

Figure 1.10: Size distributions of various airborne particles

In order for particles to penetrate to the lungs and into the alveoli, they must have a settling velocity of approximately 3×10^{-3} m/s. This corresponds to a 7 μm diameter unit density sphere. Particles with a equivalent diameter of 10 μm will not penetrate beyond the nasopharynx, in addition, particles of an equivalent diameter of 50 μm will be too large to breath into the lungs. Although EAF dust contains a varied size distribution, some of its particle sizes still fall in the harmful range where it could be inhaled into the lungs.

1.3.2 Particle Penetration Into the Respiratory System

The lungs are the organs that essentially convey with the atmosphere through a series of branching tubes, as shown in Figure 1.11. The lungs are constantly exposed to particulate matter that we breath in, however, our lungs posses defences that can protect us against this airborne matter. For example, a coal minor may receive 1000g of dust in his lungs, however, upon death a doctor may only see no more than 40g of dust remaining in the victim's lungs[22]. This illustrates the lung's defences. Conversely, no defense mechanism can be perfect. Excessive inhalation of dust will result in lung disease.

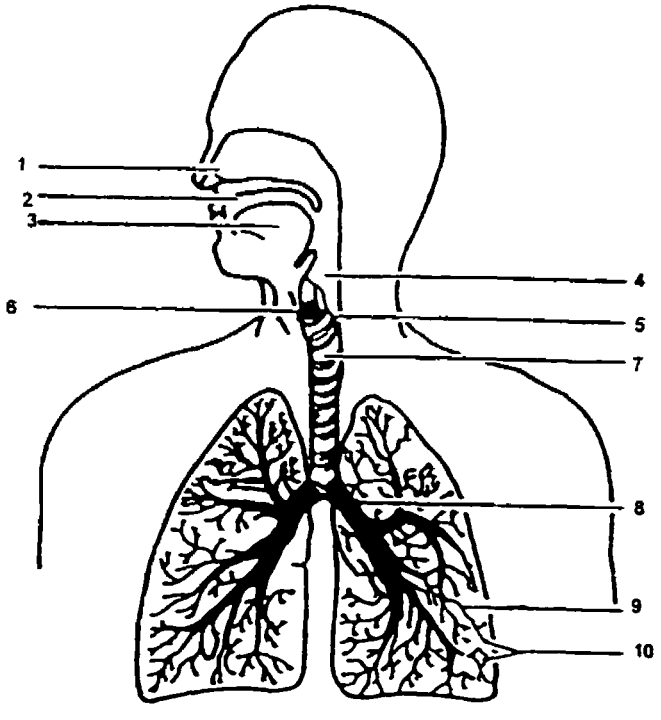

1. bones and cartilage in the nose that makes inhaled air swirl to deposit large particles
2. mouth –has no filtering system
3. tongue
4. pharynx
5. esophagus –tube leading to the stomach
6. opening of trachea
7. trachea –tube leading to the lungs
8. bronchus
9. bronchiole
10. tiny air sacs (alvioli) at the end of each bronchial "tree" branch

Figure 1.11: Diagram of airway passage to the lungs showing the routes taken by contaminated air

1.3.3 Penetration and Deposition into the Lungs

Particulate matter that penetrates into the respiratory system can have harmful effects on the lungs and other parts of the system. Soluble substances can be especially dangerous since they can be ingested into the bloodstream throughout the system.

The penetration and deposition of particles into the respiratory system can be summarized as follows:

- Particles with an equivalent diameter greater than 10μm will be retained in the upper nasal area of the respiratory system.
- For particles less than 10 μm, penetration will be increased with decreasing particle size.
- The upper limit for penetration into the alveoli is approximately 10 μm. However, very few particles of this size reach the alveoli, they are mostly found in the bronchioles.

The probable site of particle deposition can be summarised by Figure 1.12[23]. The following curves show that 65-70% of deposited particles of 3 μm diameter will be deposited in the nose, 25-30% in the pulmonary spaces, and 5-10% on the airways (i.e. esophagus). However, it must be noted that the deposition curves depend on the breathing rate[24].

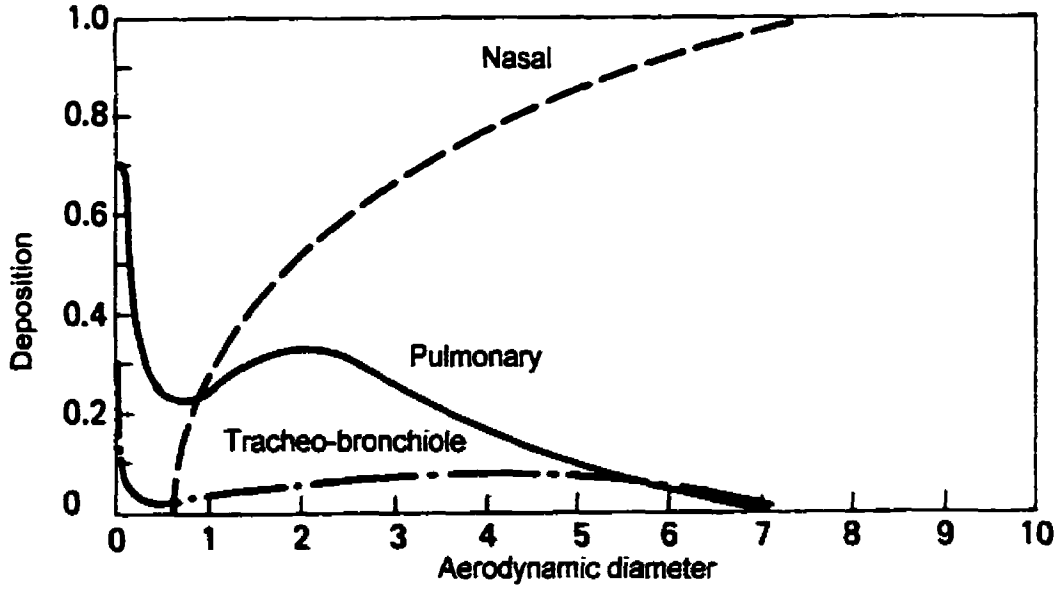

Figure 1.12: Deposition as a function of particle size for 15 respirations/min. (1450 cm^3 tidal volume

1.3.3.1 Health Effects Resulting From Particle Inhalation of Metal Bearing Particulate Matter

Metallurgical industries generate great quantities of metal bearing particulate matter that could conceivably result in adverse health effects to employees or nearby residents. The following is a partial list of common health effects resulting from the exposure to industrial particulate matter:

Pneumoconicoses: Pneumoconicoses, meaning "dusty lung", forms a group of lung related diseases resulting from the inhalation of "respirable" dust. The most serious cases of lung diseases result from the inhalation of fibres such as silica and and asbestos. However other forms of pneumoconiosis may be produced from the inhalation of excessive amounts of the following dust: beryllium (berylliosis); kaolin (kaolinosis); barium (barytosis; tin (stannaosis); talc, graphite, mica; and of special interest to the steelmaking industry, iron oxide (siderosis).

Systemic poisoning: The respiratory system provides a prevailing entry for fine particles into the body. Once inside the body they can dissolve and enter into the blood circulation and internal organs. Manganese, lead, cadmium and their compounds are examples of toxic substances that can be found in particulate form.

Cancer: An accumulation of particulate matter in the lungs can lead to cancer. Examples of particulate matter that cause cancer of the lungs after inhalation are arsenic and its compounds, chromates, particles containing polycyclic aromatic hydrocarbons, and certain nickel bearing dusts.

Irritation and inflammatory lung injuries: Although the major irritants to the respiratory system are gases, particulate matter irritants can also occur. Exposure to such irritants could induce tracheittis, bronchitis, pneumonitis and pulmonary oedema. Examples of airborne particle irritants include: cadmium fumes, beryllium, zinc chloride, chromium compounds and manganese.

Allergic responses: Deposition and retention of inhaled sensitising substances may cause allergic or other sensitivity reaction. Occupational asthma is a particular respiratory disease of allergic type caused by exposure to particulate matter. Certain metal dusts such as nickel and chromium can lead to the onset of occupational asthma.

Metal fume fever: Metal fume fever results from the exposure to fresh metal fumes such as zinc and magnesium oxides. The main symptoms include chills, fever, muscle pain, weakness and nausea.

1.4 An Update on Electric Arc Furnace Dust Treatment

EAF dust can be processed through numerous techniques. These techniques can be grouped into four main categories: (1) high temperature metals recovery (HTMR), (2) recycling, (3) stabilisation/solidification, and (4) other.

1.4.1 High Temperature Metals Recovery (HTMR)

A number of operations employ high temperature process to treat EAF dust. The EAF dust is processed in a furnace or reactor with a reductant such as coal or coke to recover the zinc, lead and cadmium in a metal or oxide state. A by-product of HTMR is an iron rich slag, which can sometimes be tapped from the furnace and recovered. High temperature processes allow for the recovery of metals such as zinc and lead in addition to producing a non-hazardous slag that can be easily disposed. The recovery of the metals defrays the cost of implementing a HTMR system.

1.4.2 Direct Recycling

Zinc content in electric arc furnace dust can vary from 5 to in excess of 40%. As a result, it is sometimes economically prudent to increase the zinc content in dust such that the final costs of recycling will be reduced due to the increased zinc concentration in the dust and the reduced volumes shipped off-site. Thus, zinc dust is introduced into the electric arc furnace along with the metal scrap during scrap melting. The reduced volume is achieved once the dust has attained the required zinc levels by various approaches such as briquetting, pelletizing, and pneumatic injection. However, it is important to note that direct recycling does not eliminate the need for further EAF dust processing, rather it makes it more attractive due to the high zinc content, while reducing the volume that has to be treated

1.4.3 Stabilisation/Solidification

Solidification and stabilisation techniques involve the addition of additives or reagents with the EAF dust in order to physically or chemically reduce the mobility of the

contaminants. Stabilisation employs a chemical modification of the dust, thus making the contaminants less soluble, mobile or toxic. However, stabilisation need not alter the physical nature of the dust. Solidification, on the other hand, changes the physical characteristics of the dust, resulting in an altered solid structure that mechanically traps the contaminants. In order for the new material to be delisted as hazardous material, it must demonstrate to appropriate environmental authorities that the waste is adequately stabilised. Delisting the hazardous waste can result in economic benefits as transportation costs for simple solid waste is lower than that of hazardous waste. In addition, the treated dust must first pass environmental regulations regarding the possible leaching of toxic material before it can be landfilled.

1.4.4 Other Types of Processes

Due to the zinc content in the dust, EAF dust in readily used in the fertiliser industry. The zinc acts a catalyst for organic reactions required in the production of fertiliser. In addition, EAF dust can be used in hydrometallurgical processes to extract the valuable zinc, through complex leaching procedures; in the production of mineral wool; in the production of ceramic products; and in the manufacture of glass beads. Thereafter; mineral wool, ceramic product and glass beads are not regulated as hazardous waste.

1.4.5 Commercially Practiced EAF Dust Management Methods

The methods employed to manage EAF dust can be grouped under the following categories: pyrometallurgical, hydrometallurgical, hybrid pyro-hydro treatment processes and stabilisation or vitrification processes. Ten methods for managing carbon steel scrap are now practiced commercially and are summarised in Table 1.5[25]. These commercially practised methods are summarised below.

Two-Stage Waelz Kiln: The two-stage Waelz kiln operation is the first HTMR process to be commercially viable in the U.S. In this method, EAF dust is fed to the first kiln in order to separate the zinc, cadmium, lead, and chloride from the non-hazardous, partially metallised iron product. Dust from the first kiln is then retreated in the second kiln to produce an impure zinc oxide used for zinc smelter feed and a lead-cadmium chloride, which requires further processing in order to separate the lead and cadmium. This method treats 80 to 85% of the dust produced by carbon steelmakers.

Single Stage Waelz Kiln: The single-stage waelz kiln process is particularly practised in Europe and Japan. It is identical to the first stage of the Two-Stage Waelz kiln process. The halide bearing lead-containing zinc oxide is an intermediary product for treatment in the Imperial Smelting Process to produce lead and zinc metal or for conversion to zinc-based chemicals and fertiliser additives.

Waelz kiln technology is a major player in the processing of EAF dust and will probably remain the industry standard until emerging technologies will prove themselves economically and technologically competitive. Fees for Waelz kiln processing may however have to be reduced as new technologies emerge.

Flame Reactor: This method requires a fine, dry EAF dust feed and oxygen to react with coke or coal reductant in a cyclone reactor. The product is a dirty zinc oxide that contains all the cadmium, halides and lead present in the dust, and is only suitable as feed to a primary zinc smelting facility which can handle halides. The present process does not have the capability of producing zinc metal since carbon supplies the energy required for reaction. The iron-rich slag produced conforms with EPA disposal requirements.

MF and Electrothermic Processes: The MF and Electrothermic processes are in use in a limited scale in Japan. They are adaptations of primary zinc processes and are practised in facilities previously used for primary smelting, using modified equipment. These processes produce and intermediary lead-containing zinc oxide for further processing.

ZTT Ferrolime Process: Raw EAF dust is treated in a rotary kiln with coke and coal as a reductant for the zinc oxide present in the dust. The fumed zinc oxide, containing lead, cadmium, and halides, is collected following the afterburner and washed in order to remove the halides. The product is an upgraded zinc oxide for sale to primary zinc smelters and a mixed salt for sale as a drilling fluid additive. The partially metallized iron-bearing product, called Ferrolime can be returned to EAF steel plants for recycle; if it meets specifications.

Laclede Steel Process: The simple process directly feeds an EAF dust and a reductant into an electric furnace. The oxide reduction reactions are effected and the resulting zinc/lead/cadmium vapour is condensed to zinc metal in a zinc splash condenser

preceded by several gas handling steps. The iron-rich slag is appropriate for disposal. However, the quality of the resulting zinc metal is deemed to be quite poor, rendering unsatisfactory for internal galvanising use.

Table 1.5: Summary of EAF dust management methods

Status	Process	Type	Zn-bearing product	Fe-bearing product	Other products
Commercial	Waelz Kiln (2 stage)	Pyro	ZnO	Iron oxide/metallized iron	$PbCl_2/CdCl_2$ fume
	Waelz Kiln (1 stage)	Pyro	ZnO	Iron oxide/metallized iron	-
	Flame Reactor	Pyro	ZnO	Slag	-
	ZTT Ferrolime	Pyro	ZnO	Ferrolime	Salt mixture
	MF/Electrothermic	Pyro	ZnO	Slag/residue	Salt mixture
	MRT	Hydro/Pyro	High purity ZnO	Iron oxide/metallized iron	Pb/Cd metals
	Laclede Steel	Pyro	Zn metal	Slag	Pb/Cd metals
	EZINEX	Hydro	Zn metal	Iron oxide	Salt mixture
	Super Detox	Stabilization	-	-	Stabilized dust
	IRC	Vitrification	-	-	Glassy granules
Emerging	Ausmelt	Pyro	ZnO	Slag	-
	MetWool	Pyro	ZnO	Pig iron	Mineral wool
	Enviroplas	Pyro	Zn metal or ZnO	Slag	-
	All Met	Pyro	Zn metal	Fe/Fe_3C	Salt mixture
	IBDR-ZIPP	Pyro/Hydro	ZnO	Pig iron	Salt mixture
	ZINCEX	Hydro	Zn metal	Residue	Pb/Cd cement
	Rezada	Hydro	Zn metal	Iron oxide	Salt mixture. Pb/Cd cement
	Cashman	Hydro	High purity ZnO	Iron oxide/metallized iron	Salt mixture. Pb/Cd cement
	Terra Gaia	Hydro	ZnS	Iron oxide	$PbCl_2$, Pb/Cd cement

MRT Process: The MRT Process is the first hydrometallurgical process to be commercially viable in North America for the treatment of EAF dust[26]. Dust is leached with hot ammonium chloride to dissolve most of the zinc, lead and cadmium oxides present in the raw dust. The leach slurry is then filtered to separate the unleachable iron oxide. The leach solution is then treated with zinc dust to precipitate the dissolved lead and cadmium as cement, which is further separated into metallic lead and metallic cadmium for sale. The clean solution passes to a crystalliser where

high purity zinc oxide crystals are produced. The ammonium chloride solution is recycled as the leachant.

EZINEX Process: This hydrometallurgical treatment was developed in Italy by Engitec Impianti[27]. In this process, dust is leached in an ammonium chloride solution to solubilise the zinc, cadmium and lead oxides. The leach solution is filtered and treated with zinc dust in order to cement the lead and cadmium and subsequently electrowon to produce hot-dip grade zinc for galvanising or zinc metal for sale. The spent electrolyte is recycled to leaching. The iron–rich, zinc-ferrite-containing leach residue is dried, pelletised with coal, and recycled to the EAF. This process offers the advantage of producing no by-products that require subsequent disposal. A mixed NaCl-KCl salt is recovered through crystallisation and sold as a flux.

Super Detox Process: The Super Detox process was the first stabilisation method to receive approval by the EPA. As a result, the stabilised product could then be disposed in non-hazardous landfills. Super Detox involves mixing the dust with alumino-silicates, lime and other additives. The heavy metals are chemically altered to their least soluble states through precipitation and oxidation/reduction followed by being physically bound in the alumino-silicate matrix. The material will solidify to become a concrete-like substance and is fairly impermeable.

IRC Process: This process mixes EAF dust with additives and melts the resulting material in a specially designed furnace. The molten, vitrified product from the furnace is converted into a granular product for sale. The zinc, lead, cadmium, and iron are not removed and recovered for re-use or recycling.

EAF dust is a complex by-product of the industrial process of steelmaking. There are many remediation techniques used to try and minimise the environmental impact of this toxic product. From this review, it is apparent that there are a significant amount of techniques used to try and re-use the dust in subsequent steelmaking operations, however, there are very few commercial applications in place. As such, steel manufacturers are increasingly looking into methods which would reduce the toxic metal impact of the dust through new methods of toxic metal stabilisation.

2 PURPOSE AND OBJECTIVES

2.1 Purpose

The proposed research will aim at understanding the behaviour of stainless steel dust with the objective of developing optimal conditions for the thermal treatment and destruction of hazardous dust and the neutralization of toxic metals. Thus, the mass and volume in addition to the environmental impact of this dust can be reduced. Consequently, the cost of transportation will be considerably reduced due to the reduction of the dust volume and mass. In addition, thermally treated dust could be de-classified as a hazardous material and possibly re-used as a co-product in the construction industry. The thermal treatment technology will be based on the application of the multi-zone temperature concept to dispose of the hazardous waste. In this method, waste is initially fed into a low-temperature region (<1000°C), then subjected to a high temperature treatment (1600°C) which is followed by another low-temperature zone (<<1000°C). The experiments simulating the events were conducted in a high-temperature furnace at McGill University.

2.2 Research Objectives

1. **Establish optimum conditions for the clean and efficient thermal treatment of stainless steel dust.** The method based on the application of the multi-zone temperature regions (low-high-low) within the high temperature furnace will aim at establishing the optimum operating conditions to ensure the following: (1) minimisation of dust volume; (2) maximisation of weight loss, and (3) neutralisation of toxic metals in the final product. As a result, the hazardous characteristics of the dust will be minimised and environmental risks reduced. The solid products resulting from this process will not be classified as hazardous and could be considered for re-use as particulate filler in construction materials such as concrete, and asphalt, thereby considerably reducing the dust's environmental impact.
2. **Solve the dust management problem** by reducing dust volume thus reducing transportation costs.

3. **Generate solid particles capable of neutralising toxic metals** during the thermal treatment of stainless steel dust. Thus, the potential environmental impact of dust disposal will be reduced; or even eliminated.

4. **Explain the influence of process parameters** (i.e. temperature profiles, heating rate, residence time) on dust behaviour and properties. This will allow for a better understanding of the fate of toxic metals and metal-solid interactions in high temperature dust remediation processes.

3 EXPERIMENTAL FACILITY AND ANALYTICAL INSTRUMENTS

3.1 Thermal Treatment Facility

The principal instrumentation used in this research to thermally treat the EAF dust was a combination of a Thermo-Gravimetric Analyzer (TGA) coupled to a Fourier Transform Infra-Red Spectrometer (FTIR). These two instruments are connected by a gas-sampling accessory and allow for simultaneous heating and resulting gas evolution. The procurement of data from these two units is controlled by a Data Acquisition System (DAS). A schematic of the system can be seen in Figure 3.1.

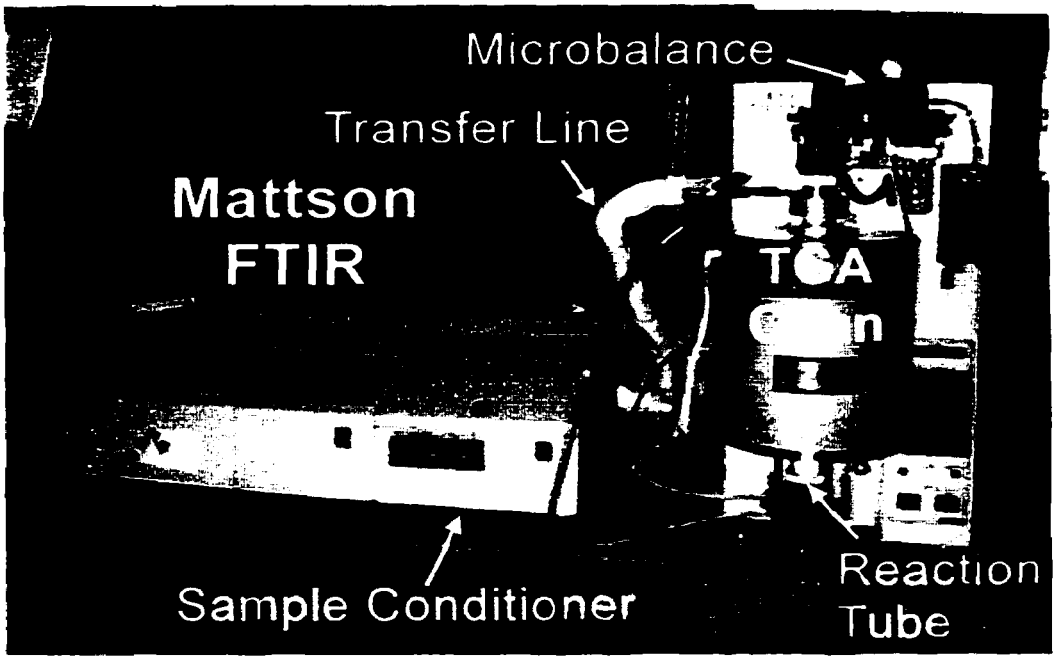

Figure 3.1: TGA FTIR System

3.1.1 Thermo-Gravimetric Analyzer (TGA)

Thermo-Gravimetric Analysis (TGA) is well established as an analytical tool. In this technique, a sample is heated in a controlled manner under a selected purge gas flow while its weight is monitored. The TGA profile is a valuable analysis tool to determine over what temperatures the weight loss occurred. In addition, the TGA can simulate the

temperature history, the residence time and environment of more industrial thermal treatment methods.

The TGA model used in this research is a Cahn TG-171. The main components of this unit are a recording microbalance, an alumina reactor, and a movable gravimetric furnace. The maximum temperature of the furnace is 1700°C, with a pressure limit of 1.0 atm. The heating rate can vary from 1.0 to 100°C/min. The microbalance sensitivity is 1μg with a limit of 100 grams and a 10 gram dynamic weight range[28].

The material to be tested is placed in an alumina crucible and is suspended by a platinum wire from the microbalance, which monitors the weight change during the experiments. The container is smooth and non-porous and cylindrical in nature. It has an inner diameter of 2 cm. The sample is heated within the container and the resulting temperature is measured by a thermocouple, which placed directly below the container.

The reactor chamber consists of a cylindrical chamber encircled by heating elements as shown in Figure 3.2. Reaction gases pass through the chamber from the

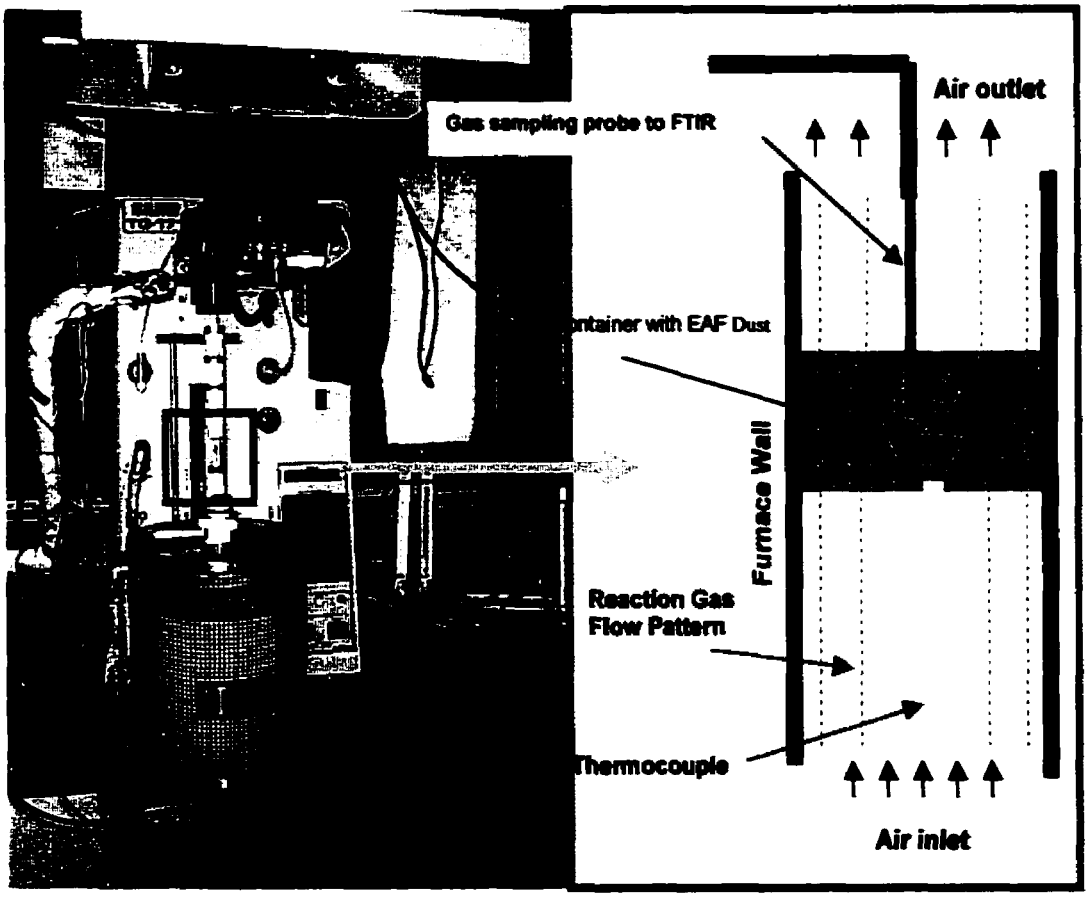

Figure 3.2: TGA reaction chamber

bottom in a portion of the chamber where the temperature is uniform. This area is referred to as the Uniform Temperature Zone or (UTZ). In order to achieve adequate experimental conditions, samples must be placed within the UTZ since in this zone, it is assumed that sample is at the same temperature as the furnace.

3.1.2 Off-Gas Sampling Accessories

The off-gases that are produced in the TGA through thermal treatment are thereafter analyzed by the FTIR. In order to connect the TGA to the external FTIR unit, gas-sampling accessories are requisite. These accessories consist of: (1) an 1/16" incanel sampling tube for low temperature analysis (<1000°C) and a 1/16" quartz tube for high temperature analysis (>1000°C); (2) a parastaltic pump which consists of a Masterflex 7543-30 pump drive coupled to a Masterflex L/S Quick load pump head operating at ~0.85 atm. and; (3) a 1/8" OD stainless steel glass-lined transfer line tube. The tip of the sampling probe sits just above the sample container as to capture a greater amount of emissions without significant purge gas dilution. The sampling tube fits into a 1/8" incanel tube, which is incorporated into a ring heated to 200°C and wrapped in K-Wool insulation as to prevent the off-gases in the tube from condensing. Thereafter, the off-gases pass through the transfer-line, which is heated to 250°C, as to once again minimize condensation of off-gases produced. The transfer-line connects the TGA to the FTIR. The off-gas flow into the FTIR is aided by the pump, which allows for an approximate flow of 60 ml./min.

3.1.3 Fourier Transform Infra-Red Spectrometer (FTIR)

The FTIR used in this research is a Mattson Galaxy 5020 Fourier Transform Infra-Red Spectrometer. FTIRs are particularly useful when high-resolution work is needed which is encountered with gaseous mixture analysis[29]. In addition, FTIR spectroscopy can collect infra-red data from very small samples. The FTIR used in this research is equipped with a liquid nitrogen-cooled Mercury Cadmium Telluride (MCT) detector, a 15 ml. gas cell and a KBr beamsplitter. The gas sampling interface can be seen in Figure 3.3. The off-gas is pumped into the sampling cell from the transfer line. The IR beam, which is generated within the instrument, is reflected off a mirror into the cell. After passing through the cell, the beam is reflected off another beam so that it can pass

through the MCT detector. The gas phase functional group composition is determined using FTIR software which contains the National Institute of Standards & Technology/Environmental Protection Agency (NIST/EPA) vapor phase library. The resolution of the FTIR was 2 $cm.^{-1}$, the scan time was set at 10 sec./spectrum, and the pump flow rate was set at 60 ml./min.

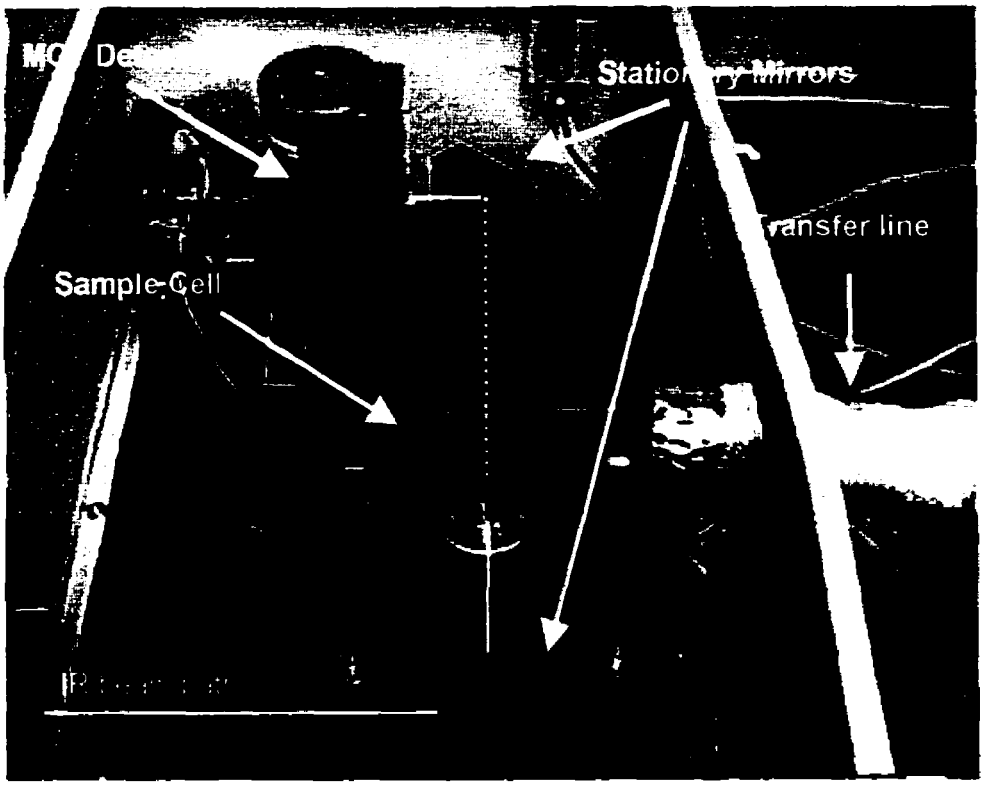

Figure 3.3: FTIR external gas sampling interface

3.1.4 TGA-FTIR System

The TGA-FTIR is an important analytical tool as it can simulate heating profiles of larger industrial processes while maintaining significant laboratory accuracy. The kinetics in industrial thermal treatment processes are mostly too fast to suitably analyze mechanisms that are occurring. However, with the TGA-FTIR system, the process can be slowed down, in order to accurately investigate mechanisms and stages in the process. This system can continuously measure temperature, weight changes and corresponding gas-evolution occurring during thermal treatment. A block diagram of the system is

shown in Figure 3.4[30]. It describes the complex interactions between the various components of the system.

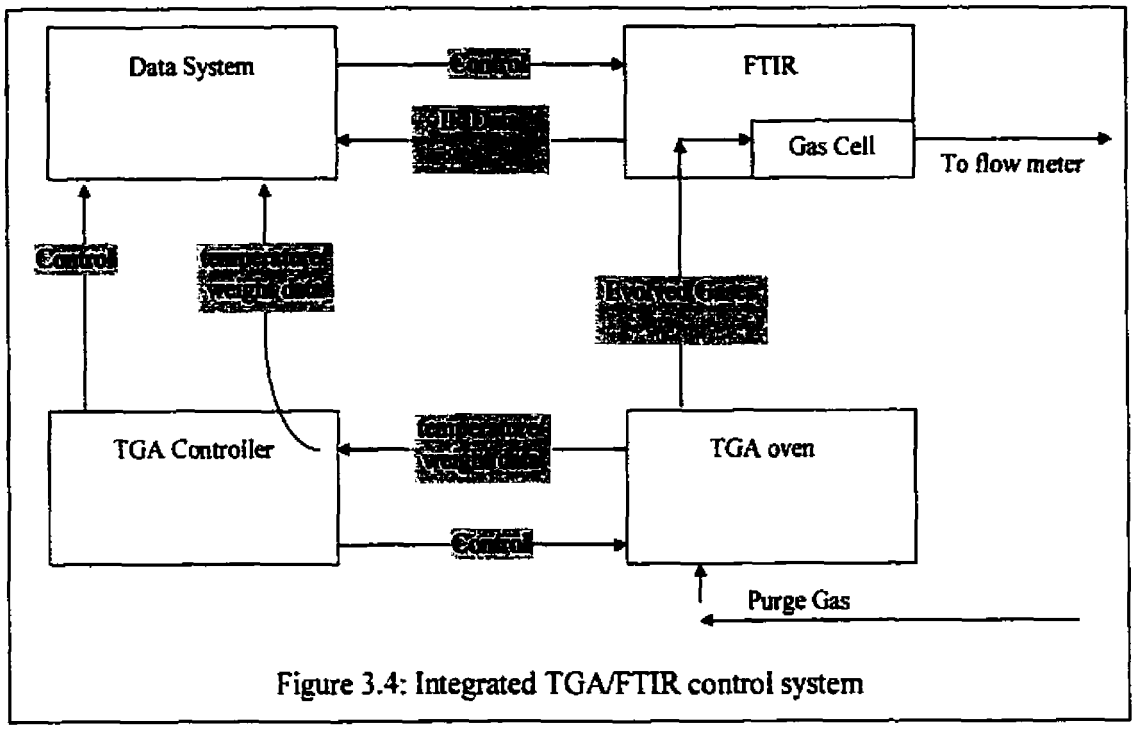

Figure 3.4: Integrated TGA/FTIR control system

3.1.5 System Limitations

The nature of the instrument resulted in the occurrence of a number of limitations during the research. Heating rates cannot be consistent throughout the temperature evolution profile. Table 3.1 displays the maximum heating rates which can be applied at different stages within the temperature evolution profile.

Table 3.1: Maximum TGA heating rate profiles

Temperature Range (°C)	Maximum Heating Rate (°C/min.)
Room Temperature-990	100
991-1290	30
1291-1390	20
1391-1700	10

Heating rates within the TGA cannot attain those used in industrial processes, which can attain thousands of degrees per minute, however during thermal treatment, one must not simply consider heating rate, but rather rate of heat input per unit of mass.

Industrial processes have high heating rates, however, the quantity of mass to be treated is also significant. The TGA's heating rates are significantly lower, however, so is the sample mass to be treated, thus providing a base of reference to industrial processes.

Another limitation with this instrument is the fact that the TGA reactor is not under vacuum. During certain pyrolysis experiments where nitrogen is the reaction gas, air infiltration can possibly occur since the reaction chamber is not under vacuum. However, the alumina reaction tube is well-sealed, with rubber o-rings and stainless steel threaded rings which attach themselves to the upper and lower baffles of the instrument. In order to minimise the effects of air, the chamber must be purged with nitrogen gas for a period of time prior to experimentation. In addition, the nitrogen gas must flow into the reaction chamber at a sufficient rate to minimise the effects of any air infiltration.

When analysing the results of FTIR analysis, one must consider the limitations of the system due to the transfer line. The transfer line can only be heated up to a temperature of 250°C due to limitations of material properties within the line. As a result, some gases will condense before reaching the sampling cell. This is the case for most metal species that are present in the gaseous phase. This signifies that the FTIR data probably omits information on gaseous products which would condense at temperatures greater than 250°C.

3.2 *Analytical Instruments*

The EAF dust samples collected during thermal treatment were subject to many tests. Particle size analysis was done through sieving; elemental analysis of the dust was performed using X-ray fluorescence (XRF); phase composition was achieved through X-ray diffraction (XRD); elemental metal distribution within the dust was accomplished through electron probe micro-analysis (EPMA); a scanning electron microscope (SEM) was used to look at particle morphology; an energy dispersive X-ray spectrometer (EDS) to examine elemental composition within the particles; and leachability tests were performed on the thermally treated samples and analysed through atomic absorption spectroscopy (AAS).

3.2.1 Sieve Analysis

Tyler Canadian Standard Sieve Series screens were used in order to dry-screen the EAF dust samples and separate them into size classes. The screen sizes, which are identified by their grid opening, started at a size of 1.70 mm. and went down to a size of 38 μm. Thirteen screen were used following a descending geometric sequence of $\sqrt{2}$. The largest size class, which did not pass through the initial 1.70 mm screen was labelled +1.70 mm, while the smallest size class which passed through the 38 μm screen and into a pan was labelled –38 μm.

3.2.2 X-Ray Fluorescence (XRF)

A Philips PW2400 X-ray spectrometer was used to perform elemental analysis of the EAF dust. In this method, the material, excited by the absorption of a beam from X-rays from an X-ray tube or a radioactive source, emits its own fluorescent X-rays. Each element emits a fluorescent wave that is amplified and counted. XRF is one of the most widely used of all analytical techniques for the qualitative and quantitative analysis of elements having atomic numbers greater than oxygen (> 8)[31].

3.2.3 X-Ray Diffraction (XRD)

The crystalline phases present in the dust were determined using an X-ray powder diffraction method. This is the only analytical method capable of providing qualitative information about compounds present in a solid. X-ray powder methods are based on the fact that an X-ray diffraction pattern is unique for each crystalline substance. Thus, if an exact match can be found between the pattern of an unknown and an authentic sample, chemical identity can be assumed. The instrumentation used in this research was a Rigaku Rotoflex goniometer. X-rays were provided through the CuK_{α} radiation of a copper tube. The voltage was set to 50 kV and the current was at 150 mA. XRD can determine material structures as well as a practical means for the qualitative identification of crystalline compounds.

3.2.4 Scanning Electron Microscope (SEM)

The thermally treated dust particles were analysed for morphology through a Jeol 840 SEM using an accelerating voltage of 10 kV. The particles first underwent gold

sputtering in order to prevent charging. Through the SEM, one could follow the evolution of particle morphology occurring through thermal treatment. The particles' surface could be well-analysed due to the high magnification of the instrument (700X). In addition, a qualitative analysis of the elements present on the particles' surface was performed though a Tracor Northern 820 energy dispersive X-ray spectrometer (EDS), which operated at a probe voltage of 10 keV.

3.2.5 Electron Probe Micro-Analysis (EPMA)

Metal distribution within the particles was performed using a Jeol Superprobe 8900 EPMA coupled with five wavelength-dispersive spectrometers (WDS) and a Tracor Northern 5520 EDS. With the electron microprobe method, X-ray emission is stimulated on the surface of the sample by a narrow, focused beam of electrons. The resulting X-ray emission is detected and analysed with though both EDS or WDS[32].

3.2.6 Atomic Absorption Spectroscopy (AAS)

Bulk metal concentrations in the leachates of thermally treated dust are analysed through a Perkin-Elmer 3110 flame atomic absorption spectrometer. AAS is a sensitive means for the quantitative determination of more than 60 metals or metalloid elements. Detection limits for Cd, Cr, Cu, Ni, Pb and Zn are 1, 3, 2, 5, 10 and 2 ng/ml respectively[33].

4 EAF DUST CHARACTERISTICS AND FORMATION

4.1 Introduction

A stainless steel mini-mill that produces over 2,000 ton/yr. of EAF dust provided EAF dust samples used in this research. Dust samples were collected from an existing 20,000 ton on-site accumulation. Stainless steel EAF dusts differ from other carbon steel dusts in their high levels of chromium in addition to other alloying elements such as zinc, lead and cadmium.

Investigations of EAF dust are sparse thus this chapter will focus on determining the physical characteristics (i.e. morphology, particle size distribution) and chemical characteristics (i.e. elemental composition, phase composition, metal distribution and metal leachability) of the particular EAF dust through a number of analytical techniques.

4.2 Physical Characteristics

4.2.1 Size Distribution

Sieve analysis was performed on the four dust samples received. Figure 4.1 represents an average particle size distribution of these four samples. It was determined that the largest size class contained particles larger than 1700 μm. However, this size class was discarded as it was not representative of dust particles, but rather of stone fragments and other entrained particles that collected with the dust during storage or handling. From Figure 4.1, it is apparent that the mass seems to be relatively equally distributed between the size classes. The bars present on the chart represent ±1 standard deviation from the mean. In general, particle size distributions are not well determined due to uncertainties in techniques, however, Stephen *et al*[34] indicated that most dust particles are in the range of 0.1-5 μm in diameter. This would indicate that the size class distribution performed on this particular EAF dust does not represent individual particles, but rather agglomerations of fine micron and sub-micron size particles. This hypothesis will be confirmed in the following section.

The EAF samples received were poured into the upper-most screen (1700 μm) and placed in a Rotap rotameter for 30 minutes. Thereafter, the largest size class was discarded (> 1700 μm) and the rest of the size classes were separated and weighed. For

this section of the research, four different dust samples received from the company were used: EAFD1, EAFD2, EAFD3, and EAFD4. This was to get a proper representation of the size distribution of the dust we were dealing with. *However, it should be noted that all further analysis and experimentation in this research uses EAFD2 as the experimental material.* This was necessary in order to keep the dust elemental composition consistent throughout the research.

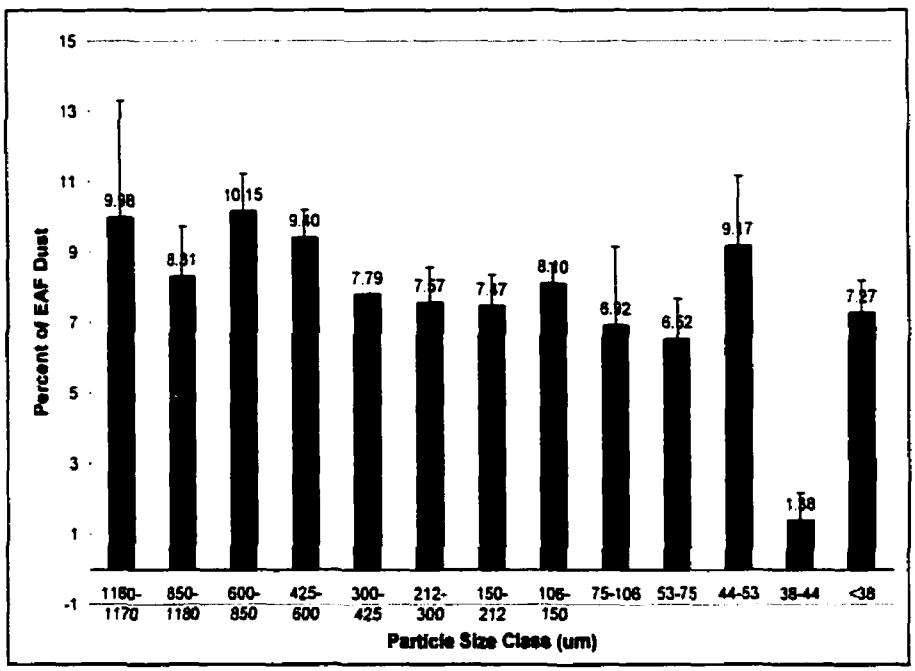

Figure 4.1: Mass percent of different size classes with respect to EAF dust samples.

4.2.2 Particle Morphology

Figure 4.2 displays SEM photos of the EAF dust. As seen from SEM images, the particles are spherical in nature and range in size from 1 to 800 μm. The dust is present as agglomerates as well as particles of sub-micron size. The agglomerations represent both homogeneously nucleated particles and entrained fugitive particles that have experienced heterogeneous condensation. The particles seem to have a fibrous appearance at the surface. This is caused by the adhesion of fine dust and fume particles that have agglomerated onto the surface of the larger particles thus providing a fibrous appearance. Due to the small nature of these particles, they were most likely produced through homogeneous nucleation. This phenomenon can be better viewed in Figure 4.2b, which is

a magnification of the surface of Figure 4.2a. The individual sub-micron and micron particles which form the larger agglomerates are clearly seen.

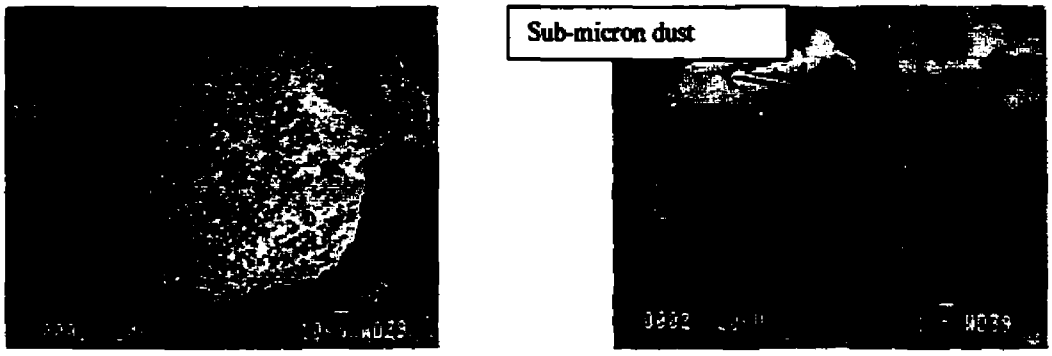

Figure 4.2 - SEM micrographs of (a) EAF dust particle; (b) particle surface

From EDS analysis, it was possible to obtain a qualitative elemental analysis of the dust particles. Particles analyzed through EDS were 100 μm or smaller in diameter since these were ideal for SEM examination. Iron peaks were quite prevalent in the EDS scans. They were followed by significant chromium peaks, which is to be expected this these two elements are the principal constituents of the dust. Aside from the initial two, smaller copper, nickel, lead, and zinc peaks were noticed on the scans. Some particles contained large calcium and silicon peaks. These particles were most probably representative of entrained refractory pieces, whose major constituents are silica and lime. Manganese was present in every particle, which is indicative of its level within the dust. Besides the major components, small aluminum, potassium, sulphur, and titanium peaks were identified in the EDS scans. In addition to these, chlorine peaks were also identified. Chlorine is a hindrance since it can act to increase metal vaporization in the melt. For example, the vaporization temperatures of nickel and lead chlorides are drastically reduced over their oxide counterparts[35]. However, this is not the case for cadmium, which does not readily form chloride species[36].

4.3 Chemical Characteristics

4.3.1 Elemental Analysis

Chemical analysis performed on the EAF dust through XRF (Table 4.1) indicated that the primary composition of the dust is for the most part Fe (34 wt%) and Cr (9.6

wt%) and to a lesser extent Si, Ca, Cu, Mn, Ni, Na, Zn and Mg. The four samples represented specimens collected from the same source but at different time periods. Composition of the dust can vary depending on the type of scrap that is used to feed the EAF. Stainless steel dusts contain greater levels of Cr, Ni, Mn, since these are main alloying elements in the stainless steel scrap in the melt. The presence of Zn and Pb principally arise from coated steel products that form the scrap metal input into the furnace. Stephen *et al.*[34] reported that in the USA, stainless steel dust is composed of 22-36% Fe, 1.8-6.2% Zn, 2.4-4.6% Mn and less than 1% each of Cr and Ni. In addition this dust contains less than 10% each of Ca, Mg, Si, K and Na. The EAF dust analyzed in this paper differs from the American values due to the extremely high levels of Cr present in the dust. In addition, the level of Ni is also slightly superior to US values whereas the level of Zn is lower.

Table 4.1: Elemental Analysis of EAF Dust

Element	Detection Limit (ppm)	EAFD1 (wt%)	EAFD2 (wt%)	EAFD3 (wt%)	EAFD4 (wt%)	EAFD Avg. (wt%)
Al	64	2.39	0.31	0.21	0.32	0.81
Ca	11	10.60	4.03	0.29	0.50	3.85
Cu	3	0.24	0.16	0.26	0.10	0.19
Cr	10	5.99	10.93	10.88	10.61	9.60
Fe	21	25.17	37.96	35.80	36.65	33.86
K	21	0.29	0.36	0.58	0.60	0.46
Mg	57	1.51	1.53	2.15	1.21	1.60
Mn	23	2.07	3.32	4.73	3.06	3.30
Na	56	2.04	1.18	3.34	0.45	1.75
Ni	3	1.71	3.77	2.67	3.89	3.01
P	15	0.02	0.03	0.27	0.13	0.11
Pb	3	0.11	0.07	0.52	0.28	0.24
Si	28	9.31	2.29	2.20	2.40	4.05
Ti	21	0.58	0.17	0.04	0.07	0.21
Zn	2	0.87	1.20	3.86	0.77	1.67
Cd (ppm)	10	37.50	107.50	43.75	350.00	134.69

4.3.2 Phase Composition

A typical XRD pattern for the EAF dust is shown in Figure 4.3. The main phases detected in the dust were mainly metal oxides. The greatest peaks within the diffraction patterns contained chromium and iron in the oxide form. This is to be expected since iron

and chromium are the two major constituents of this particular EAF dust. The iron components represented the majority of the diffraction peaks. Most iron was found to be in the oxidised state, as either Fe_2O_3 or Fe_3O_4. Chromium was mostly present as Cr_2O_3, which is a very stable and insoluble compound. In addition, it was also present as $FeCr_2O_4$. Nickel was primarily grouped with manganese to form complex compounds such as $NiMn_2O_4$ and $MnNi_2O_4$; in addition it was present in the simple oxide form as NiO. Copper is found in complex oxide forms along with iron and manganese principally as $CuMn_2O_4$, $CuFe_2O_4$ and $CuFeMnO_4$. Zinc was primarily found coupled with chromium to form $ZnCr_2O_4$. XRD patterns were measured on the different particle size classes to determine the influence of particle size class on phase composition. Samples were chosen from a range of 1.18-1.70 mm. down a size class of less than 38 μm. The resulting diffraction patterns were essentially identical, indicating the relative homogeneity of the distribution of crystal phases in particles with different sizes.

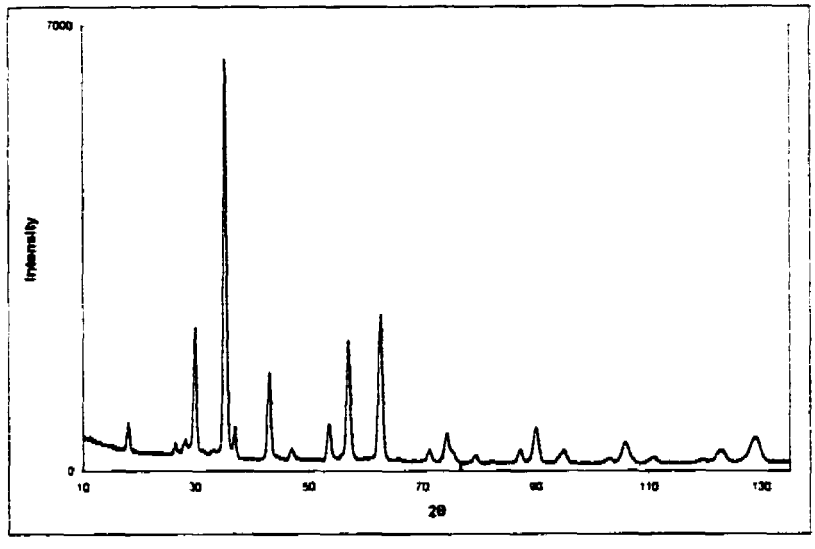

Figure 4.3: X-ray diffraction pattern of EAF dust sample

4.3.3 Metal Distribution

Figure 4.4 presents a surface map of an EAF dust particle greater than 200 μm in diameter produced through EPMA analysis. The concentration of the element is relative to its intensity on the photograph; red being the highest and orange the lowest.

The three photographs represent the three largest components of this particular EAF dust: Fe (Figure 4.4a), Cr (Figure 4.4b) and Si (Figure 4.4c). From these pictures, one can see the agglomerate nature of EAF dust particles. This is particularly true for the Fe and Si, which are not well dispersed throughout the particle. Rather, they are present as agglomerate clumps. The Fe agglomerates result from the entrainment of steel particles into the off-gas due to the agitation of the EAF melt. In the same manner, Si agglomerates in the dust result from the addition of fluxes into the turbulent EAF bath. The chromium appears to be more finely dispersed within the agglomerate particle. The chromium is present in smaller particles that were homogeneously particles nucleated from the gas phase and are eventually agglomerated onto the surface of the larger particle due to electrostatic forces.

The EAF dust sample for EPMA was prepared by placing an amount of dust on a microscope glass sample holder. It was then compacted and coated with a thin epoxy layer. Thereafter, the sample was polished down to one micron and carbon coated. The instrument probed a cross sectional area of 2 mm^2.

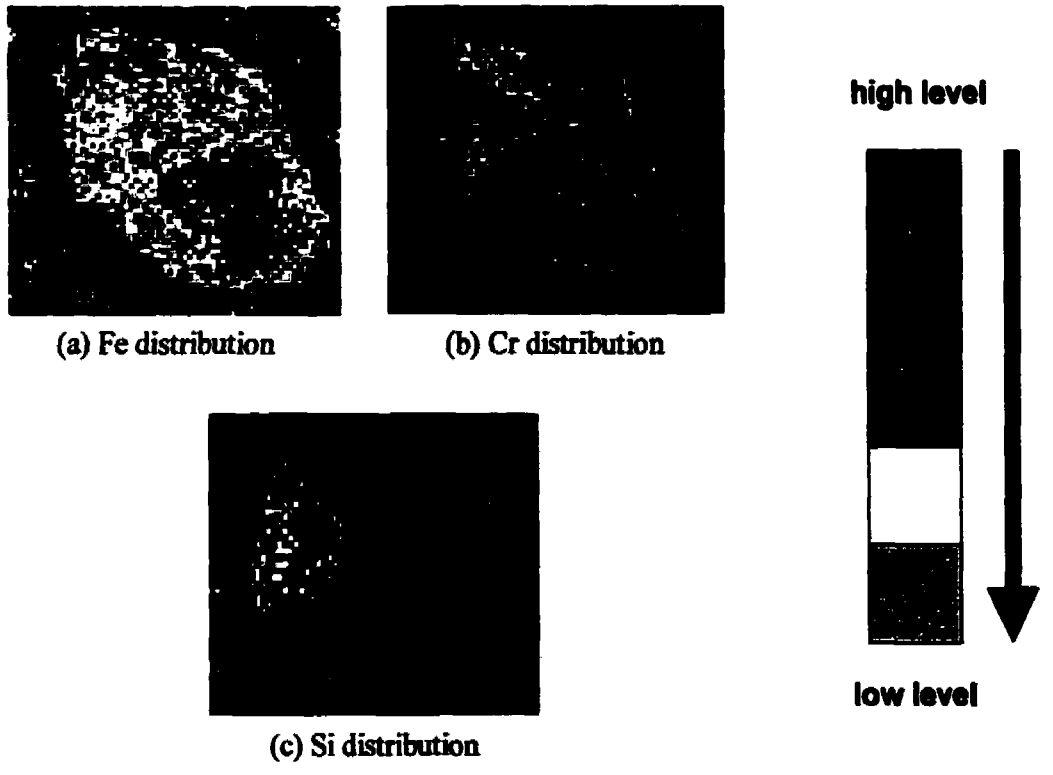

(a) Fe distribution (b) Cr distribution

(c) Si distribution

Figure 4.4: EAF dust metal distribution

4.3.4 EAF Dust Leachability

The leachability of this EAF dust is of utmost concern due to the fact that it can contaminate soils and groundwater supplies. The EAF dust was leached with an acidic leaching solution recommended by the MEF. It consisted of 10:1 liquid to solids ratio and a leaching time of 24 hours. The leachate produced from the overnight test was then filtered and tested using AA spectroscopy. The dust was tested for six toxic metals included in the MEF's Hazardous Waste Regulation: cadmium, chromium, copper, nickel, lead and zinc. Cadmium and chromium are used for corrosion resistance, Ni is usually added to steel for strengthening purposes, Pb and Zn are added as steel coatings. Table 4.2 shows the results of leachability tests performed on the particular EAF dust. The levels of cadmium, copper, nickel, lead and zinc were all under regulatory limits. This was to be expected due to the low levels of these elements present in the dust.

The majority of the Cr in the dust is of a trivalent form. Cr^{3+} is very stable nature and is not considered toxic. However, the chromium leaching out of the dust is of the hexavalent phase[37] since the latter is very unstable and thus soluble. Cr^{6+} is considered to be carcinogenic. The levels of Cr^{6+} within the dust greatly surpass MEF guidelines for maximum allowable Cr limits contained in leachates of solid materials. Elevated Cr^{6+} levels in the blood is considered dangerous.

Table 4.2 - EAF dust leachability

Element	MEF Norm[38] (mg/L)	EAF Dust (mg/L)
Cd	2.0	-
Cr	5.0	270
Ni	10.0	0.50
Pb	5.0	0.14
Zn	10.0	0.27

4.4 Dust Formation Mechanism

In this section, we will examine the possible formation mechanism of the particular dust. The formation of the EAF dust occurs within the melt. Due to agitation in the EAF melt, elevated melt temperatures (~1600°C) and high heating rates, volatile metals will vaporise or react with oxygen, sulphur or chlorine to form species that will vaporise and be present within the gaseous phase as illustrated in Figure 4.5.

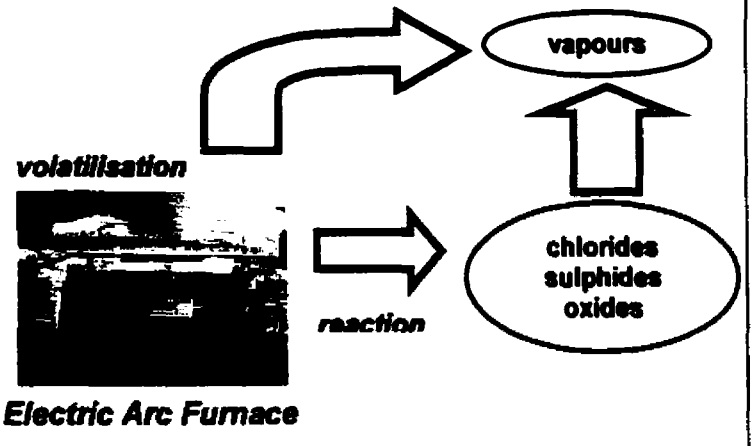

Figure 4.5: Vaporisation of metal species

There are two mechanisms in which the metals species present in the gaseous phase can react to form the EAF dust (Figure 4.6). The first mechanism is that of heterogeneous condensation[39] (Figure 4.6a). In this process, metals will heterogeneously condense onto the surface of small particles that have been entrained into the off-gas stream due to the violent reactions of the melt; such is the case with metal fragments or fugitive dust. Most metal condensation will occur onto surfaces of small particles since they provide the best surface area/volume ratio. Thereafter, these particles will mechanically agglomerate into larger particles that can attain 800 μm in diameter. Stephen *et al.*[34] suggested that surface charge and magnetic properties result in the agglomeration of EAF dust. Chung-Lee *et al.*[40] have suggested that EAF dusts are agglomerated through a $ZnCl_2 \bullet 4Zn(OH)_2 \bullet H_2O$ or $ZnCl_2 \bullet 4Zn(OH)_2$ binding substance which is formed when condensed $ZnCl_2$ reacts with ZnO in the EAF gas cooler. The reactions are as follows:

$$ZnCl_2 + 4ZnO + H_2O \xrightarrow{167\text{-}266^\circ C} ZnCl_2 \bullet 4Zn(OH)_2 \quad (1)$$

$$ZnCl_2 \bullet 4Zn(OH)_2 + H_2O \xrightarrow{110\text{-}147^\circ C} ZnCl_2 \bullet 4Zn(OH)_2 \bullet H_2O \quad (2)$$

The second mechanism of dust formation is that of homogeneous nucleation and particle growth (Figure 4.6b). If not enough surface area is available for condensation, metal species in the gas phase will homogeneously nucleate to form sub-micron nuclei. Thereafter, through collisions or particle adhesion, particle size will increase. In addition, the favourable surface area/volume ratio of the sub-micron nuclei will make them sinks for heterogeneous condensation, thus producing particles in the range of 0.02-1.0 μm. These smaller particles can then mechanically agglomerate onto the surface of larger particles.

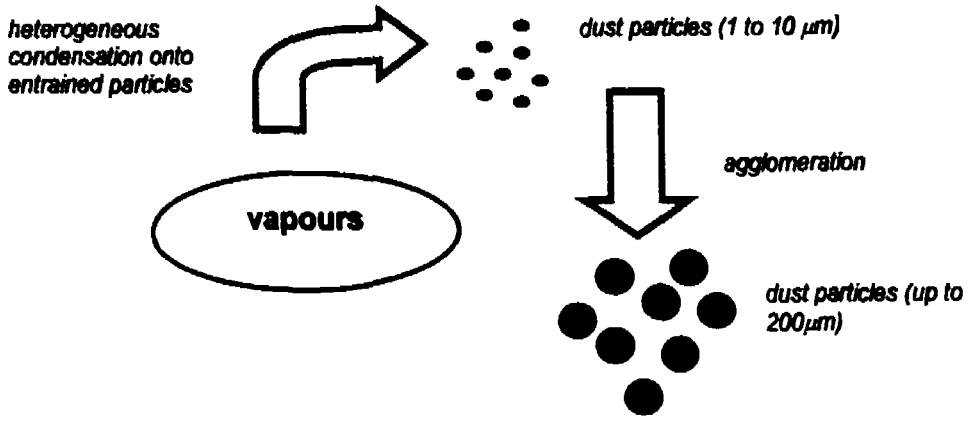

(a) Heterogeneous nucleation

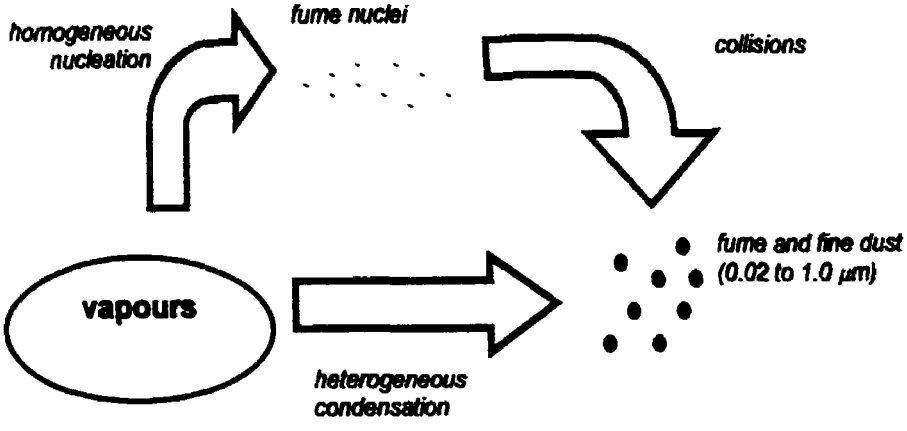

(b) Homogeneous nucleation

Figure 4.6 - Mechanisms of dust formation

5 EXPERIMENTAL METHODOLOGY

5.1 Experimental Designs

Research within the field of waste destruction incorporates many different types of wastes, treatment facilities and operating parameters. In order to obtain the best possible treated product, a researcher must find the best mix of parameters and conditions. However, running experiments according to classical scientific methods (i.e. one variable at a time) requires thoroughness, adequate funding and time. These resources are luxuries that are not always available; especially in industry, where time is of an essence. Major processes require the study of the influence of numerous parameters and as such, are quite laborious in nature. A possible way to reduce the amount of experimentation required is to study multiple parameters at a time. One such method is the Design of Experiments[42] (DOE). DOE is a discipline that applies statistics to the experimental process. It allows researchers to systematically vary a number of independent (input) variables in order to evaluate their effect on dependent output variables or responses.

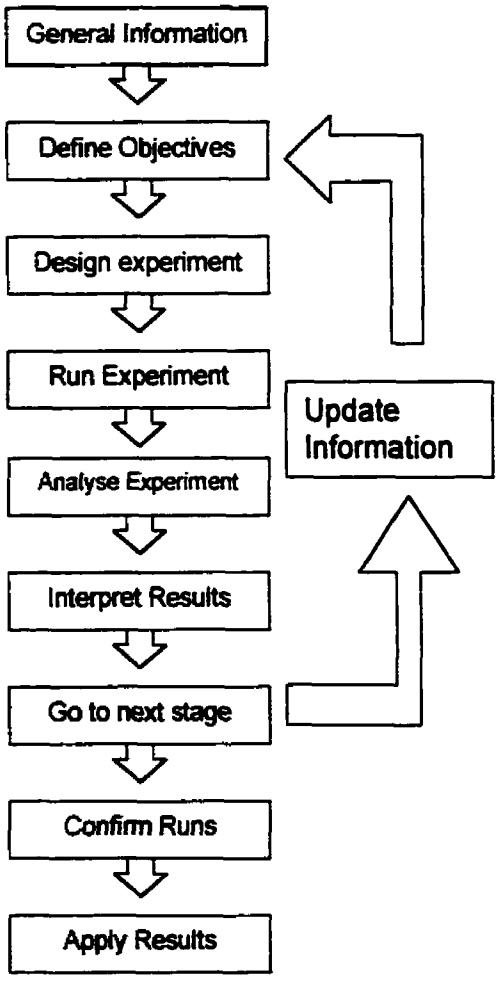

Figure 5.1[41]: Strategic approach to experimental design

In order to optimise the use of DOE, it is recommended to follow a strategic approach to the methodological application (Figure 5.1). The first step in the process is to gather information. Researchers determine what they know and what they need to know about the research. Based on this preliminary brainstorming, they next define the objectives for the experiment. Once the researchers gather information and define their

objectives, they then select an appropriate experimental design. They review the chosen design for feasibility. If the design is viable, it is run according to the plan. If it is impractical, alternative designs can be considered or the objective can be modified and new tests run. After the experiment is run, the responses are analysed through appropriate software packages. Finally, the results are interpreted in light of the stated objectives. At this point, financial constraints play a role in determining whether more experimentation is needed. A screening design should be used if one would want to rank the variables or a full response-surface design should be used if one would want to confirm the results.

5.2 Determination of Optimal Research Conditions

5.2.1 Design of Experiments (DOE)

In the DOE system, independent variables and the responses that result are viewed as an interactive relationship within the system. As the variables are changed in the experimental process, their relationships, effects and interactions are measured, analysed and mapped. Statistical models of the system play a key role in this strategy.

According to DOE principles, an experiment is a system composed of independent input variables and dependent output variables. When an experiment is designed, the values or settings for numerous input variables are systematically changed. The experiment then measures and analyses the effect of these changes on the output variables.

In the present research into EAF dust thermal treatment, we are considering the influence of three input parameters (temperature, heating rate and residence time) in affecting two dependent output variables (weight loss and metal leachability within the treated product). The three input variables will be tested at three different conditions. One can visualise this experimental matrix as a cube (Figure 5.2) defined by three values for three control variables. In this graphical representation, an input variable can be located anywhere in the cube, and its co-ordinates are defined by its three values. An output response can similarly be pictured as a point in another cube.

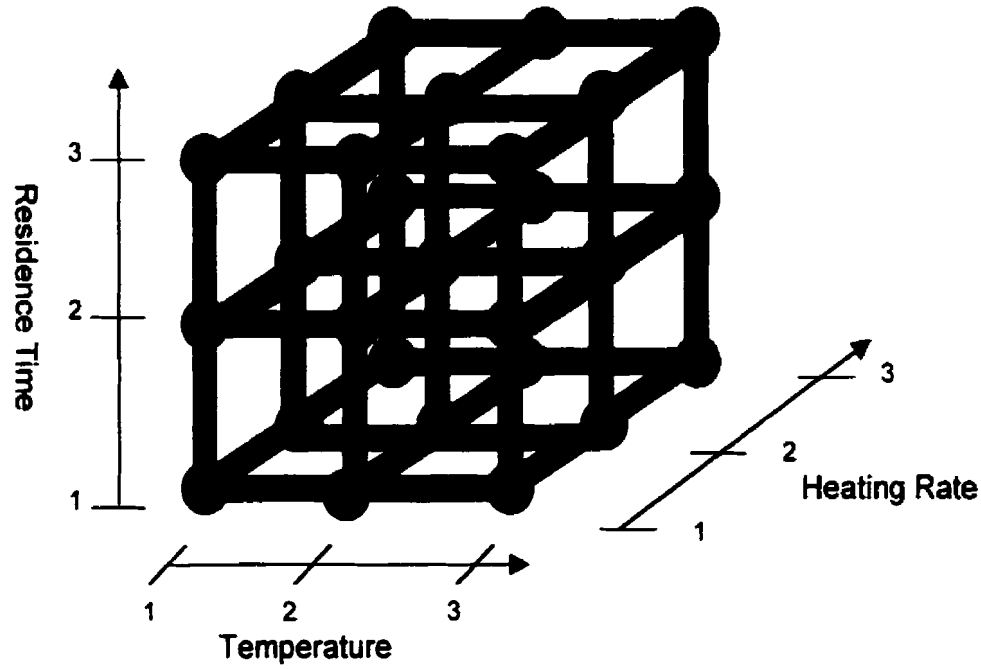

Figure 5.2: Schematic Cube diagram of input parameters

DOE provides many designs, which tell us how to choose the variables (the axes on the cube), the values (the boundaries of the cube), and the number of conditions for each variable (points along the axes). Since it would be unpractical to test all possibilities within the system, a factorial design was developed to realise the goal of obtaining the most significant input variable.

Interaction or factorial designs look at fewer variables (usually three to six) than other designs. One of the fundamental characteristics of DOE is the assumption that input variables often interact. Factorial designs help quantify such relationships. Factorial designs include experimental runs for all combinations of conditions represented by the circles at the cube junctions.

In this research, we have three input variables at three conditions. Through factorial design, this would amount to 27 separate experiments (3^3=27), which are represented by the cube junction points. 27 experiments seems like a reasonable number, however if we had five variables at five different conditions, 3125 (5^5) experiments would need to be run in order to evaluate parametric significance. As a result, cross-

experimentation methods must be employed to reduce the level of experimentation. Using this technique, 3125 experiments can be reduced down to 25, while maintaining a representation of the system. In the case of the current research, the initial 27 experiments can be reduced down to nine through the chosen cross-experimental method[43]. Table 5.1 demonstrates the cross-experimental technique, while Figure 5.3 graphically displays the experiments to be performed on the cube. This cross-experimental can be represented by the designation[44], $L_9\ (3^3)$, which indicates that nine experiments are being conducted, varying three different input variables at three different conditions.

Table 5.1: Sample cross-experimental table

Experiment Number (row number)	Input Variables		
	A	B	C
1	1	1	1
2	1	2	2
3	1	3	3
4	2	1	2
5	2	2	3
6	2	3	1
7	3	1	3
8	3	2	1
9	3	3	2

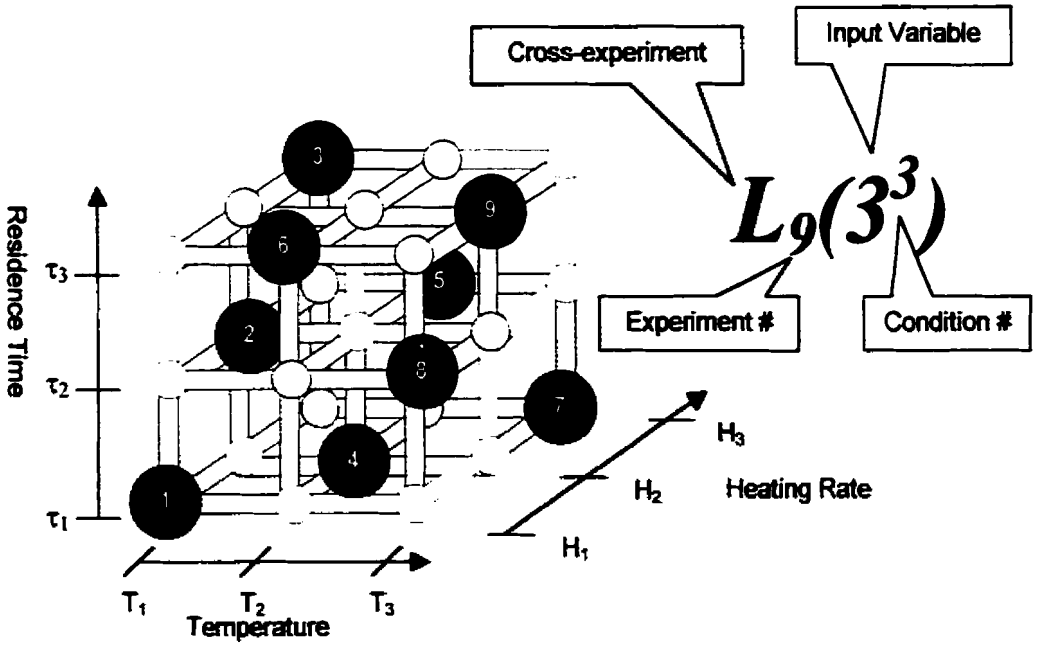

Figure 5.3: Schematic diagram of cross-experiments

As previously mentioned, the present research into thermal treatment of EAF dust will focus on three input variables or parameters within the TGA system (Figure 5.4): maximum thermal treatment temperature (T_{max}, °C); residence time at the maximum thermal treatment temperature (τ, min.); and the heating rate to attain the maximum temperature (H, °C/min.). Through the strategic approach to experimental design and through limitations within the thermal treatment facility, three conditions were chosen for each input parameter, thus giving the L_9 (3^3) cross-experimental matrix.

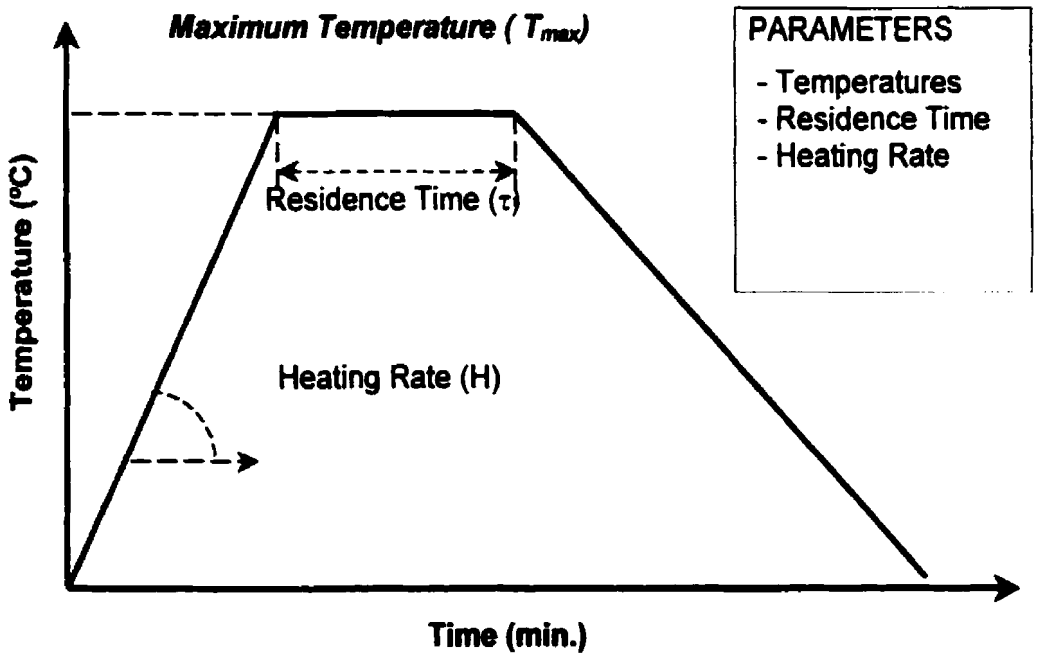

Figure 5.4: Experimental Parameters

Through the cross-experimentation design, conditions can be studied in order to establish the influences of the different parameters on the results. In addition to the latter, one can also determine the optimum combination of conditions within the parameters that will yield the most desired results. In order to achieve this goal, an experimental table was constructed (Table 5.2). Within the table is a column referred to as 'Combining Devices'. This column defines the combination of the different parametric conditions within the experiment. The last column refers to the results obtained and will be in terms of weight loss and leachability of zinc, nickel and chromium. The latter result is extremely important since leachability of chromium in the dust surpasses government

regulations. Nine experiments were conducted, analysing the three different parameters at three conditions. The three different maximum temperatures (T_{max}) used were 900, 1200 and 1500°C; heating rates of 10, 40 and 75°C/min. were used to attain T_{max}; and finally, the samples experienced residence times of 5, 15 and 30 minutes at T_{max}. Experiments used 2.1g. of EAF dust as the initial material and were conducted in the TGA using air as the thermal treatment gas.

Table 5.2: Cross-experimental table

Test #:	Combining Devices	Experimental Conditions			Results
		T_{max} (°C)	τ (min)	H (°C/min)	
1	$T_1\tau_1H_1$	900	5	10	Y_1
2	$T_1\tau_2H_2$	900	15	40	Y_2
3	$T_1\tau_3H_3$	900	30	75	Y_3
4	$T_2\tau_1H_2$	1200	5	40	Y_4
5	$T_2\tau_2H_3$	1200	15	75	Y_5
6	$T_2\tau_3H_1$	1200	30	10	Y_6
7	$T_3\tau_1H_3$	1500	5	75	Y_7
8	$T_3\tau_2H_1$	1500	15	10	Y_8
9	$T_3\tau_3H_2$	1500	30	40	Y_9

5.2.2 Determination of Optimal Experimental Parameters

Once the experimentation is complete, the dependent output variables are statistically analysed in terms of their significance through a mathematical average value of the results obtained at a specific condition (e.g. at a residence time of 30 minutes). The difference (D) between these average values at different conditions within the parameter is then calculated. Once D-values are obtained for each parameter, they are compared to see which parameter plays the greatest role in influencing the results. As such, the D-value is directly proportional to the influence of the particular parameter.

Through the cross-experimental design, results were obtained for the nine tests and are shown in Table 5.3. The 'Final Weight' column indicates the percent of the initial sample weight remaining after thermal treatment and is given by the recording microbalance in the TGA system. Metal leachability is determined through atomic absorption analysis of the resulting leachate of the treated sample after undergoing leachability tests.

Table 5.3: Results of cross-experimentation

Test #	Final Weight (%)	Metal Leachability (ppm)		
		Cr	Ni	Zn
Y_1	97.97	660	3.75	0.56
Y_2	97.63	540	4.28	0.30
Y_3	97.71	560	3.37	0.28
Y_4	97.60	129	0.44	0.22
Y_5	96.80	120	0.40	0.10
Y_6	96.51	250	0.32	0.29
Y_7	94.07	13	0.21	0.16
Y_8	95.02	2	0.09	0.06
Y_9	93.85	5	0.30	0.12

Cross-experimental methods cannot gather a direct correlation of a single parameter's influence on the results since other parameters vary during the experiments. For example, it cannot directly be said which is the optimal condition within the residence time parameter, 5, 15 or 30 minutes, since the other two parameters (temperature and heating rate) are not kept constant throughout the cross-experimental test runs. However, by determining the D-values of the parameters, one can determine their influence on affecting results. The D-value technique was introduced earlier in this section and will now be implemented to calculate parametric influence. Using the results (Y_{1-9}) in Table 5.3 the appropriate D-values were calculated and shown in terms weight loss and metal leachability in Table 5.4 and Table 5.5-5.7 respectively.

The D-value will provide us with an idea on the effect of temperature, residence time and heating rate on weight loss and metal leachability. Calculation of the D-value is shown in Figure 5.5. It demonstrates how D-values were obtained in terms of the 'weight loss' results output variable. The first step in obtaining the D-value is a summation of the weight loss results of every test containing a particular condition (i.e. $\Sigma T_1(900°C) = Y_1+Y_2+Y_3$). Thereafter, this summation is divided by the number of tests containing this particular condition (i.e. $T_{1\ (avg.)} = \Sigma T_1/3$). Once the average results have been calculated for every condition within a parameter, the D-value can be calculated by obtaining the maximum difference between the average conditions within a parameter (i.e. $T_{i\ (avg.\ max)} - T_{i(avg.\ min)}$).

Part 1: summation of the weight loss results of every test containing a particular condition

$\Sigma H_{1\ (10°C/min)}=Y_1+Y_6+Y_8=97.97+96.51+95.02=289.50$ $\Sigma H_{2\ (40°C/min)}=Y_2+Y_4+Y_9=97.63+97.60+93.85=289.08$ $\Sigma H_{3(75°C/min)}=Y_3+Y_5+Y_7=97.71+96.80+94.07=288.58$	$\Sigma \tau_{1(5\ min)}=Y_1+Y_4Y_7=97.97+97.60+94.07=289.64$ $\Sigma \tau_{2(15\ min)}=Y_2+Y_5+Y_8=97.63+96.80+95.02=289.45$ $\Sigma \tau_{3(30\ min)}=Y_3+Y_6+Y_9=97.71+96.51+93.85=288.07$	$\Sigma T_{1\ (900°C)}=Y_1+Y_2+Y_3=97.97+97.63+97.71=293.31$ $\Sigma T_{2\ (1200°C)}=Y_4+Y_5+Y_6=97.60+96.80+96.51=290.91$ $\Sigma T_{3(1500°C)}=Y_7+Y_8Y_9=94.07+95.02+93.85=282.94$

Part 2: Average results for a particular condition within a parameter

$H_{1(avg)}=\Sigma H_{1(10°C/min)}/3=289.50/3=96.50$ $H_{2(avg)}=\Sigma H_{2(40°C/min)}/3=289.08/3=96.36$ $H_{3(avg)}=\Sigma H_{3(75°C/min)}/3=288.58/3=96.19$	$\tau_{1(avg)}=\Sigma \tau_{1(5\ min)}/3=289.64/3=96.55$ $\tau_{2(avg)}=\Sigma \tau_{2(15\ min)}/3=289.45/3=96.48$ $\tau_{3(avg)}=\Sigma \tau_{3(30\ min)}/3=288.07/3=96.02$	$T_{1(avg)}=\Sigma T_{1(900°C)}/3=293.31/3=97.77$ $T_{2(avg)}=\Sigma T_{2(1200°C)}/3=290.91/3=96.97$ $T_{3(avg)}=\Sigma T_{3(1500°C)}/3=282.94/3=94.31$

Part 3: calculation of the D-value through the difference of the maximum and minimum average for each parameter

$D_{value}(H)=96.50-96.19=\mathbf{0.31}$	$D_{value}(\tau)=96.55-96.02=\mathbf{0.52}$	$D_{value}(T)=97.77-94.31=\mathbf{3.46}$

Figure 5.5: Calculation of D-value

Table 5.4: Calculation of D-value in terms of the 'weight loss' result

Parameters	Summation		Average	D value
T_1 (900°C)	$Y_1+Y_2+Y_3$	293.31	97.77	***3.46***
T_2 (1200°C)	$Y_4+Y_5+Y_6$	290.91	96.97	
T_3 (1500°C)	$Y_7+Y_8+Y_9$	282.94	94.31	
τ_1 (5 min.)	$Y_1+Y_4+Y_7$	289.64	96.55	***0.52***
τ_2 (15 min.)	$Y_2+Y_5+Y_8$	289.45	96.48	
τ_3 (30 min.)	$Y_3+Y_6+Y_9$	288.07	96.02	
H_1 (10°C/min.)	$Y_1+Y_6+Y_8$	289.50	96.50	***0.31***
H_2 (40°C/min.)	$Y_2+Y_4+Y_9$	289.08	96.36	
H_3 (75°C/min)	$Y_3+Y_5+Y_7$	288.58	96.19	

Mass loss and volume reductions are two important aspects of thermal treatment of wastes since they contribute to the bottom line. Residual waste resulting from the thermal treatment of waste is adverse since it must be further processed through transportation and subsequent landfilling. As such, the viability of such treatment methods is dependent on generating the least amount of residual so as to reduce further processing costs. Consequently, this research aims to determine the parameter that has the greatest influence over weight loss within the cross-experimental framework. The chart in Figure 5.6 shows the influencing degree of the three parameters with respect to weight loss. Since the D-value denotes the degree of influence of a particular parameter within the thermal treatment process. The higher the D-value, the greater its effect in influencing the output variables. From the results, it is evident that the maximum temperature of thermal treatment plays the greatest role in influencing weight loss. Its D-value is an order of magnitude higher than those of residence time and heating

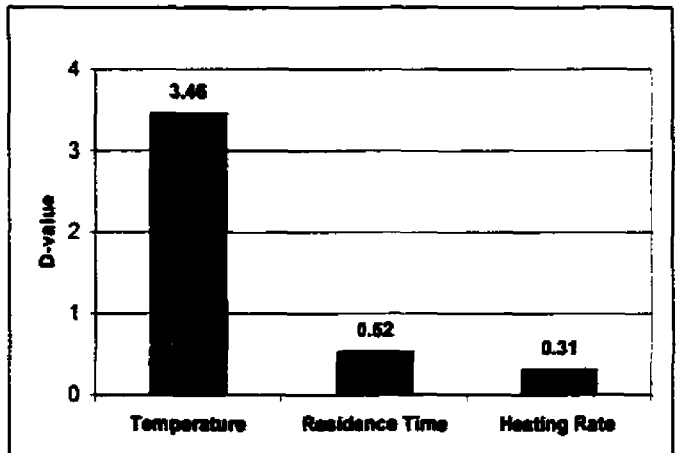

Figure 5.6: Influencing degree of parameters in terms of weight loss

rate. The level of influence of the parameters follows the following trend: $D_T > D_\tau > D_H$, where maximum temperature has an overwhelming influencing effect; followed by the residence time at the maximum temperature; and finally, the least influencing factor, being the heating rate necessary to attain the maximum temperature. The latter two parameters were quite similar in terms of influencing degree over the weight loss. As such, their variance had little effect on the final weight. It should be noted that the weight loss within the dust during thermal treatment is quite insignificant as it ranges between 6-7 wt% at 1500°C. This is to be expected since the dust is composed mainly of oxides, which are quite stable under the high-temperature oxidative conditions of the cross-experimental runs.

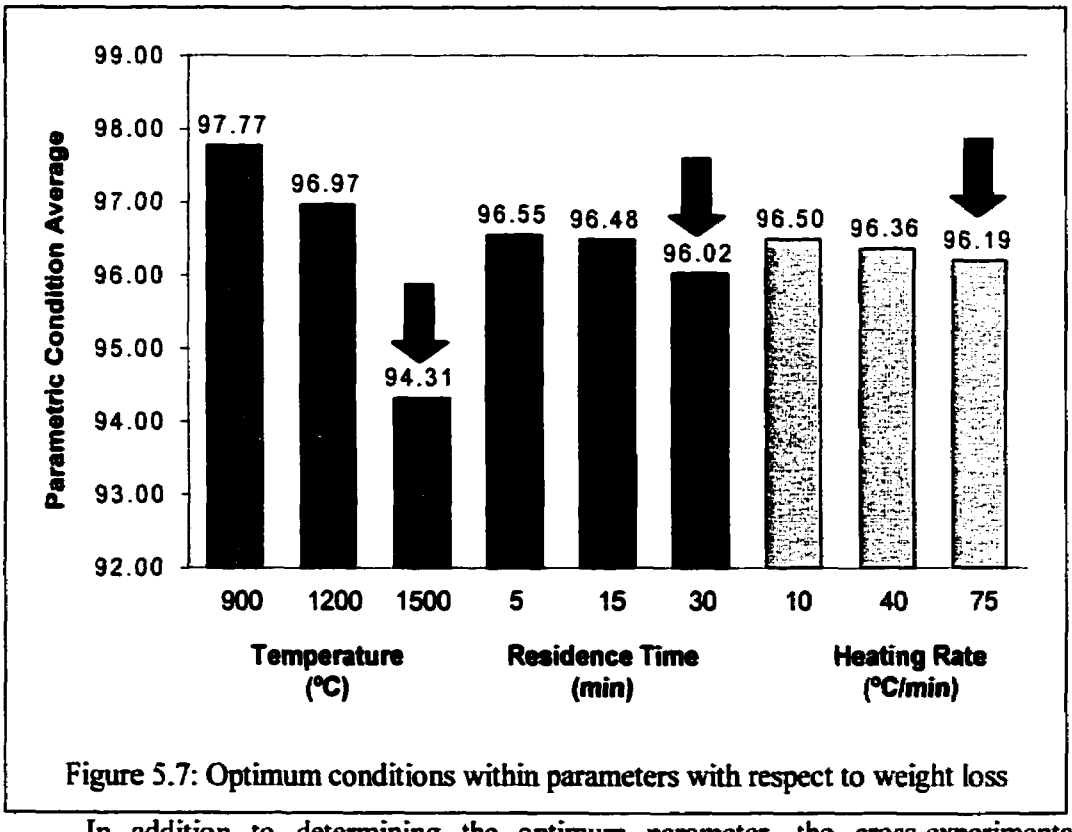

Figure 5.7: Optimum conditions within parameters with respect to weight loss

In addition to determining the optimum parameter, the cross-experimental technique also provides information on the prime conditions within each parameter so as to optimise results during future experimentation. Within the chart in Figure 5.7, Each bar represents an average EAF dust final weight per parametric condition. The lowest final weights are indicated by arrows, and represent the optimal conditions within the parameters. These optimal conditions occur at the highest levels of each condition, i.e. at

a maximum temperature (T) of 1500°C, a residence time (τ) of 30 minutes, and a heating rate (H) of 75°C/min. It should however be noted that it is unfeasible to draw definite conclusions about optimum conditions within the parameter since the average values for each parametric condition are quite similar; which is especially true for the latter two parameters, i.e. residence time and heating rate. One could conclude that these two parameters are inconsequential in determining weight loss within the dust. Nonetheless, this study into parametric optimisation does provide us a base of knowledge into parametric applications during further experimentation throughout this research.

Table 5.5: Calculation of D-value in terms of the 'Cr leachability' result

Parameters	Summation		Average	D value
T_1 (900°C)	$Y_1+Y_2+Y_3$	1760	586.67	***580.00***
T_2 (1200°C)	$Y_4+Y_5+Y_6$	1229	409.67	
T_3 (1500°C)	$Y_7+Y_8+Y_9$	20	6.67	
τ_1 (5 min.)	$Y_1+Y_4+Y_7$	802	267.33	***4.33***
τ_2 (15 min.)	$Y_2+Y_5+Y_8$	662	220.67	
τ_3 (30 min.)	$Y_3+Y_6+Y_9$	815	271.67	
H_1 (10°C/min.)	$Y_1+Y_6+Y_8$	912	304.00	***116.67***
H_2 (40°C/min.)	$Y_2+Y_4+Y_9$	558	186.00	
H_3 (75°C/min)	$Y_3+Y_5+Y_7$	562	187.33	

Table 5.6: Calculation of D-value in terms of the 'Ni leachability' result

Parameters	Summation		Average	D value
T_1 (900°C)	$Y_1+Y_2+Y_3$	11.4	3.80	***3.60***
T_2 (1200°C)	$Y_4+Y_5+Y_6$	1.16	0.39	
T_3 (1500°C)	$Y_7+Y_8+Y_9$	0.6	0.20	
τ_1 (5 min.)	$Y_1+Y_4+Y_7$	4.4	1.47	***0.14***
τ_2 (15 min.)	$Y_2+Y_5+Y_8$	4.77	1.59	
τ_3 (30 min.)	$Y_3+Y_6+Y_9$	3.99	1.33	
H_1 (10°C/min.)	$Y_1+Y_6+Y_8$	4.16	1.39	***0.06***
H_2 (40°C/min.)	$Y_2+Y_4+Y_9$	5.02	1.67	
H_3 (75°C/min)	$Y_3+Y_5+Y_7$	3.98	1.33	

Table 5.7: Calculation of D-value in terms of the 'Zn leachability' result

Parameters	Summation		Average	D value
T_1 (900°C)	$Y_1+Y_2+Y_3$	1.14	0.38	***0.27***
T_2 (1200°C)	$Y_4+Y_5+Y_6$	0.61	0.20	
T_3 (1500°C)	$Y_7+Y_8+Y_9$	0.34	0.11	
τ_1 (5 min.)	$Y_1+Y_4+Y_7$	0.94	0.31	***0.08***
τ_2 (15 min.)	$Y_2+Y_5+Y_8$	0.46	0.15	
τ_3 (30 min.)	$Y_3+Y_6+Y_9$	0.69	0.23	
H_1 (10°C/min.)	$Y_1+Y_6+Y_8$	0.91	0.30	***0.12***
H_2 (40°C/min.)	$Y_2+Y_4+Y_9$	0.64	0.21	
H_3 (75°C/min)	$Y_3+Y_5+Y_7$	0.54	0.18	

Another important aspect within the field of thermal treatment of wastes is the leachability of toxic metals from the residual final product since the latter contains concentrated levels of heavy metals within its structure. Toxic metal leachability is a determining factor in deciding whether a material can be de-classified as a hazardous product. As such, it is important to produce structures within the thermally treated product which will not easily leach out toxic metals present thus complying with environmental regulations.

EAF dust samples were treated according to the design of the cross-experimental matrix. Thereafter, the treated product was leached according to environmental guidelines and test through AA for metal leachability in terms of chromium, nickel and zinc; three metals contained in the dust and present under Quebec's Hazardous Waste Regulation Act.

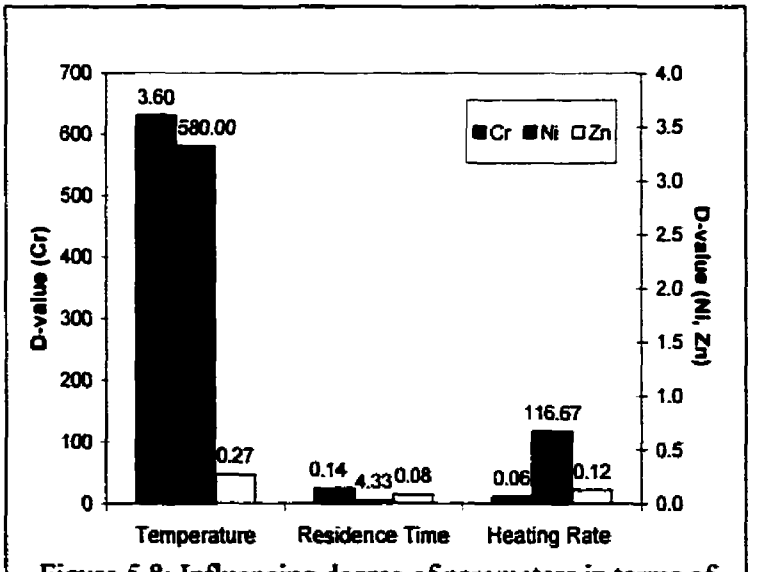

Figure 5.8: Influencing degree of parameters in terms of metal leachability

The leachability of the final product will determine whether it can be placed in a regular landfill or re-used as a co-product in other industries; or whether it needs to be placed in a hazardous landfill, which is the more expensive option.

The chart in Figure 5.8 shows the influencing degree of the three parameters with respect to metal leachability. Chromium D-values are represented by the left-hand y-axis while nickel and zinc D-values are represented by the y-axis on the right. The higher the D-value, the greater the degree of influence of a particular parameter within the thermal treatment process. Once again, it is evident that the maximum temperature of thermal treatment plays the greatest role in influencing the output parameter; that of metal leachability. In the case of chromium, parametric influence follows the subsequent trend: $D_T > D_\tau > D_H$. Temperature (T) is the most important parameter in influencing Cr leachability followed by the heating rate (H). Residence time (τ) at the maximum temperature does not seem to influence metal leachability a great deal. In terms of nickel and zinc, no directs trends could be observed since the levels of these metals in the leachate were quite low resulting in very low D-values. Thus, it was unclear whether residence time and heating rate generally affected the leachability of these two metals. However, the influence of temperature could still be noted in influencing the leachability of both nickel and zinc.

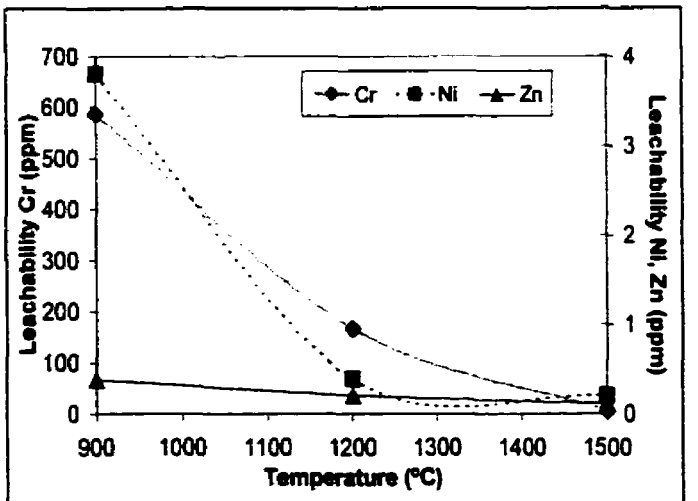

Figure 5.9: Optimal condition in terms of maximum temperature (T)

Parametric optimisation analysis was performed on the dust samples in terms of metal leachability. The maximum temperature was an important factor in determining metal leachability. Metal leachability decreased dramatically as the thermal treatment temperature increased (Figure 5.9). This is due to the fact that the dust structure changed after thermal treatment at high temperatures (beginning at 1200°C), that resulted in the sintering of the initial product. This stronger structure caused in a reduction in metal leachability.

The effect of residence time on metal leachability is minimal, as there does not seem be a clear-cut optimal condition for the metals (Figure 5.10). Chromium and zinc show a minimum leachability at a residence time of 15 minutes, while there seems to be a minimum leachability at 30 minutes in terms of nickel. As such, the results seem to conflict, as the influence of this parameter is rather insignificant.

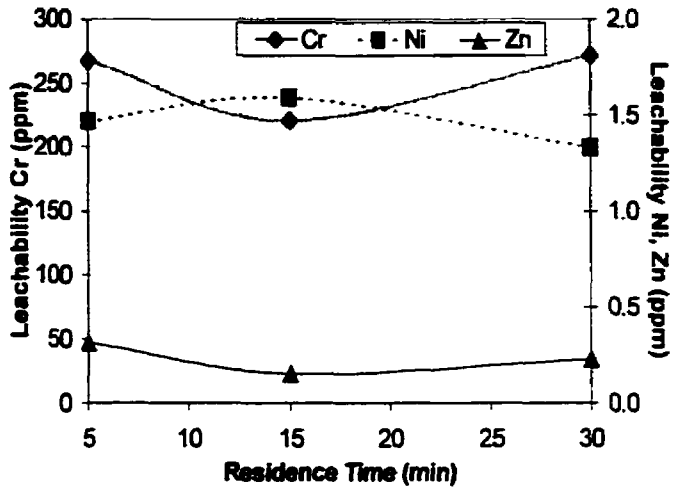

Figure 5.10: Optimal condition in terms of residence time (τ)

Heating Rate (H) seemed to affect the levels of chromium leachability within the samples (Figure 5.11). As the heating rate was increased, the leachability of Cr decreased by ~100 ppm. The optimal condition in terms of chromium leachability was determined to occur at a heating rate of 75°C/min. This decrease in Cr leachability is however unsubstantial and cannot be confirmed through the other two metals (i.e. Ni, Zn). The levels of these latter two metals are insignificant, as a result, they do not demonstrate any marking trends within this parameter.

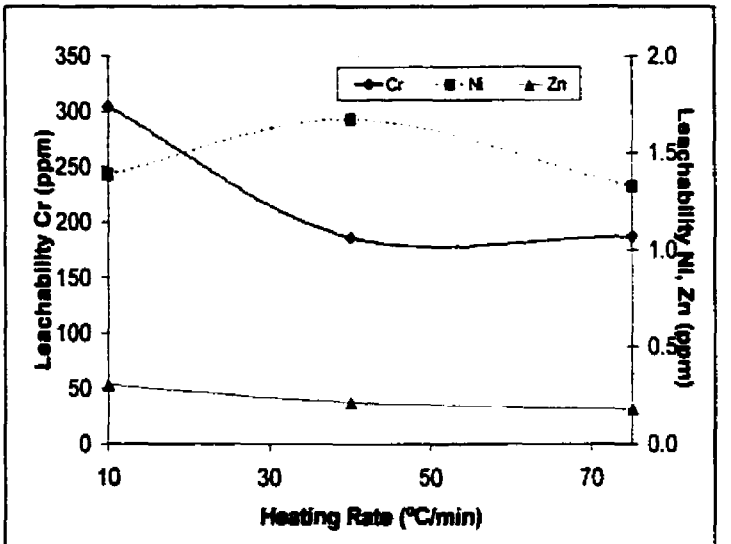

Figure 5.11: Optimal condition in terms of heating rate (H)

The optimum parameter in terms of metal leachability is the maximum temperature of thermal treatment. This is confirmed by its high D-value, indicating

parametric significance. The effect of both residence time and heating rate were minimal in influencing leachability results. Chromium levels within the dust were high enough to show consequential trends within the parametric optimisation analysis. However, the levels of nickel and zinc within the dust were too small to establish any optimal conditions.

5.3 Thermal Treatment Evolution

Once the cross-experimental tests concluded, appropriate parametric conditions could be applied for the following segment of the research: a thermal evolution profile of the EAF dust. Since the maximum temperature was the most influential parameter in determining weight loss and metal leachability, it was decided to vary this parameter from a low value to the highest level possible permitted by the TGA system, thus obtaining a complete temperature profile of the EAF dust. The residence time (τ) chosen was 15 minutes. Although this was not the optimal condition in terms of weight loss, its parametric influence was rather minimal. The time period chosen was regarded as adequate to stabilise the temperature at the maximum level. The heating rate (H) chosen was 40°C/min. This level was not the optimal level in terms of weight loss, however, as in the case of the residence time, the influence of the parameter was insignificant. Thus, in order not to overstress the TGA system by applying an undue high heating rate (i.e. 75°C/min), a more moderate rate was chosen. The maximum temperature varied from a minimum of 600°C and continued up to a maximum of 1600°C, in increments of 200°C. Thus tests were performed at the following set temperatures: 600°C, 800°C, 1000°C, 1200°C, 1400°C and 1600°C. After a residence time of 15 minutes at the set temperature the dust samples were subsequently cooled down to room temperature. The sample cools at a similar rate as the furnace as it eventually drops back down to room temperature. The cooling rate in the furnace after the set temperature is attained was 15°C/min. Thermal treatment experiments were performed under both oxidative and pyrolitic conditions, as shop air and nitrogen were the respective purge gases used in the tests. These two thermal treatment conditions were applied to gain a comparative understanding of the process. 2.1 grams of EAF dust was used per experiment. The helium flowrate was set at 60 ml/min. and the purge gas flowrate was 100 ml/min. Experiments were repeated twice for statistical accuracy.

5.4 Mass Balance Experiments

Samples produced through thermal evolution experiments underwent mass balance tests in order to determine the decrease in levels of certain metals occurring during thermal treatment. Acid digestion tests were performed on samples using methods described by the Ministry of the Environment of Quebec. Hydrochloric acid (HCl) was mixed with nitric acid (HNO_3) in a 3:1 ratio. Sample were heated and left overnight. The leachate was separated from insoluble particles and tested using atomic absorption spectroscopy. The metals that were tested for included chromium, copper, nickel, lead and zinc since these were all toxic metals contained within the dust.

5.5 Metal Leachability Experiments

Leaching tests were carried out on the thermal evolution samples according to procedures established by the MEF. A leaching solution was prepared using 49 g. of acetic acid and 37 g. of sodium anhydrate in a litre of distilled water[45]. The leaching solution and EAF dust sample was mixed with distilled water in a 1:1:9 mass ratio. The sample was rotated at 30 rpm for 24 hours at room temperature. The samples were then centrifuged to separate the leachate from the residual solids. The resulting leachates were analysed for Cd, Cr, Ni, Pb and Zn concentrations using atomic absorption.

6 BEHAVIOUR OF EAF DUST DURING THERMAL TREATMENT

6.1 Weight Loss

The first condition studied within the thermal treatment of EAF dust was its weight loss. An insignificant weight loss within the EAF dust samples was anticipated since the latter contained mostly metal oxides and little carbonaceous material. The primary object of studying the weight loss was to obtain a reference as to study the thermal evolution of the EAF dust as it was treated from 600°C up to a maximum of 1600°C. Certain inflections on the weight loss curves can give rise to corresponding manifestations which occur within the sample.

Weight loss curves were constructed from the thermal evolution of EAF dust in oxidative and pyrolitic atmospheres respectively. Figure 6.1 and Figure 6.3 represent the curves as they are plotted as weight loss (%) versus time (sec.). In addition to the weight loss curves, derivative curves (dw/dt), to determine the locations of the maximal weight loss/gain rates, were constructed. These derivative curves are shown in Figure 6.2 and Figure 6.4. During thermal treatment experiments, the dust was placed in a crucible. Throughout these experiments, it was assumed that the temperature of the dust, which was measured by a thermocouple placed directly below the crucible, was at the same temperature as the furnace. This assumption was plausible since the thermocouple was placed at close proximity to the sample in addition to fact that the small quantity of dust used per experiment would negate any possible thermal gradient within the material thus allowing heat to rapidly dissipate throughout the sample.

Data collection was recorded throughout the experimental runs (i.e. during heating and cooling up to room temperature), however, no noticeable changes in weight loss occurred during the cooling process after a temperature of ~700°C was attained. As a result, the experimental run-time represented on the curves by the x-axis is cut at around 5000 sec. or ~83 minutes. From the resulting weight loss curves, appropriate zones can be designated on the graphs, which can provide insight into the different stages of thermal evolution.

6.1.1 Weight Loss During Oxidative Treatment

Figure 6.1 displays the weight loss (% weight loss) and temperature (°C) evolution of the EAF dust with respect to time using oxygen as the reaction gas. From the

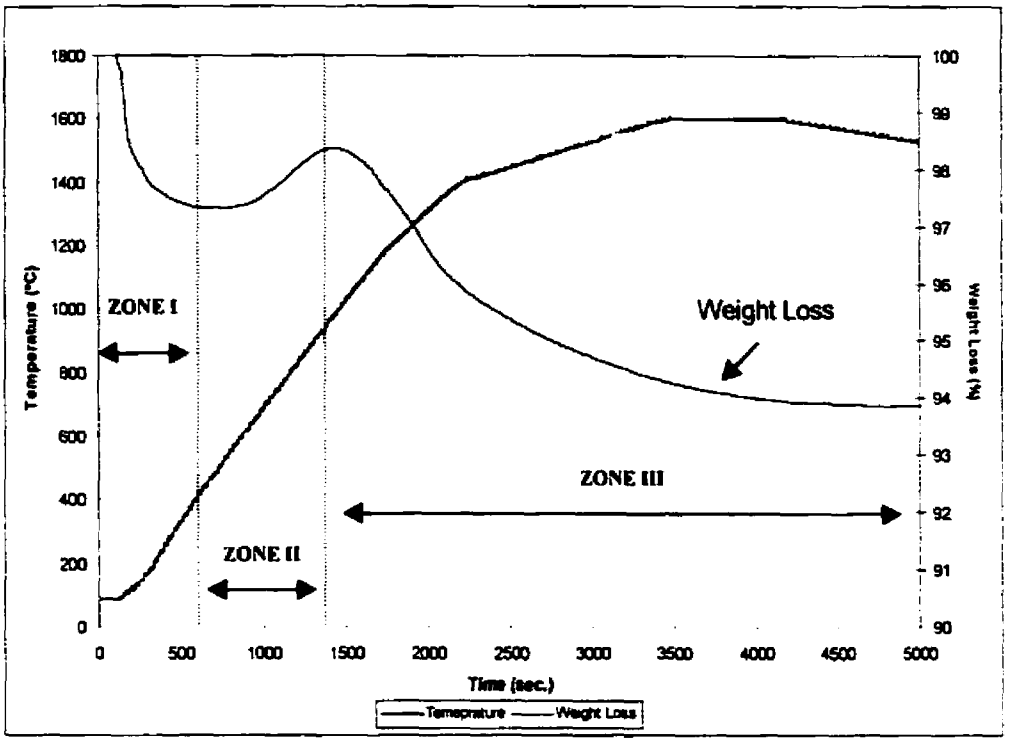

Figure 6.1: Thermal evolution of EAF dust under oxidative conditions

resulting curve, the evolution of EAF dust under oxidative conditions can be separated into 3 distinct zones. These zones are characterised by different weight loss/gain rates within the sample. Zone I encompasses a temperature region of room temperature to ~450°C. Approximately 2.5 wt.% weight loss occurs within this zone, resulting in 36% of the entire weight loss in the sample. At the end of Zone I, the EAF dust sample has achieved 42% of its final weight loss occurring through the thermal evolution process. By calculating the weight loss (in mgs) over the time equivalent of the zone, it is possible to obtain an average weight loss rate over the zone. Within Zone I, this corresponds to an average weight loss rate of 4.05 mg/min over the time length of the zone. At the heating rate used (i.e. 40°C/min.), this coincides to the first 9 minutes of the evolution process. The sharpest weight loss rate occurs inside this zone and is most likely due to the evaporation of moisture and oxidation of residual carbon present in the EAF dust. This will be further analysed within the 'Gas Evolution' section of this chapter. Zone II is a

brief phenomenon which occurs during oxidative thermal treatment, encompassing the temperature range of 470-1000°C. In this zone, oxygen reacts with metal or metal oxides species present in the dust to make them into oxides or to render them into a more advanced oxidative stage, which results in a temporary weight gain within the sample of ~1.5 wt.%. At the end of this zone, the sample has achieved but 17% of its final weight loss, decreasing from a level of 42% at he end of Zone I due to the temporary increase in weight. The weight gain rate in the sample corresponds to 2.4 mg/min. At the heating rate of 40°C/min., this transitory phenomenon persists for 19 minutes. Thereafter, the thermal evolution of the sample leads to Zone III. Within this zone is observed a gradual weight loss of ~5 wt.% up to the maximum final weight loss in the sample of 6 wt.%. Indeed 64% of the entire weight loss is achieved in this zone. As a result of the conditions applied, the duration of the zone is approximately 60 minutes. Zone III is gradual in nature as the weight loss rate is but 1.63 mg/min. The boundary of the zone lies 83 minutes into the experimental run whereupon the final weight of the EAF dust has stabilized. Thereafter, minimal weight fluctuations are noticed. Weight loss within this zone is most likely due to the slow volatilization of metal and metal oxide species into the off-gas.

Figure 6.2 displays the 3 distinct peaks that can be seen within the curve, corresponding to three different weight loss/gain rates within the sample. Peak I is representative of the weight loss within Zone I. A high yet brief weight loss rate is evident in Peak I which corresponds to the rapid evaporation of moisture and reaction of residual carbon in the dust. Peak II denotes the momentary weight gain experienced by the sample around the temperature range of 470-1000°C though oxidation. Peak III is a small but sustained peak that encompasses the weight loss of Zone III. The large area of this peak represents the bulk of the weight loss occurring in the sample as the sample reaches the target temperature of 1600°C. The bulk of the weight loss can be attributed to the vaporisation of metal and metal oxide species.

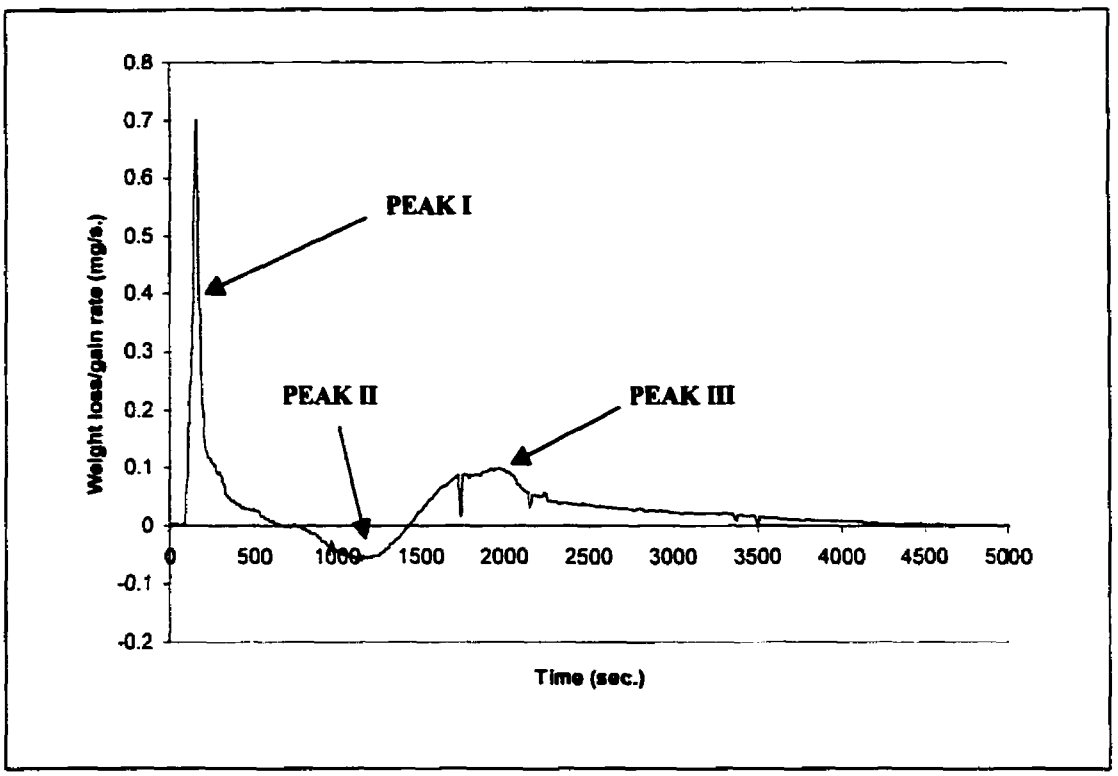

Figure 6.2: DTG Profile obtained during oxidative thermal treatment of EAF dust @ 1600°C

6.1.2 Weight Loss During Pyrolitic Treatment

Thermal treatment of the EAF dust was also performed under pyrolitic conditions as nitrogen was used as the purge gas during the experiments. The goal of this trial was to determine the differences between thermal treatment under oxidative and pyrolitic conditions. The weight loss evolution of the EAF dust can be viewed in Figure 6.3. As with the oxidative experiments, the evolution of EAF dust under pyrolitic conditions can be separated into 3 distinct zones. These zones are characterised by different weight loss rates within the sample. Zone I encompasses a temperature region of room temperature to ~400°C. Approximately 5% weight loss occurs within this zone, resulting in 70% of the entire weight loss in the sample. The average weight loss rate within Zone I is 9.80 mg/min over the time length of the zone. At the heating rate used (i.e. 40°C/min.), this coincides to the first 10 minutes of the evolution process. As in the previous set of experiments, the sharpest weight loss rate occurs inside this zone. It is most likely due to the evaporation of moisture and possible oxidation of residual carbon due to free oxygen

present in the EAF dust. This will be further analysed within the 'Gas Evolution' section of this chapter.

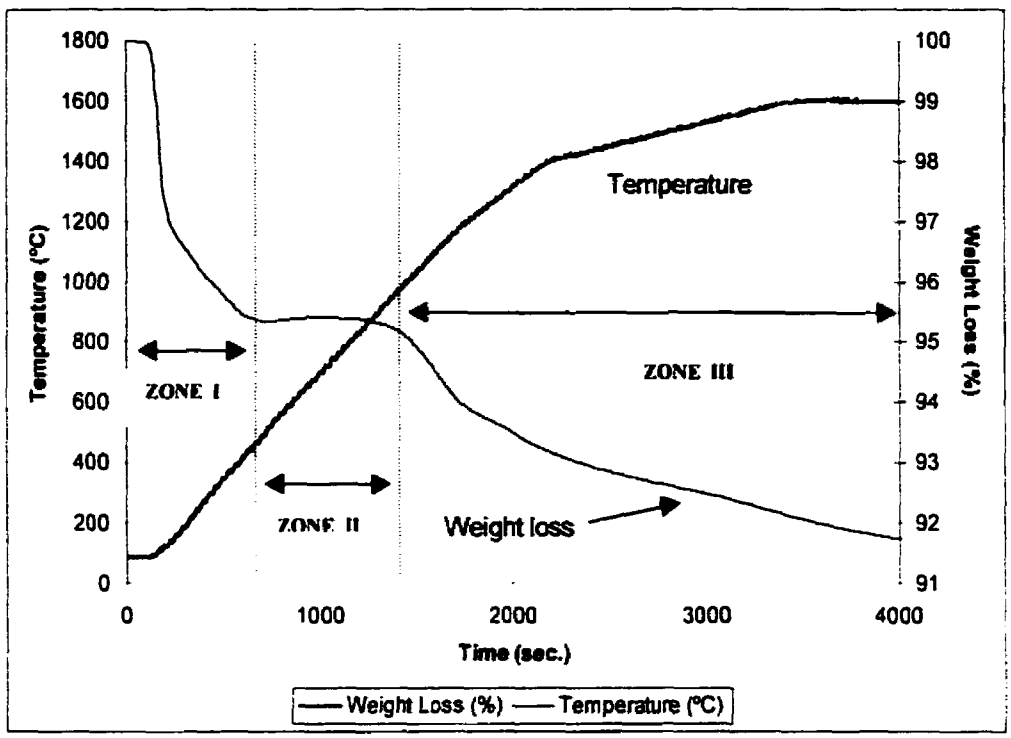

Figure 6.3: Thermal evolution of EAF dust under pyrolitic conditions

Zone II is a plateau which occurs during the treatment process. This zone represents the counter-balance of evaporation of metal species and probable oxidation of other metal species resulting from free oxygen present in the dust, which results in a minimal weight decrease of less than one percent within the dust. The weight loss rate in the sample corresponds to 0.2 mg/min. In addition, at the heating rate of 40°C/min., this transitory phenomenon persists for 12 minutes.

Thereafter, the thermal evolution of the sample leads to Zone III. Within this zone is observed a gradual weight loss of ~2 wt.% up to the maximum final weight loss in the sample of 7.1 wt.%. Indeed, 28% of the entire weight loss is achieved in this zone. As a result of the conditions applied, the duration of the zone is approximately 45 minutes. Zone III is gradual in nature as the weight loss rate is but 1.1 mg/min. The boundary of the zone lies 67 minutes into the experimental run whereupon the final weight of the EAF dust has stabilised. Thereafter, minimal weight fluctuations are noticed. Weight loss

within this zone is most likely due to the slow volatilisation of metal and metal oxide species into the off-gas.

Figure 6.4 displays the 2 distinct peaks that can be seen within the curve. These two peaks correspond to the two weight loss slopes that can be seen in within Zone I of Figure 6.3. A high yet brief weight loss rate is evident in Peak I, which corresponds to the rapid evaporation of moisture. This peak occurs from approximately 90°C to 150°C. Peak II is also representative of the initial weight loss within the sample, however, the weight loss rate within this stage is considerably slower than in the previous peak although it is more sustained. Weight loss within this region corresponds to the reaction of free carbon in the dust, which produces carbon dioxide off-gas. It occurs within a temperature range of 150°C to 450°C. The greatest weight loss within the dust sample occurs in Zone I. which is verified by the DTG curves. Subsequent weight loss in the sample is minimal. which is reflected in Figure 6.4 by the insignificant weight loss rates observed.

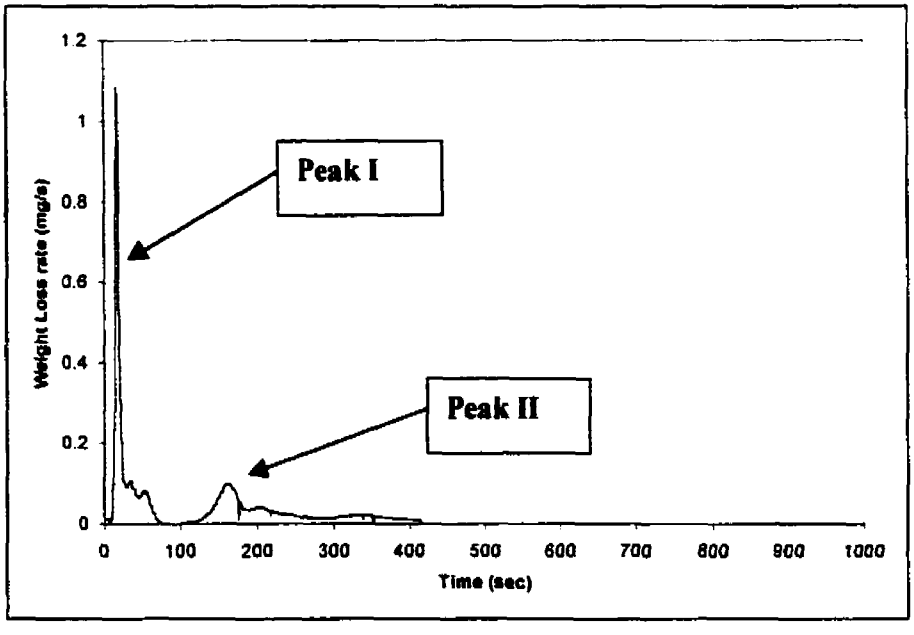

Figure 6.4: DTG Profile obtained during pyrolitic thermal treatment of EAF dust @ 1600°C

6.1.3 Comparison of Thermal Treatment Methods

Both thermal treatment methods (oxidative and pyrolitic) exhibit some similarities in terms of their weight loss curves. These curves show three distinct zones. The first

zones of both treatments are similar as they show a sharp decrease with respect to the totality of the curve. The initial zones last for the first 8 to 10 minutes of the thermal treatment experiments and end when the temperature surpasses 450°C. The majority of the weight loss in this initial zone is attributed to the vaporisation of moisture present in the dust and formation of carbonaceous off-gasses. Thereafter, the weight loss evolution of the processes starts differing. Within the dust treated under an oxidative atmosphere, a brief weight gain is noticed, which occurs within a temperature range of 450-1000°C. The latter phenomenon can be attributed to oxidation of metal species present within the dust. In the pyrolitic weight loss curve, a steady plateau is seen within a temperature range of 450-1300°C, which represents the counter-balance of weight gain occurring from oxidation of metal species due to the presence of free oxygen in the dust; and the weight loss resulting from the vaporisation of metal species within the dust. The latter stages of the thermal evolution of the dust are once again similar for both treatment methods. In the case of the oxidative method, vaporisation of metal species occurs once the temperature surpasses 1000°C and results in the remainder of the weight loss in the sample. The pyrolitic dust sample experiences the remainder of the final weight loss once all the free oxygen has been depleted in the dust. The weight loss in this final section is quite small due to the relatively slow heating rate in the reactor, which results in the gradual vaporisation of metal species in the dust.

6.2 *Volume Reduction*

Thermal evolution in terms of volume reduction (Figure 6.5) shows that at lower temperatures (600-1000°C), volume reduction is insignificant. In this case, the treated product is present as the fine particulate matter, which is observed in the original dust. However, at higher

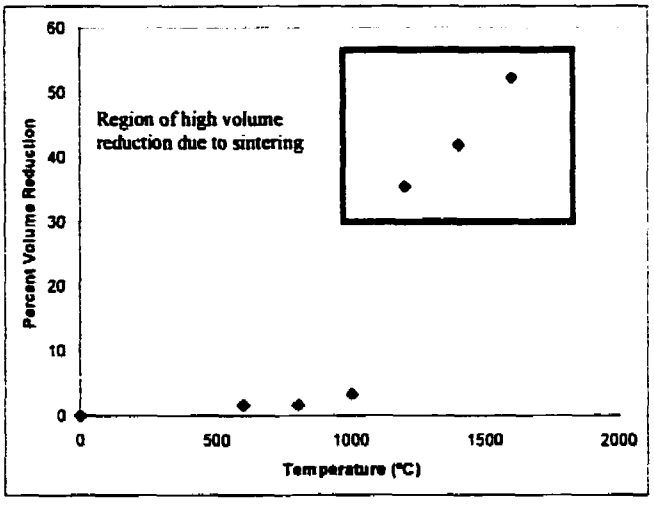

Figure 6.5: Volume reduction in thermally treated dust samples

temperatures (1200-1600°C), a significant volume reduction occurs within the dust sample which results in a volume reduction of greater than 50% in the case of the treated

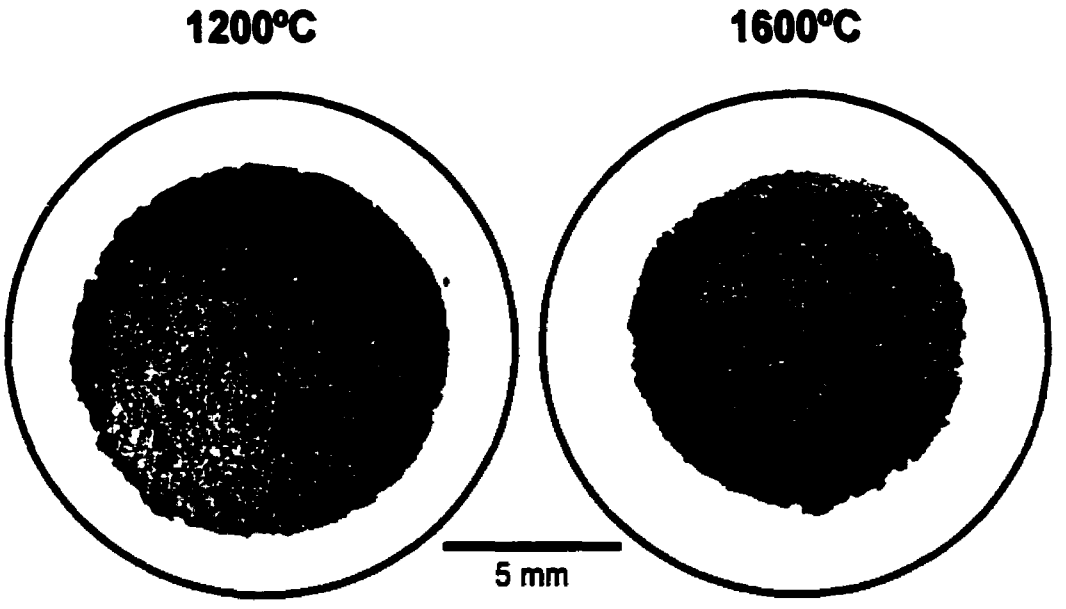

Figure 6.6: Sintered structures formed at 1200°C and 1600°C respectively

product at 1600°C. The main reason for the dramatic volume reduction is the sintering process that occurs within the dust particles at these elevated temperatures. The result of the sintering process is the creation of a strong pellet-like structure, which will be further examined in the following chapter. The sintering process results in the densification of the dust and the elimination of pores within the resulting structure. An example of this sintering can be seen in Figure 6.6, which displays the cross-sectional images of two treated products formed at 1200°C and 1600°C under oxidative conditions respectively. Although the initial particles are agglomerated, the final structure created is a cylindrical pellet structure mimicking the container structure in which it is originally placed. The circles represent the diameter of the container in which the dust was placed and compacted in. After the treatment, the thickness and the diameter of the treated product decreased, as seen in the Figure. This resulted in an average volume reduction of 35% in the dust treated at 1200°C, and over 50% volume reduction in the 1600°C treated product.

6.3 Gas Evolution During Thermal Treatment

Due to the insignificant weight loss in the treated dust, the off-gas generated by

the oxidative treatment of the sample in the TGA was minimal. Through FTIR analysis (Figure 6.7) it was determined that the main off-gases formed was (1) CO_2, resulting from free carbon present in the dust and, (2) moisture. The levels of CO_2 evolved during thermal treatment are insignificant due to the low levels of carbon present in stainless steel dust.

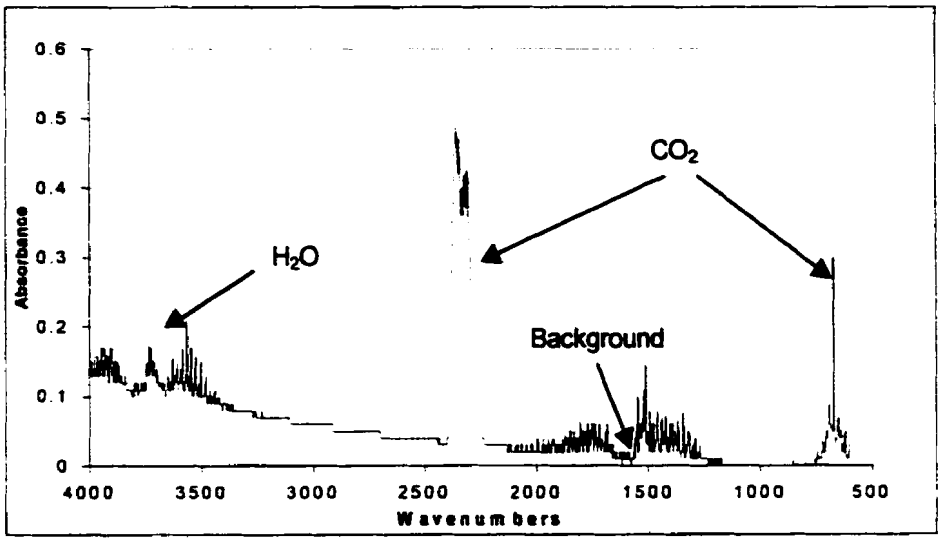

Figure 6.7: FTIR spectra obtained during thermal treatment @ 1600°C under O_2

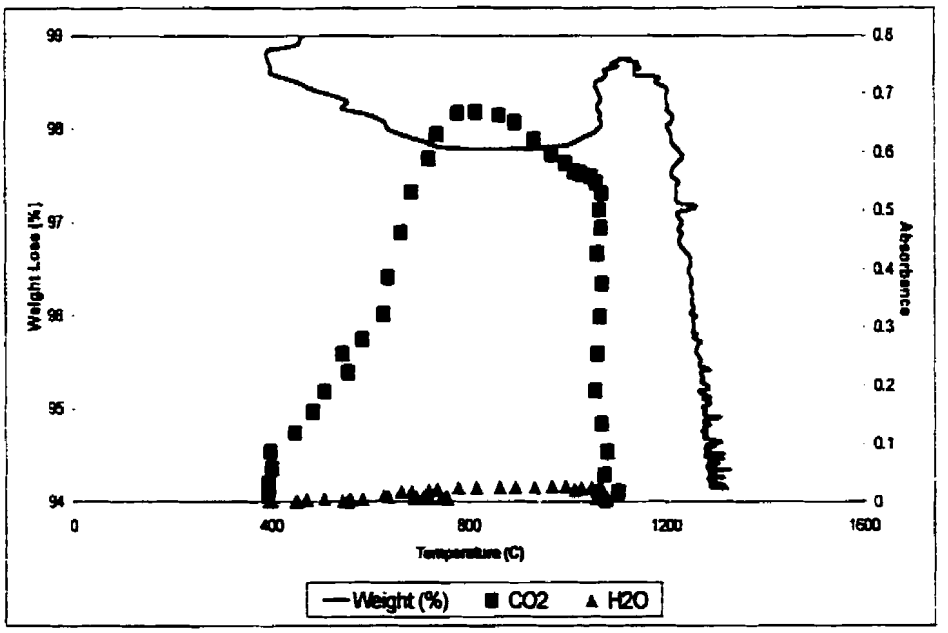

Figure 6.8 - Gas evolution during thermal treatment of EAF dust @ 1600°C

Figure 6.8 displays the evolution profiles of CO_2 and water obtained during thermal treatment of the dust sample at 1600°C. The gas evolution profiles were similar for all thermal treatment experiments run at varying set temperatures. CO_2 evolution was significant at a temperature range of 400-1000°C during the heating process. This temperature range corresponds to the area of rapid weight loss noticed at the end of Zone II during the oxidative thermal treatment process. From the profile, evaporation of moisture seems insignificant. However, since the FTIR's off-gas recording only started at 400°C, most of the evaporation was disregarded by the system. Gas evolution profiles obtained from the pyrolitic experiments revealed the same general trend as in the oxidative tests. CO_2 was the primary off-gas detected by the FTIR, followed traces of water vapour.

6.4 *Processes During Thermal Treatment*

Based on the data presented, the thermal treatment of EAF dust can be divided into three separate stages as seen in Table 6.1.

Table 6.1: Possible processes occurring during thermal treatment of EAF dust

Stages	Temperature Range (°C)	Possible Processes
Stage 1 Initial vaporisation	90-150	Vaporisation of moisture present within the initial EAF dust
	250-600	Formation of $CO_{2\,(g)}$ resulting from the reaction of free carbon in the dust and the oxidative environment and/or oxygen present in the dust.
Stage 2 Transition	600-1000	Oxidation of metal species present in the dust
	800-1100	Volatilisation of certain metal species present in the dust.
Stage 3 Final Sintering	1200-1600	Structure hardening and densification

The first stage of the thermal treatment process is initially associated with the evaporation of moisture and secondly with the formation of $CO_{2\,(g)}$ due to the reaction of free carbon with oxygen, which is subsequently revealed through FTIR analysis. As the temperature increases past 500°C, the detection of $CO_{2\,(g)}$ decreases up to its eventual disappearance, thus indicating the depletion of free carbon in the dust. Since the dust is

inorganic in nature, no burning occurs during this stage of the thermal evolution process, and thus weight loss is minimal (2-3%).

The second stage of the thermal evolution process is characterised by the possible oxidation of metal species present within the dust according to the following reaction type[46]:

$$M + O_2 \Rightarrow MO_x \qquad (1)$$

This has the effect of slightly increasing the sample weight in experiments that are run under an oxidative environment. The oxidation of metal species occurs concurrently with the volatilisation of certain metal species, which acts to reduce the overall weight of the sample. Many heavy metals are volatilised during this stage of thermal evolution such as cadmium, lead and zinc and do not remain in the final thermally treated product[47]. When the off-gas cools down, these metals condense onto the reactor's uptake equipment and thus cannot be analysed by the FTIR. During this stage of thermal evolution, the sample experiences little or no weight loss.

The third stage of the EAF dust evolution is the final sintering stage in which densification and particle agglomeration occurs. The surfaces of the particles begin to fuse together and produce a very dense compact structure. This results in a decrease in mass diffusion from the inside to the outside of the structure as the material flow is hindered by a lack of grain boundaries in which to travel. Thus heavy metals could potentially be trapped within the resulting structure before being able to volatilise. However, some volatilisation of metal compounds will continue from the surface of the structure to the increasing temperature[48]. which in turn contributes to the reduction in sample weight by around 3-4%.

6.5 *Metal Balance Within the Thermally Treated Product*

Metal balance experiments were carried out in order to determine the fate of the toxic metals within the EAF dust during the thermal treatment process using acid digestion tests previously described in the "Experimental Methodology" chapter. Table 6.2 represents an average of the six sets of duplicate samples which were analysed at each thermal treatment temperature. From the results, it is evident that significant amounts of metal vaporisation occurs during the thermal treatment process at high temperatures. As a result, the levels of toxic metals present at elevated temperatures are quite negligible. The

resulting thermally treated ash is low in toxic metal content, however, this content is higher than the maximum leachability allowed from leachates of solid matter.

Table 6.2: Toxic metal content within the EAF dust during thermal treatment

Temperature (°C)	Metal levels (mg/l)					
	Cd	Cr	Cu	Ni	Pb	Zn
Initial	5	5010	220	1930	119	1170
600	4	5000	213	1910	108	1100
800	0.2	4510	200	1870	80	980
1000	0.1	4280	165	1590	14	560
1200	0	413	82	170	11	340
1400	0	356	50	50	6	55
1600	0	30	25	13	2	33

Table 6.3[49] demonstrates metal volatility temperatures of certain metals. It should be noted that chromium is one of the most stable metals and only begins to volatilise beyond a temperature of 1600°C. When chromium does volatilise. it can do so in a hexavalent form (e.g. CrO_3). The decrease in chromium content in the dust resulting from increased thermal treatment temperature can possibly be explained through a presence of chlorine within the dust or in the atmosphere. As Figure 6.9 shows[50], chromium can vaporise at much lower temperatures if amounts of chlorine are present in the flue gas. A small fraction of hexavalent CrO_3 (g) is formed at high temperatures under all chlorine conditions. However, Figure 6.9 suggests that chlorine might promote the formation of carcinogenic hexavalent chromium in a temperature window of around 800°C. It should be emphasised that the equilibrium predictions may not be realised if either other chromium species not considered in this calculation are important, or kinetic rates are too slow to allow equilibrium to be reached.

Table 6.3: Metal Volatility Temperatures

Metal	Volatility Temperature (°C)	Principal Species
Chromium	1613	CrO_2/CrO_3
Nickel	1210	$Ni(OH)_2$
Lead	627	Pb
Cadmium	214	Cd

6.6 *Leachability of Thermally Treated EAF Dust*

Leaching tests were performed on the treated dust to examine the effects of thermal treatment on leachability properties. The treated dust was subject to the same leaching

treatment as the initial dust samples and analysed for metal leachability through AA analysis. As in the initial case, the dust was analysed for five metals which are contained in the MEF hazardous waste guidelines: Cd, Cr, Ni, Pb and Zn. Table 6.4 reveals the level of metals found in the leachate solutions of the treated dust samples. The levels of Cd, Ni, Pb and Zn were already below regulatory limits in the initial dust and as expected, this trend continues in the treated samples. Beyond 1000°C, there is no noticed leachability of the aforementioned metals. The Cr levels detected in the leachate decrease as the temperature of thermal treatment increases. However, at lower temperatures, there is no significant reduction in leachability of this treated product as its levels of Cr are still elevated compared to regulatory limits by two orders of magnitude. At higher temperatures (≥ 1200°C), the levels of Cr found in the leachate dramatically decrease. This is due to the fact that the treated product at 1200°C is sintered into a resistant cylindrical pellet. The pellet properties act to decrease the leachability of the metals in the dust. The sample treated 1600°C does not exhibit measured leachability of Cr. The leachability of the chromium falls below MEF guidelines of 5 mg/l. It must be noted that the levels of toxic metals contained within the dust decrease at a dramatic rate due to the volatilisation of metal species. This contributes to an overall decrease in metals present within the leachate of the treated dust.

Table 6.4: Leachability of metals from thermally treated EAF dust

	Leachability (mg./l.)					
	Cd	**Cr**	**Cu**	**Ni**	**Pb**	**Zn**
Initial	0	270	0.1	0.8	0.1	0.3
600°C	0.04	300	0.1	0.9	0.1	0.3
800°C	0	289	0.1	0.9	0	0.3
1000°C	0	300	0	0.2	0	0.2
1200°C	0	56	0	0.2	0	0.2
1400°C	0	10	0	0	0	0
1600°C	0	0	0	0	0	0

6.7 Phase Evolution During Thermal Treatment

The main phases present within the EAF dust did not change during the thermal treatment process, indicating no crystalline change. The main phases detected during thermal treatment were oxides within the chromium and iron form. Iron constitutes the strongest peaks and is primarily found under the Fe_2O_3 or Fe_3O_4 oxidised form. Chromium is mainly found under the Cr_2O_3 oxidised species or mixed with iron as $FeCr_2O_4$. Nickel, copper and zinc were also present in the final thermally treated products as complex oxide products usually coupled with chromium or manganese. Hexavalent chromium compounds peaks are not visible through XRD since it is present in minute quantities within the dust.

During the evolution of the dust in the oxidative environment, transitory crystalline phases appeared between 800°C and ended once the dust reached a temperature greater than 1200°C (Figure 6.10). These transitory phases correspond to the momentary weight gain noticed during oxidative thermal evolution within the same temperature range and are represented by the new peaks that formed within the XRD spectra. The new peaks represent transitory species that were created within the oxidative environment. These transitory phases are unstable resulting in probable volatilisation at higher temperatures. Although the exact composition of these phases was not determined, it was most likely the result of an intermediary unstable oxidative phase appearing during thermal treatment. These transitory phases were not noticed within the dust samples which experienced pyrolitic thermal treatment thus indicating stability within the inert atmosphere.

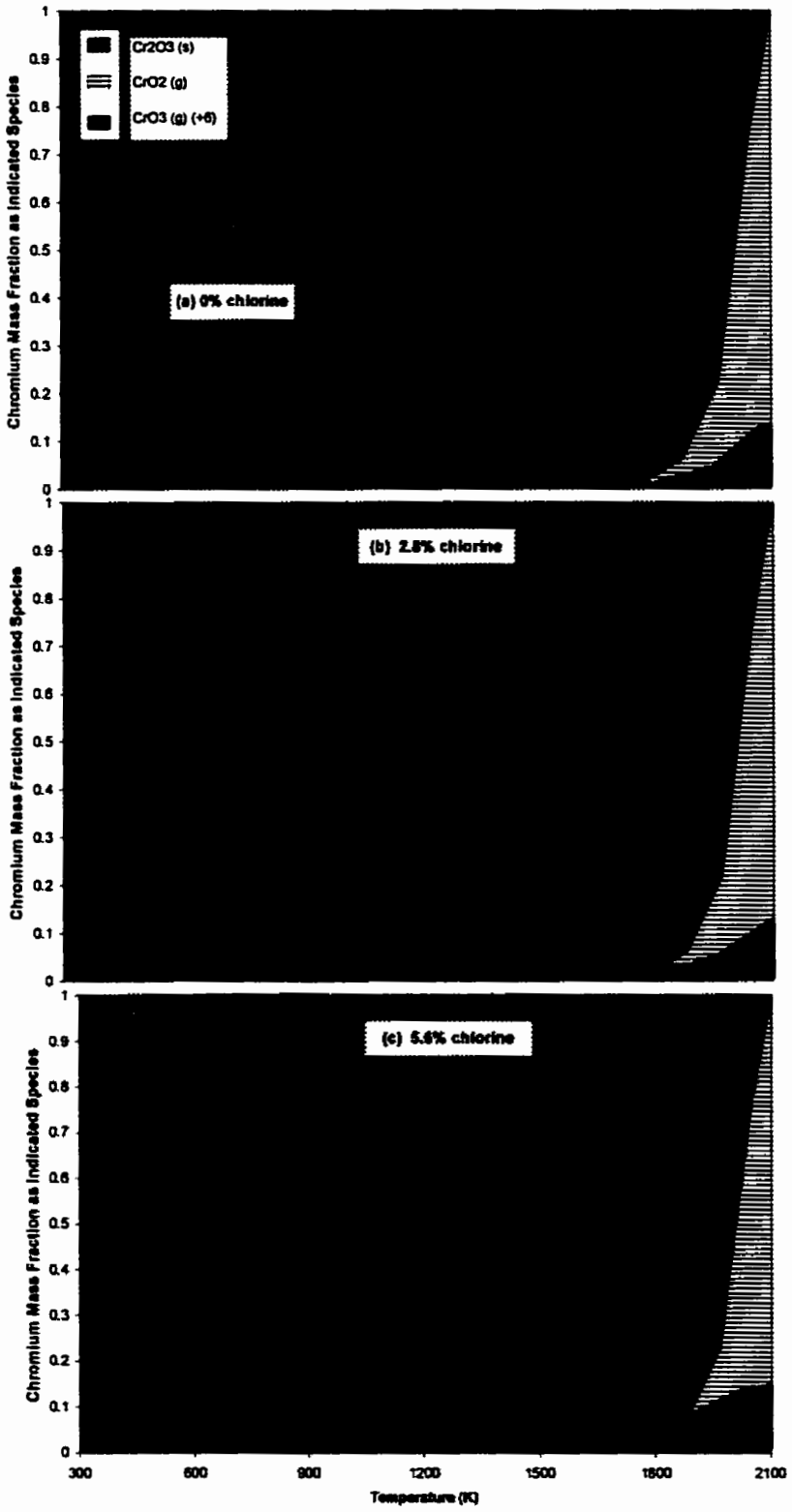

Figure 6.9: Equilibrium predictions of chromium valence as a function of temperature in a simulated environment

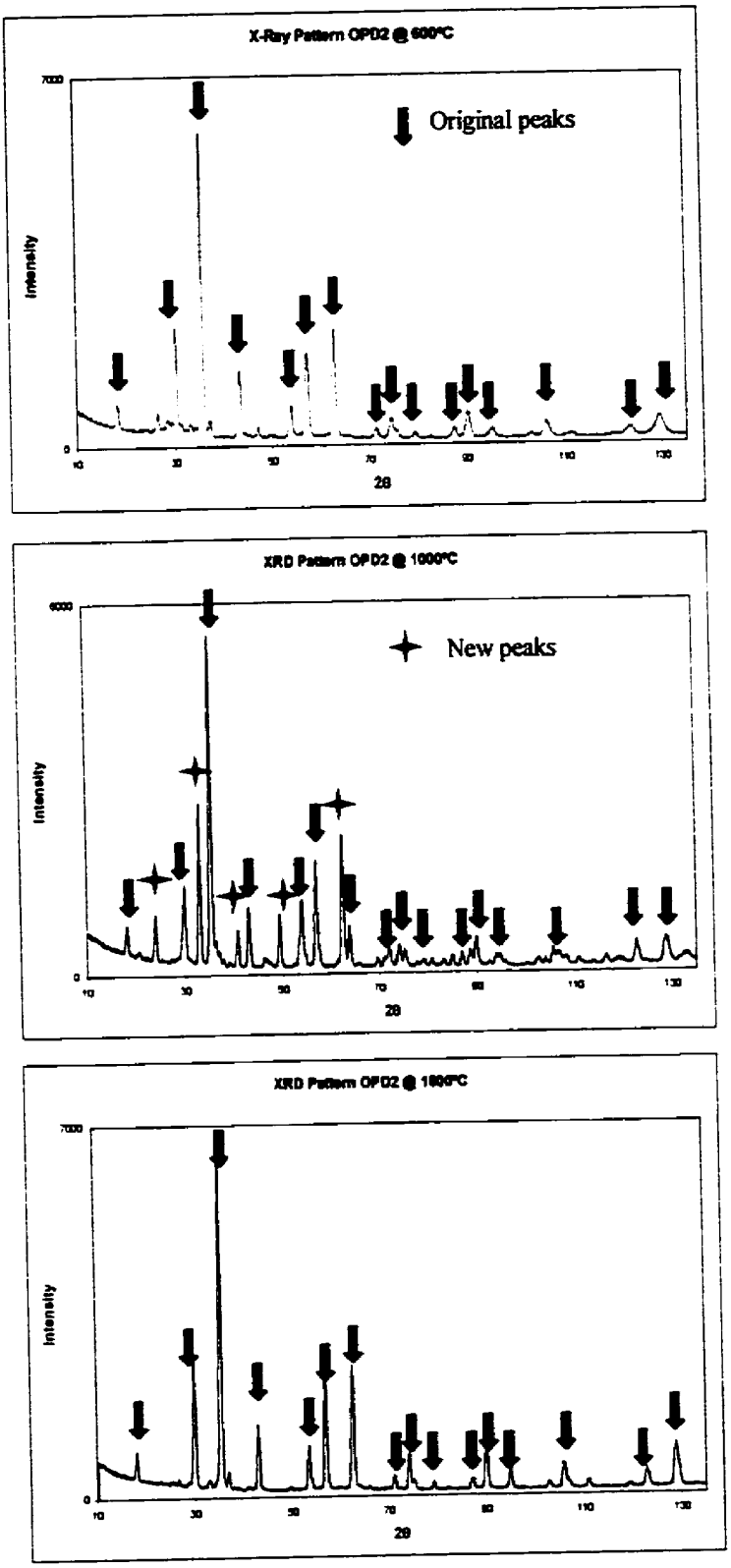

Figure 6.10: X-ray diffraction patterns of the EAF dust samples at 600°C, 800°C and 1600°C

7 MORPHOLOGICAL CHANGES DURING THERMAL TREATMENT

The following chapter will reflect the physical changes that the EAF dust underwent during the thermal treatment procedure. The morphology of the particles will be closely examined with respect to temperature and the thermal treatment environment: atmospheric thermal treatment in air and pyrolitic treatment in N_2 (g). Particle morphology is an important feature of the treated dust particle since an appropriate dust structure can result in metal encapsulation.

7.1 Influence of Temperature

From the analysis on parametric influence on EAF dust behaviour, it was concluded that temperature played the greatest role in influencing dust properties. As previously mentioned, EAF dust particles are spherical in nature and have a varying size range as it present as agglomerates as well as particles of sub-micron size. The particles can be seen as individual structures within the surface. This is caused by the adhesion of fine dust and fume particles that have agglomerated onto the surface of the larger particles thus providing a fibrous appearance. Thermally treated dust morphologies can be divided into the three stages of thermal evolution: Stage 1: *Initial Vaporisation*; Stage 2: *Transition* and Stage 3: *Final Sintering*.

7.1.1 Ash Morphology During Stage 1: Initial Vaporisation

This initial stage of the thermal evolution process occurs from approximately 100°C to 600°C. This stage is characterised by a marked weight loss within the dust sample due to the vaporisation of moisture and the reaction of free carbon present in the dust. From a morphological perspective, the treated dust particle greatly resembles the initial particle. The treated dust is present as agglomerates (Figure 7.1a) as well as particles of sub-micron size. The agglomerates seem to have a fibrous appearance at the surface due to the adhesion of fine dust and fume particles that have clustered onto the surface of the larger particles thus providing a fibrous appearance. The individual sub-micron and micron particles that form the larger agglomerates are clearly seen at the particle surface level (Figure 7.1b). These particles appear to be slightly shrunken over their original state due to the effects of thermal treatment.

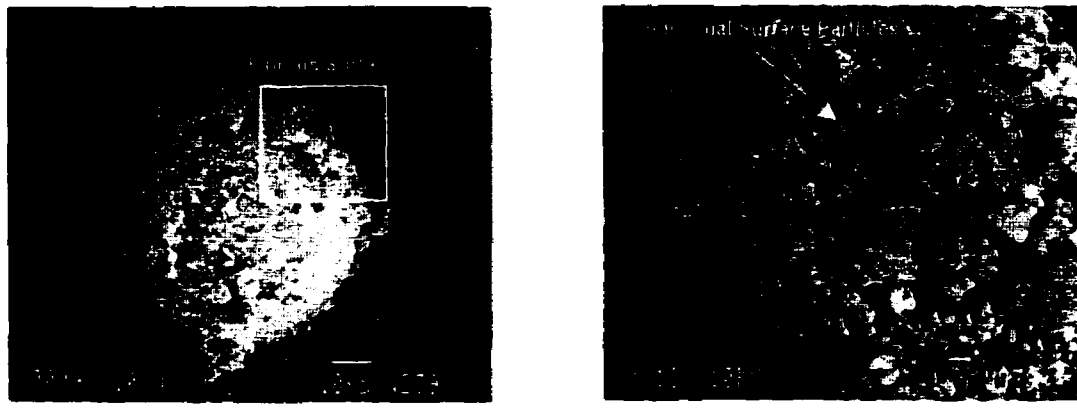

(a) (b)

Figure 7.1: (a) Particle occurring during initial stage, treated at @600°C,
(b) Particle Surface treated at 600°C

7.1.2 Ash Morphology During Stage 2: Transition

The transition phase of the thermal treatment process occurs from a temperature range of 600°C to 1100°C and is accompanied by oxidation reactions. It can be seen that in this stage of treatment the dust particles begin to change morphology. The particles (Figures 7.2a,c) still demonstrate a fibrous appearance, however, the effects of shrinkage appear to be taking place. When examining the particle surfaces (Figure 7.2b,d), it is evident that the boundaries between the micron and sub-micron particles are disappearing. In addition, significant particle shrinkage can be noticed at the surface. Small areas of liquid can be noticed at the surface of the particles. Some of the SiO_2 and K present in the dust form a glassy binary SiO_2-K_2O/Na_2O system with a low melting point below 1100°C[51]. This liquid phase is quite limited due to the insignificant levels of these compounds in the dust. The resultant glass phase is too limited to create a strong impenetrable structure that could trap metals within its matrix. The formation of the liquid pockets and the particle shrinkage does however result in a more resistant treated product as compared to the original EAF dust.

(a) Particle

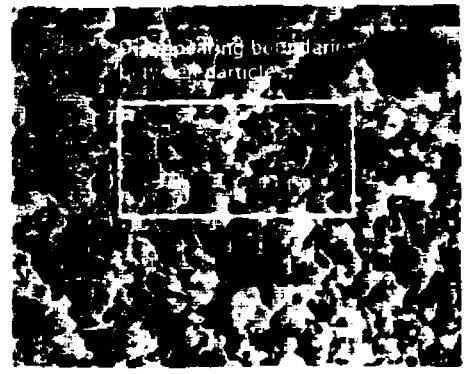

(b) Particle Surface

EAF Dust Treated at 800°C

(C) Particle

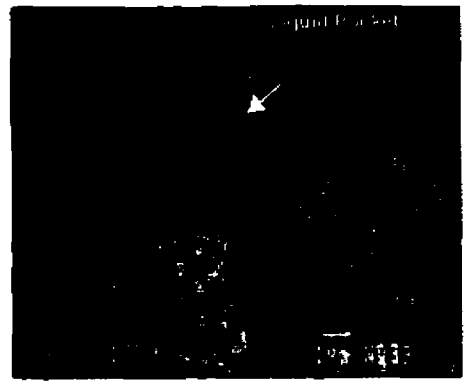

(d) Particle Surface

EAF Dust Treated at 1000°C

Figure 7.2: Particle Structures occurring during the Transition Stage of Thermal Treatment

7.1.3 Ash Morphology During Stage 3: Final Sintering

The morphology in Stage 3 occurs between a temperature range of 1100°C to 1600°C. This stage is characterised by the final sintering of the dust resulting in a strong pellet-like structure at high temperatures. Through the examination of the particles (Figure 7.3 a, c, e), it is evident that the particles have gone through a sintering process. The fibrous appearance of the particle has disappeared to be replaced by a smooth plate-like structure. Analysis of the particle surfaces (Figure 7.3, b, d, f) reveals that the micron and sub-micron particles are no longer evident and have been replaced by a smooth continuous-phase. The porosity in the sample is considerably diminished due to the formation of the regular structures.

(a) Particle

(b) Particle Surface

EAF Dust Treated at 1200°C

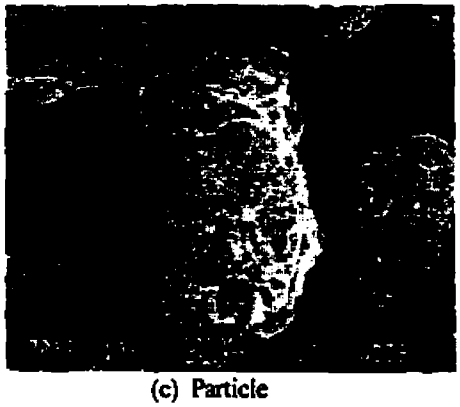

(c) Particle

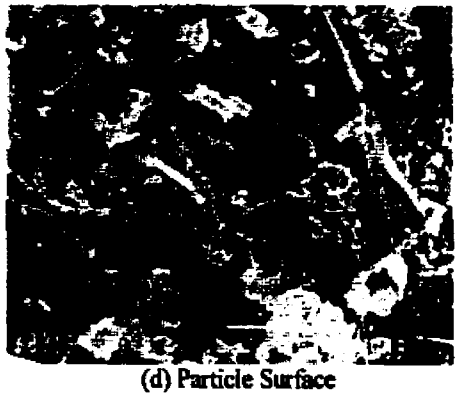

(d) Particle Surface

EAF Dust Treated at 1400°C

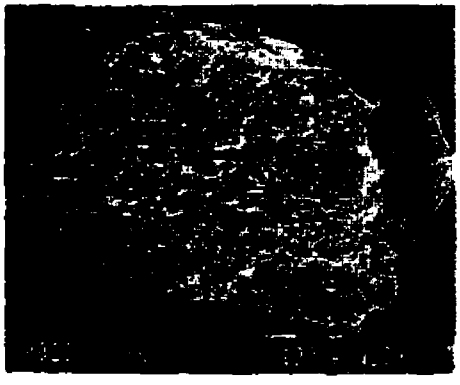

(e) Particle

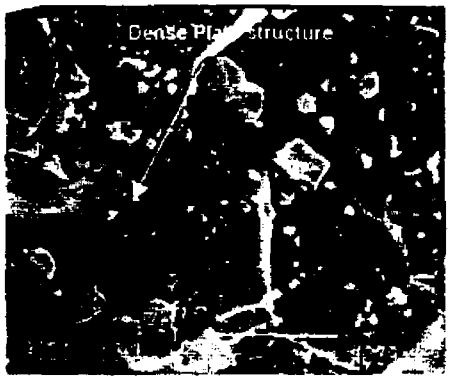

(f) Particle Surface

EAF Dust Treated at 1600°C

Figure 7.3: Particle Structures occurring during the Sintering Stage of Thermal Treatment

7.1.4 Theory of Sintering

The process of sintering is the densification of the oxide particles within the initial EAF through the removal of pores between particles through shrinkage, combined with growth and strong bonding between adjacent particles. The following criteria must be met in order for sintering to proceed: (1) A method of material transport must be available and, (2) a source of energy to activate and sustain this material transport must be made available[52]. Transport occurs mainly through diffusion and viscous flow. The energy is mainly provided through heat, in conjunction with energy gradients due to particle-particle contact and surface tension.

The process of sintering can be divided into three stages[53] as shown in Table 7.1.

Table 7.1: Sintering Stages

Stages	Phenomena
Stage 1:	
	Rearrangement
	Neck formation
Stage 2:	
	Neck Growth
	Grain Growth
	High Shrinkage
Stage 3	
	Much grain growth
	Discontinuous pore phase
	Grain boundary pores eliminated

The initial stage (Figure 7.4b) incorporates the rearrangement of particles, which consists of slight rotation of adjacent particles as to form more points of contact. In addition, the formation of a necking contact point occurs between adjacent particles due to the high probability of material transport in these areas of high surface energy.

The second stage of sintering (Figure 7.4c) is referred to as the *intermediate sintering stage*. In this stage, the size of the neck between the particles grows, resulting in a decrease in porosity as the particles move closer together. Shrinkage results due to the motility of the particles. The boundaries between the particles (which will now be referred to as grains) begin to move so that one grain begins to grow to the detriment of the smaller grains; this allows for a change in geometry that will accommodate further

necking and porosity removal. Intermediate sintering continues as long as pore channels are interconnected and ends when pores become isolated. Most of the shrinkage during the sintering process occurs during this stage.

The third and final stage of sintering (Figure 7.4d) is referred to as *final sintering*. In this stage, final porosity is removed by diffusion along the grain boundaries. Therefore pores must remain close to the grain boundaries. Additionally, grain growth occurs in this stage due to surface energy. The forces of nature reduce surface area to a minimum to minimise surface free energy, such as water drops which form into spheres. These same forces act on solid materials during sintering. Grains will grow in such a way as to increase their radius of curvature (i.e. they will straighten out). The smaller grains have a smaller radius of curvature, thus providing them more energy for motility and ultimately consumption by larger grains. The final distribution of grains and pores is referred to as the *microstructure*.

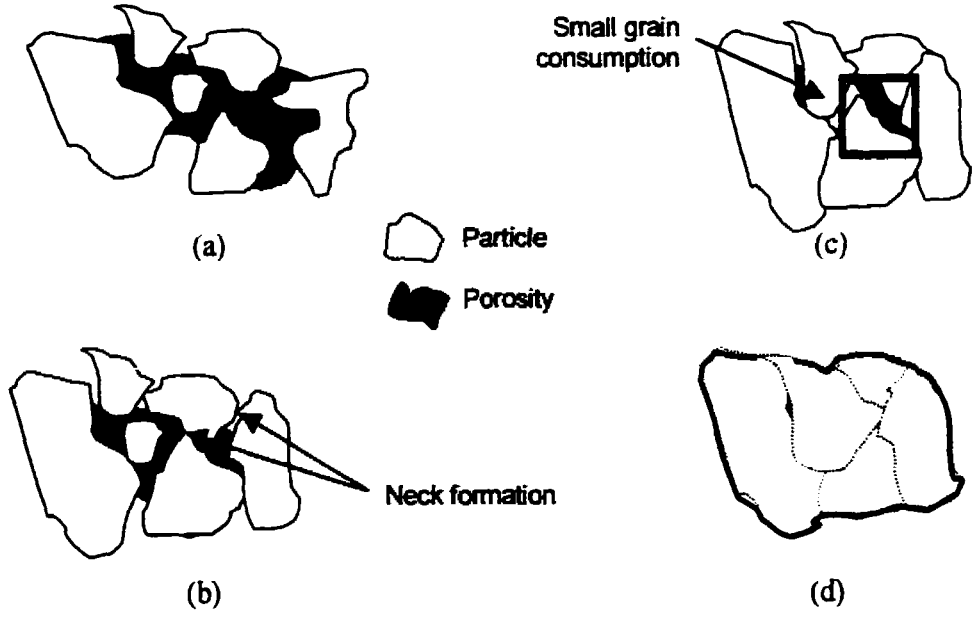

Figure 7.4: The three stages of sintering, (a) EAF dust in its original state, (b) First stage, (c) Second or Intermediate stage and, (d) Final sintering

The mechanism of sintering which occurs during the thermal treatment of the EAF dust is that of solid-state sintering. Solid-state sintering involves volume diffusion as illustrated in Figure 7.5. Diffusion can consist of atomic or vacancy movement along a surface or grain boundary or through the volume of the dust. Surface diffusion will not result in shrinkage, however volume diffusion whether through the grain boundaries or through the dislocations will result in shrinkage[54].

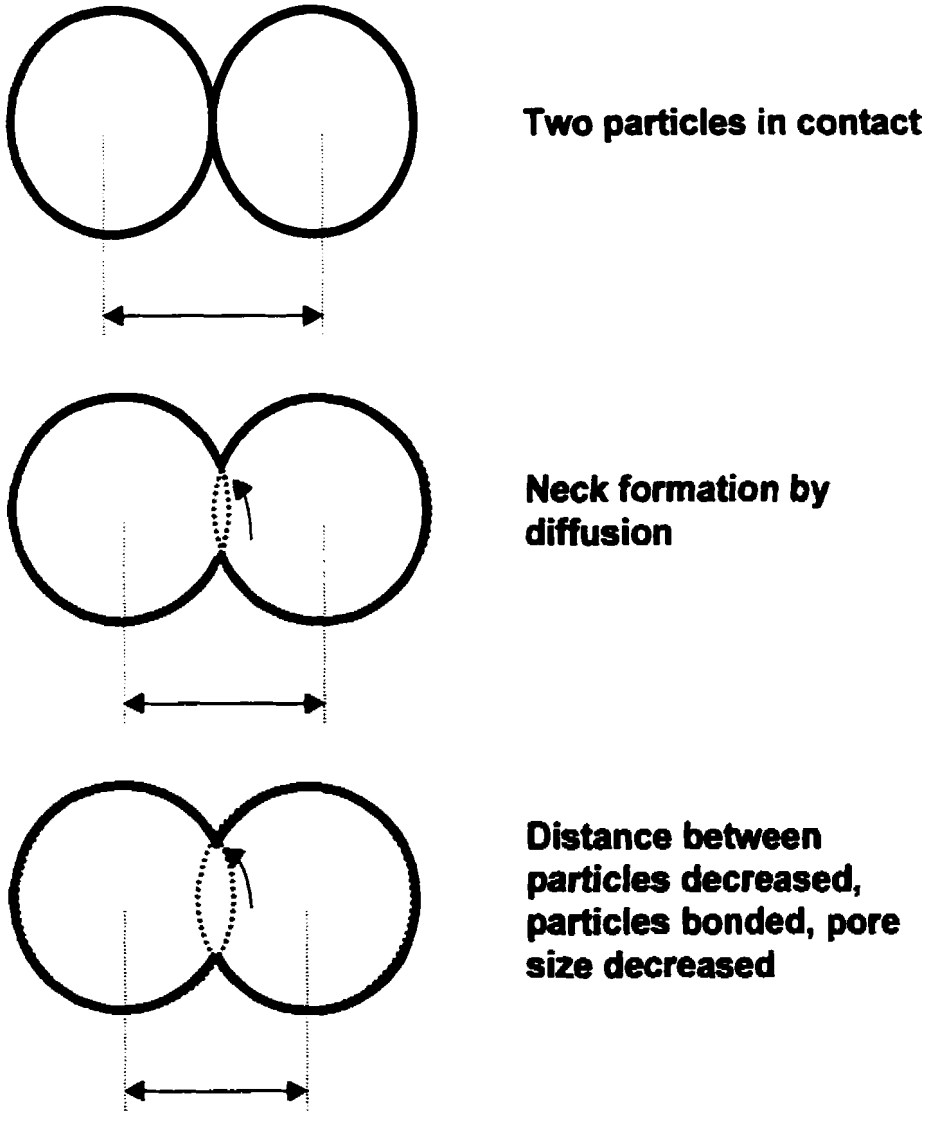

Figure 7.5: Solid-state materials transport

The driving force for solid-state sintering is the difference in free energy or chemical potential between the free surfaces of the particles and the points of contact between the adjacent particles. The equation representing the model of the mechanism of transport of material by lattice diffusion between from the line of contact between two particles to the neck region is[55]:

$$\frac{\Delta L}{L_0} = \left(\frac{K\gamma a^3 D^* t}{kTd^n} \right)^m$$

Where,
$\Delta L/L_0$ = linear shrinkage (equivalent to the sintering rate)
γ = surface energy
a^3 = atomic volume of the diffusing energy
D^* = self-diffusion coefficient
k = Boltzmann constant
T = temperature
d = particle diameter (if we assume equal-size spherical starting particles)
t = time
K = constant dependent on geometry
The exponent *n* is typically close to 3 and the exponent *m* is in the range of 0.3 to 0.5.

From this equation, it is evident that the greatest influence on the sintering rate is particle diameter. The smaller the particles, the greater the rate. In addition, temperature also plays a role in influencing the sintering rate. This is due to the exponential relationship between temperature T, and the diffusion coefficient.

7.2 Influence of Pyrolitic Environment

Figure 7.6 shows the morphology of the EAF dust treated in a pyrolitic environment as N_2 (g) was passed through the reaction chamber. The resulting thermally treated products demonstrate the same structures and morphologies as those produced in the atmospheric environment indicating that the pyrolitic environment does not have an influence on the resulting product characteristics. The thermally treated products present the three stages of treatment: Vaporisation, Transition and Sintering. During the vaporisation phase, the dust particles present a fibrous surface due to the loosely agglomerated micron and sub-micron particles on its surface. During the transition phase,

particle shrinkage starts to occur and the boundaries between the micron and sub-micron particles begin to disappear. Within the final sintering stage, fusion between the particles is noticed and a dense, smooth final structure is produced.

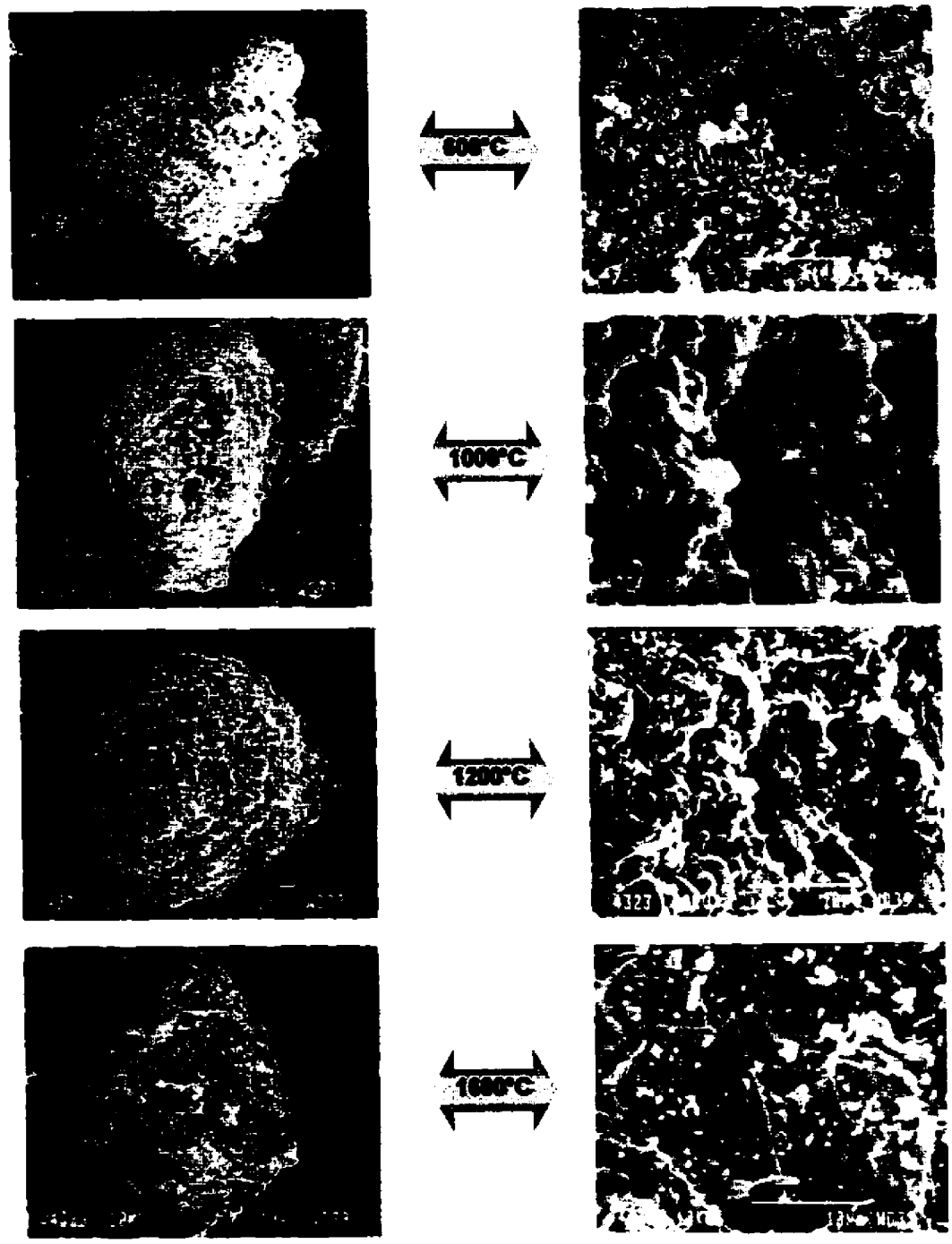

Figure 7.6: Morphological evolution of the thermally treated EAF dust in a pyrolitic environment

8 CONCLUSIONS AND RECOMMENDATIONS

The current research has provided some insight into EAF dust, through its initial physical and chemical characteristics and the transformations that occur within the original product throughout the thermal treatment process. From the results obtained, it is clear that it may be eventually possible to recommend an efficient and safe thermal remediation technique to deal with the abundance of toxic EAF dust.

The following conclusions and recommendations can be established:

The EAF dust particles in question are randomly distributed between <38 μm and 1.17 mm. The particles represent spherical agglomerations of homogeneously nucleated particles and entrained particles, the latter providing an adequate surface area for heterogeneous condensation to occur. Chromium and iron are the predominant elements present in the dust. Si, Ca, Mn, Ni, Na, Zn and Mg are also present in the dust in a lesser extent. The high level of Cr present in the dust is due to the fact that the dust was obtained from a stainless steel mill. The main phases present in the EAF dust are Fe_2O_3/Fe_3O_4 and Cr_2O_3.

The Design of Experiments (DOE) technique is introduced in this research and was greatly beneficial as it reduced research time while providing insightful results. During the thermal treatment of the EAF dust, temperature is determined to be the major influencing parameter in the process as it plays the greatest role in affecting weight loss in addition to diminishing the leachability of toxic metals from the dust product. The other two parameter researched; heating rate and residence time played a negligible role in influencing weight loss and metal leachability. As a result of the parametric experimentation, an optimum set of parametric conditions is established: a heating rate of 40°C/min., a residence time of 15 min. and a maximum temperature of 1600°C.

Thermal treatment of EAF dust can be characterised into three main stages: (1) Initial Vaporisation (90-600°C), where moisture present within the dust evaporates and free carbon reacts with oxygen to produce $CO_{2\,(g)}$; (2) Transition (600-1100°C), where oxidation and volatilisation of metal species begins; and (3) Final Sintering (1200-1600°C), where structure hardening and densification occurs.

Thermal evolution profiles reveal an insignificant weight loss occurring in the dust throughout thermal treatment. During both atmospheric and pyrolitic thermal treatment the weight loss curves exhibit three distinct zones. During atmospheric thermal treatment, the middle zone experienced a slight weight gain as re-oxidation of certain metal species occurred. In pyrolitic treatment, the middle zone was delineated as a plateau, representing the opposing effects of weight loss through volatilisation and weight gain through oxidation of metal species resulting from fine amounts of free oxygen present within the dust. Through thermal treatment, a maximum of 6 to 8 wt% can be achieved a final temperature of 1600°C. through analysis of the off-gas, this weight loss mostly occurs through the evolution of CO_2 gas and minimal amounts of water vapour.

Thermal treatment of EAF dust above 1200°C can lead to significant volume reduction in the dust due to the effects of sintering. Thus, the original EAF dust is transformed into a resistant pellet-like structure. In addition, metals mass balance experiments indicate that the toxic metal concentration in the initial dust diminishes to negligible levels at temperatures greater than 1200°C. This type of structure can be beneficial in subsequent landfilling operations due to its strength, compactness and resistance to leachability.

Temperature plays an important role in the morphology of the final EAF dust product. The different stages of thermal treatment reveal different ash morphologies. The dust product produced during the *Initial Vaporisation* stage is very similar to the initial EAF dust as it is present as agglomerates with a very loose fibrous surface. The particles created do not form an adequate structure to prevent metals leachability. The particles formed during the *Transition* stage present aspects of shrinkage and liquid eutectic formation. However, as in the previous case, the particulate nature of the dust product during this stage would not be sufficiently resistant for disposal. The dust product formed during the *Final Sintering* stage provides a plate-like, dense morphology. The resulting pellet produced contains very resistant qualities which would provide an adequate matrix to prevent the leaching of toxic metals present within the dust.

The leachability of the thermally treated EAF dust decreases dramatically as thermal treatment temperatures increase. At temperatures greater than 1200°C, leachability is significantly reduced due to the resistant pellet structure that is created. At 1600°C the leachability of all toxic metals falls bellow environmental guidelines to create a product that is environmentally safe to dispose or to re-use as a filler product in other materials.

Due to the fact that thermal treatment of EAF dust results in volatilisation of toxic metal species, it is important to study the parameters which affect the volatilisation behaviour of toxic metals such as hexavalent chromium. Operating conditions and waste composition are two such parameters which can greatly influence thermal treatment.

Thermal remediation procedures require high temperatures to treat EAF dust. Effective remediation can only result at temperatures greater that 1200°C. It would be beneficial to research thermal remediation techniques which employ co-products to reduce the treatment temperatures.

The greatest challenge to thermal remediation concept is its ability to treat various toxic materials and to do so through a cost and operations effective manner without creating secondary emissions. Thus, it is essential to design techniques which will continuously demonstrate safe operation and high performance. In doing so, public fears regarding this waste disposal option will be allayed.

9 REFERENCES

[1] Sims *et al.*, "Electric Arc Steelmaking", v.1, AIME. New York, 1962, 396p.

[2] Robiette, A.G.E., "Electric Melting Practice", Griffin Publishing, London. 1972, 412p.

[3] Beddows, R., Doble, M. and Emmott, R., "Resource Options are Critical to EAF Steelmaking Decisions", Steel Times. Int. 1996, v.20, n.4, p.34, 3p.

[4] "Electric Furnace Roundup", Iron & Steelmaker. 1996, v.23, n.5, p.22, 2p.

[5] McIntyre, E.H. and Landry, E.R., "EAF Stelmaking-Process and Practice Update", Iron & Steelmaker. 1993, v.20, n.5, p.61, 6p.

[6] Aydin, S., Taptik, Y. and Arslan, C., "Scrap, Recycling and Steel production: a General Perspective and Turkey's Standpoint", Ironmaking & Steelmaking. 1996, v.23, n.3, p.242, 5p.

[7] Taylor, C.R. *et al.* "Electric Furnace Steelmaking", Iron and Steel Society. 1985, 391p

[8] Donald, J.R. and Pickles, C.A., "A Review of Plasma-Arc Processes for the Treatment of Electric Arc Furnace Dusts", Proc. Int. Syp. Res. Cons. Env. Tech. Met. Ind.. CIM. 1994, p.3, 21p.

[9] Donald, J.R. and Pickles, C.A., "Kinetic Study of the Reaction of Zinc Oxide With Iron Powder", Metallurgical and Materials Transactions - Series B, 1996, v.27, n.3, p.363, 12p.

[10] Li, Chung-Lee; Tsai, Min-Shing, "A crystal phase study of zinc hydroxide chloride in electric-arc-furnace dust", Journal of Materials Science, 1993, v.28, n.17, p.4562, 9p.

[11] Later, D.W. and Sorensen, G., "A Primer on the Toxicity Characteristic Leaching Procedure, A Laboratory's Perspective", Air and Waste Management Association. 1993.

[12] Goodwill, J.E. and Schmitt, R.J., "An Update on Electric Arc Furnace Dust Treatment in the United States", Proc. Int. Syp. Res. Cons. Env. Tech. Met. Ind., CIM. 1994, p.25, 9p.

[13] "Règlement sur les déchets dangereux (D. 1000-85 117 G.O. II, 3235 [c. Q-2, r.3.01]", Ministère de l'environnement et de la faune du Québec. 1985

[14] "Procédure d'évaluation des charactéristiques des déchets solides et des boues pompables", Ministère de l'environnement et de la faune du Québec. 1986

[15] Campbell, W.W. and Fullerton, R.W., "Development of an Electric Dust-Control System", J. Air Poll. Cont. Assoc. v.12, 1962, p.514

[16] Wilcox, M.S. and Lewis, R.T., "A New Approach to Pollution Control in an Electric Furnace Meltshop" Iron and Steel Eng. v.45, 1968. p.113

[17] Brown, K.A., "USS Duquesne Works Electric Furnace Shop Gas Cleaning System", IISI Symposium on Environmental Control in the Steel Industry, Japan

[18] Erikson, O.E., "Electric Steel Foundries Control Dust Emissions in the Los Angeles Area", J. Metals. v.5, 1953, p.1625

[19] Smith, G.F. and Critchley, P., "Development in Fume Extraction at Dunfurd Hadfields Ltd. and Brown Bayley Steels Ltd.", Ironmaking and Steelmaking. v.4, 1976, p.215

[20] "Evaluation of Exposure to Airborne Particles", World Health Organization. Geneva, 1984

[21] Dosman, J.A. and Cotton, D.J., "Occupational Pulmonary diseases: Focus on Grain Dust and Health", Academic Press. New York, 1980

[22] Bertolini, R., "Dust and its Effect on the Lungs", Canadian Centre for Occupational Health and Safety. 1988

[23] Task Group on Lung Dynamics to I.C.R.P. Committee 2: Deposition and Retention Models for Internal Dosimetry of the Human Respiratory Tract, Health Physics. v.12, 1966, p.173, 34p.

[24] Lippmann, M., "Respirable Dust Sampling", American Hygiene Assoc. Journal. v.31. 1970, 138p.

[25] Zunkel, D., "What to do with your EAF dust", Steel Times International, 1996, v.20, n.4, p.46, 5p.

[26] Beckovich, C M., "Treating and Managing Electric Arc Furnace Dust", Iron and Steelmaker, 1996, v.23, n.4, p.39, 4p.

[27] Corsini, T., "Treatment of EAF dust by leaching", Steel Times, 1994, v.222, n.10, p.400, 2p.

[28] (D.A.C. Compton, D.J. Johnson, "Integrated TGA-FTIR System to Study Polymeric Materials". FTS/IR Notes No. 70. July 1989).

[29] D.A. Skoog and J.J. Leary, "Principles of Instrumental Analysis" Fourth Edition, Sauders College Publishing, 1992, pp.266-267

[30] D.A.C. Compton, "On-line FTIR Analysis of the Gaseous Effluent from a Thermogravimetric Analyzer: Applications of an Integrated TGA/FTIR System", FTS/IR Notes No.54 1987

[31] R. Jenkins, X-Ray Fluorescence Spectrometry". New York: Wiley, 1988

[32] L.S. Birks, "Electron Probe Microanalysis", 2nd Edition. New York: Wiley Interscience. 1971

[33] V.A. Fassel and R.N. Kniseley, "Analytical Chemistry", 1974, 46, 1111A. Copyright 1974 ACS

[34] L.L. Stephen, F.L. Wayne, G.S. Janet and W.K. Gary. Bureau of Mines. Report of Investigation 8750 (1983).

[35] (C.R. Dempsey and E.T.Opppelt, "Incineration of Hazardous Waste: A critical Review Update", Air & waste, Vol. 43, January 1993. pp.25-63.

[36] W.R. Seeker, "Waste Combustion," in Proceedings of the Twenty-Third Symposium (international) on Combustion, The Combustion Institute, pp. 867-885. 1990

[37] J.E. Goodwill and R.J. Schmitt, "An update on electric arc furnace dust treatment in the United States," Res. Cons. Environ. Tech., 1994. pp. 25-33

[38] "Règlement sur les déchets dangereux (D.1000-85, (1985) 117 G.O. II, 3235 [c. Q-2, r.301])," Ministère de l'environment et de la faune. 1985

[39] Linak, W.P. and Wendt, J.O.L., "Toxic Metal Emissions from Incineration: Mechanisms and Control," Progress in Energy and Combustion Science 1993, Vol.19. No.2, pp. 145-185.

[40] Chung-Lee Li and Min-Shing Tsai, "A crystal phase study of zinc hydroxide chloride in electric-arc-furnace dust"Institute of minerals, metallurgy and Material Science. National Cheng-Kung University, Tainan, Taiwan. 1993

[41] K.K. Hockman and D. Barengut. "Design of Experiments", Chemical Engineering, November 1995, pp. 142-147.

[42] K.K. Hockman and M.W. Jenkins, "Design of Experiments: Neglected Key to Competitive R&D", Industrial Engineering, February 1994, pp. 50-51.

[43] X. Wei, Research Methods in Non-Ferrous Metallurgy. Northeast University of Technology, China. 1982

[44] G. Zheng, S. Di Lalla and J.A. Kozinski, "Experimental Methodology and Determination of Optimum Operating Parameters During Solid Waste Burning", Trans IChem, Vol. 76, Part B, February 1998, pp.19-30

[45] Procédures d'évaluation des caractéristiques des déchets solides et des boues pompables, MEF bibliothèque nationale du Québec. 1986

[46] G. Zheng, "Ash Morphology and Metals Distribution during Combustion of De-Inking Sludge", Department of Mining & Metallurgical Engineering, McGill University

[47] W.R. Seeker, "Waste Combustion," Proceedings of the Twenty-Third Symposium (International) on Combustion, The Combustion Institute, pp. 867-885, 1990.

[48] J.P Stumbar, et *al*, "The Fate of Heavy Metals I EPA'a Mobile Incineration System," presented at the American Flame Research Committee 1989 International Symposium on Combustion in Industrial Furnaces and Boilers.

[49] W.R. Seeker, "Waste Combustion," in Proceedings of the Twenty-Third Symposium (International) on Combustion, The Combustion Institute, pp. 867-885. 1990

[50] W.P. Linak and J.O.L Wendt, "Toxic Metal Emissions from Incineration: Mechanisms and Control" Prog. Energy Combust. Sci. 1993, Vol. 19, pp. 145-185

[51] Alpor A.M., "High Temperature Oxide Part – Refractory Glasses, Glass – Ceramics, and Ceramics", Academic Press, Inc. (London) Ltd., 1971

[52] Richerson, D.W., "Modern Ceramic Engineering", Second Edition, Marcel Dekker, Inc. (New York).,1992, pp. 519-521

[53] Richerson, D.W., Ceramic Fabrication – Densification, Lesson 12 from "Introduction to Modern Ceramics", ASM Materials Engineering Institute Course 56. ASM International, Materials Park, Ohio, 1990

[54] R.L. Coble, Sintering Crystalline solids. I. Intermediate and final state diffusion models and II. Experimental test of diffusion models in powder compacts, *J. Appl. Phys.* 32 (5), 787-799 (1961)

[55] J.S. Reed, "Principles of Ceramic Processing", Wiley, New York, 1988